Elsevier Editorial System(tm) for Energy Conversion and Management
Manuscript Draft

Manuscript Number: ECM-D-18-05037R1

Title: Performance analysis and optimization of a combined cooling and power system using low boiling point working fluid driven by engine waste heat

Article Type: Original research paper

Section/Category: 1. Energy Conservation and Efficient Utilization

Keywords: Internal combustion engine; Brayton cycle; Waste heat recovery; Dual-pressure organic Rankine cycle; Ejector refrigeration cycle; Optimization

Corresponding Author: Dr. Jiangfeng Wang, Ph.D.

Corresponding Author's Institution: Xi'an Jiaotong University

First Author: Wenge Huang

Order of Authors: Wenge Huang; Jiangfeng Wang, Ph.D.; Jiaxi Xia; Pan Zhao, Ph.D.; Yiping Dai

Abstract: This paper develops a combined cooling and power system, which consists of a carbon dioxide Brayton cycle, a dual-pressure organic Rankine cycle and an ejector refrigeration cycle, to recover waste heat from exhaust gas and jacket water in internal combustion engines. Thermodynamic models of the system are performed and exergoeconomic methods are used to calculate the levelized exergy cost of the component products. Effects of seven parameters, including Brayton cycle turbine inlet temperature and inlet pressure, organic Rankine cycle turbine high-pressure side and low-pressure side inlet temperature and ejector primary inlet pressure, are evaluated. Single-objective optimization is carried out by means of genetic algorithm to obtain the minimum levelized exergy cost of system product. Results show that the increase of pressure at Brayton cycle turbine inlet and high-pressure and low-pressure side of the organic Rankine cycle turbine inlet contributes to the decrease of levelized exergy cost of the system product. Optimization results show that minimum levelized exergy cost for system product is 53.25 $ (MWh)-1. When system product levelized exergy cost is minimum, system net power output, cooling capacity and exergy efficiency are 374.37 kW, 188.63 kW and 37.31%, respectively.

Dear Editor:

We are sending a manuscript entitled “Performance analysis and optimization of a combined cooling and power system using low boiling point working fluid driven by engine waste heat”, which we should like to submit for publication in Energy Conversion and Management. We investigate a combined cooling and power system driven by exhaust gas and jacket water from an internal combustion engine. The mathematical model of the system is established to simulate the cycles under steady-state conditions. A parametric analysis of seven key parameters is conducted to examine their effects on the thermodynamic and exergoeconomic performance of the system. An optimization is conducted by genetic algorithm to obtain better system performance.

We declare that the manuscript has not been previously published, is not currently submitted for review to any other journal and will not be submitted elsewhere before one decision is made. Its publication is approved by all authors. If accepted, it will not be published elsewhere in the same form, in English or in any other language.

We appreciate your consideration of our manuscript, and we look forward to receiving comments from the reviewers.

Sincerely,

Jiangfeng Wang (on behalf of the authors’ team)

Institute of Turbomachinery

Cover letter

Shaanxi Engineering Laboratory of Turbomachinery and Power Equipment

State Key Laboratory of Multiphase Flow in Power Engineering

School of Energy and Power Engineering

Xi’an Jiaotong University, Xi’an, China

Highlights

A combined cooling and power system driven by engine exhaust gas and jacket water is proposed.

Thermodynamic and exergoeconomic performance of the system are analyzed.

Optimization for the combined cooling and power system is conducted by genetic algorithm.

Performance analysis and optimization of a combined cooling and power system using low boiling point working fluid driven by engine waste heat

Wenge Huang, Jiangfeng Wang*, Jiaxi Xia, Pan Zhao, Yiping Dai

Institute of Turbomachinery, Shaanxi Engineering Laboratory of Turbomachinery and Power Equipment, State Key Laboratory of Multiphase Flow in Power Engineering, School of Energy and Power Engineering, Xi'an Jiaotong University, Xi'an 710049, China

Corresponding author: Jiangfeng Wang

Mailing address:

Institute of Turbomachinery, Shaanxi Engineering Laboratory of Turbomachinery and Power Equipment, State Key Laboratory of Multiphase Flow in Power Engineering, School of Energy and Power Engineering

Xi'an Jiaotong University, Xi'an 710049, China

E-mail address: jfwang@mail.xjtu.edu.cn (JF Wang).

Performance analysis and optimization of a combined cooling and power system using low boiling point working fluid driven by engine waste heat

Wenge Huang, Jiangfeng Wang*, Jiaxi Xia, Pan Zhao, Yiping Dai

Institute of Turbomachinery, Shaanxi Engineering Laboratory of Turbomachinery and Power Equipment, State Key Laboratory of Multiphase Flow in Power Engineering, School of Energy and Power Engineering, Xi'an Jiaotong University, Xi'an 710049, China

Abstract

This paper develops a combined cooling and power system, which consists of a carbon dioxide Brayton cycle, a dual-pressure organic Rankine cycle and an ejector refrigeration cycle, to recover waste heat from exhaust gas and jacket water in internal combustion engines. Thermodynamic models of the system are performed and exergoeconomic methods are used to calculate the levelized exergy cost of the component products. Effects of seven parameters, including Brayton cycle turbine inlet temperature and inlet pressure, organic Rankine cycle turbine high-pressure side and low-pressure side inlet temperature and ejector primary inlet pressure, are evaluated. Single-objective optimization is carried out by means of genetic algorithm to obtain the minimum levelized exergy cost of system product. Results show that the increase of pressure at Brayton cycle turbine inlet and high-pressure and low-pressure side of the organic Rankine cycle turbine inlet contributes to the decrease of levelized

exergy cost of the system product. Optimization results show that minimum levelized exergy cost for system product is 53.25 \$ (MWh)$^{-1}$. When system product levelized exergy cost is minimum, system net power output, cooling capacity and exergy efficiency are 374.37 kW, 188.63 kW and 37.31 %, respectively.

Nomenclature

Latin symbols		ρ	density, kg m^{-3}
A	area, m^2	μ	dynamic viscosity, m^2 s^{-1}
B_o	boiling number	η	efficiency, %
c	levelized average cost, \$(MWh)$^{-1}$	δ	thickness, m
c_p	specific heat, kJ kg^{-1} K^{-1}	*Subscribes*	
C	cost rate, \$ year^{-1}	1-31	state points
D	diameter, m	g1-g3	state points
e	exergy, kJ kg^{-1}	w1-w3	state points
E	exergy flow rate, kJ s^{-1}	Bt	Brayton cycle turbine
E_y	exergy flow rate per year, kJ year^{-1}	BM	bare module
F	multiplying factor	cond	condenser
f	friction factor	comp	compressor
G	mass flow rate, kg s^{-1}	D	destruction
h	enthalpy, kJ kg^{-1}	elec	electricity
H	depth, m	es	equivalent diameter
i_{eff}	interest rate	ev	evaporation/evaporator
l	length, m	ex	exergy

M	mass flow rate, kg s^{-1}	F	fuel
n	lifetime, year	g	exhaust gas
Nu	Nusselt number	gh	gas heater
P	pressure, MPa	he	heat exchanger
Pr	Prandtl number	L	loss
Pt	center distance between tubes, m	l	liquid
P_r	reduced pressure	M	material
Q	heat transfer rate, kW	Ot	ORC turbine
Q_{cool}	cooling capacity, kW	P	product
q_{m}	average imposed wall heat flux, W m^{-2}	p1	pump 1
r_{f}	enthalpy of vaporization, kJ kg^{-1}	p2	pump 2
T	temperature, K	p3	pump 3
U	overall heat transfer coefficient, W m^{-2} K^{-1}	p4	pump 4
W	power, kW	pf	primary flow
W_{y}	annually power, MWh $year^{-1}$	prec	precooler
x	vapor quality	preh	preheater
Z	annually levelized cost value, \$ $year^{-1}$	s	shell
z	capital cost, k\$	t	tube
Acronyms		th	thermal
BC	Brayton cycle	turb	turbine
CBC	CO_2 Brayton cycle	vg	vapor generator
CCP	combined cooling and power	w	tube wall

CRF	capital recovery factor
CEPCI	chemical engineering plant cost index
DORC	dual-pressure organic Rankine cycle
ERC	ejector refrigeration cycle
GA	genetic algorithm
TEG	thermoelectric generator
AARC	ammonia absorption refrigeration cycle
Greek symbols	
α	convection heat transfer coefficient, W m^{-2} K^{-1}
λ	heat conductivity, W m^{-1} K^{-1}

1. Introduction

Nowadays, internal combustion engine (ICE) is the major motive power source in energy field, which are widely used in transport, construction, agriculture, etc. Over 50 % of the total transportation fuel is consumed by ICEs [1]. However, only 30-45 % of the fuel energy is converted into effective power output, while the remaining energy is discharged to the environment via exhaust gas, jacket water and charge air, causing a large amount of waste fuel energy [2]. Thus, technology for waste heat recovery from ICEs has drawn much interest of researchers in the last decade. Much effort has been devoted to the study of organic Rankine cycle (ORC) based ICE waste heat recovery system for its advantages of high efficiency and simple structure [3].

There are two important pathways that will lead to the improvement of the ORC system for ICE waste heat recovery. One will be selecting organic working fluids which are suitable for the system under certain conditions. Another is to optimize the system configuration to make full use of the waste heat.

The work of selecting suitable organic working fluids for ORC was carried out by many researchers to improve the efficiency of the ICE waste heat recovery. Tian et al. [4] evaluated the performance of 20 different working fluids in an ORC system for ICE waste heat recovery. Rijpkema et al. [5] compared the performance of twelve working fluids in an ORC-based ICE waste heat recovery system to find the suitable candidate. Su et al. [6] developed a theoretical efficiency model about working fluids selecting for ORC-based ICE waste heat recovery system via strict mathematical derivation.

Configuration optimization in ORC-based ICE waste heat recovery system mainly focuses on reducing the system irreversible rate to fully utilize the engine waste heat. Vaja and Gambarotta [7] added a preheater and a recuperator separately to a simple ORC system to improve the performance for the ICE waste heat recovery. Kim et al. [8] proposed a novel single-loop ORC system to recovery engine waste heat. They employed two recuperators in series to heat the working fluid. Comparison showed that the net power output of the system was 35.6 % more than simple ORC system. Because that the maximum power output of single-loop ORC is lower than that of the dual-loop ORC system [9], more attention has been focused on dual-loop ORC based ICE waste heat recovery system in recent years. Wang et al. [10] modeled a dual-loop ORC system for engine waste heat recovery. The high-temperature loop absorbed heat from exhaust gas and its residual heat acted as heat source for the low-temperature loop. Wang et al. [11] investigated a dual-loop ORC system for ICE waste heat recovery. The high-temperature loop absorbed heat from exhaust gas for the first time. Then the low-temperature loop absorbed heat from the residual heat of the exhaust gas to realize the cascading utilization of the waste heat. Huang et al. [12] proposed a complex dual-loop ORC system for engine waste heat recovery. The high-temperature loop absorbed heat from the exhaust gas and residual heat from both the exhaust gas and the high-temperature loop provided heat for the low-temperature loop.

When referring to heat transfer in the high-temperature loop, thermal stability of organic working fluid is necessary to be considered. In previous studies, refrigerants were most selected as working fluids. The decomposition temperatures of refrigerants are relatively low (200-300 ℃) [13], while the temperature of exhaust gas is above 450 ℃ [14]. Direct heat transfer between high-temperature exhaust gas and refrigerant caused the risk of working fluid decomposition. Though high decomposition temperature working fluids such as siloxanes and alkanes were adopted by some researchers, their flammability hindered their further applications [15]. Though placing a heat transfer oil intermediate loop between the exhaust gas and the ORC system could address this issue [16], it would cause a large amount of the high-temperature waste heat unharnessed. Therefore, some other high-temperature loops for waste heat recovery were employed by researchers to couple with the ORC. Miller et al. [17] introduced thermoelectric generator (TEG) technology. High-temperature exhaust gas was first exploited by the TEG, then the cooled exhaust gas could drive the ORC safely. But the energy conversion capacity of TEG is low because of the material limitation. Steam Rankine for its high efficiency and stable operation attracted much attention of researchers. Shu et al. [18] placed a steam Rankine cycle between the ORC and the exhaust gas. Yu et al. [19] coupled a steam Rankine cycle with an ORC for the ICE waste heat recovery. However, the large bulk of the components in steam Rankine cycle limits further applications (such as application in vehicles) [20]. Considering the requirement of high thermal efficiency and compact configuration, Brayton cycle could be a compromise solution. Brayton cycle with CO_2 (carbon dioxide) as working fluid has the advantage of low environmental impact and good thermodynamic performance [21]. Few studies about ORC system coupled with CO_2 Brayton cycle (CBC) for ICE waste heat recovery have been published. Though Zhang et al. [20] carried out some relevant studies, their attention was focused on comparing the performance of CBC, TEG and steam Rankine cycle when coupled with the same bottom ORC. Detailed analysis of the CBC was not given and the energy in jacket water was not harnessed.

Jacket water, though containing large amounts of energy [22], obtained little attention in the previous studies. For its relatively low temperature, jacket water was mainly used to preheat the organic working fluid in the ORC system. In the ORC-based ICE waste heat recovery system designed by Zhang et al. [23] jacket water was used to preheat the organic working fluid. Then the organic working fluid was heat by the high-temperature exhaust gas to vapor state and expanded in the ORC turbine. In Yang's [24] ICE waste heat recovery system, jacket water and secondary exhaust gas were used to preheat the organic working fluids in ORC. In the dual-loop ORC based ICE waste heat recovery system investigated by Song et al. [25], jacket water was used to preheat the low-temperature-loop. Yu et al. [26] calculated the energy recovery efficiency from an ORC-based ICE waste heat recovery system. 75 % waste heat could be recovered from the exhaust gas, while only 9.5 % waste heat was recovery from jacket water. The relatively low utilization rate of jacket water energy in the ORC system is caused by the mismatch of working fluid mass flow rate in the preheater and the evaporator. Thus, the utilization of energy in jacket water could be further explored.

Multigeneration system driven by waste heat has drawn increasing interest of researchers in light of the trend towards reducing emissions, increasing the efficiency of energy use and providing variable energy. Li et al. [27] modeled a combined cooling, heating and power system to highly utilize the waste heat. Yari et al. [28] proposed a waste heat recovery system to provide power, distilled water and heat. Bai et al. [29] investigated a cooling, heating and power system driven by exhaust gas to recovery the waste heat. Combined cooling and power (CCP) systems driven by ICE waste heat were also investigated by some researchers. Chen et al. [30] designed an ammonia-water combined cooling and power system using the waste heat from the ICEs. Ammonia-water was heated by exhaust gas and jacket water. One part of the ammonia-water vapor flew into the turbine to provide power and the other part flew into the evaporator to provide refrigeration. Salek et al. [31] coupled an ammonia absorption refrigeration cycle and a bottoming Rankine cycle with internal combustion engine to produce power and cooling capacity.

Ammonia absorption refrigeration cycle (AARC) were widely used in the combined cooing and power system for its large refrigeration output. However, the complex cycle structure and high driven temperature requirement of AARC might sometimes limit its applications. On the contrary, ejector refrigeration cycle (ERC) exhibits the advantages of easy maintenance and high reliability [32] and it can be driven by low-temperature heat source such as the jacket water. Thus, ICE waste heat recovery system with ERC driven by jacket water not only simultaneously generate power and refrigeration but also fully utilized the jacket water waste heat.

In this study, a combined cooling and power system is developed, which comprises a CO_2 Brayton cycle, a dual-pressure organic Rankine (DORC) cycle and an ejector refrigeration cycle. The CO_2 Brayton cycle absorbs heat from the high-temperature exhaust gas directly to prevent the decomposition risk. The turbine exhaust in the CO_2 Brayton cycle and the engine exhaust gas after heat transfer are respectively regarded as the heat sources for the high-pressure side and low-pressure side of the dual-pressure ORC, realizing the cascading utilization of exhaust gas. Meanwhile, organic working fluids in high-pressure side and low-pressure side are both preheated by jacket water which increases the mass flow rate of the organic working fluid preheated by jacket water. What’s more, the ejector refrigeration cycle is adopted to produce refrigeration and fully utilize waste heat in jacket water. Thermodynamic and exergoeconomic analysis is carried out to examine the effects of key parameters on system performance. Then a system optimization is conducted to obtain the minimum levelized exergy cost for the system product by means of genetic algorithm (GA).

The innovative features of this paper are as follow:

- A CO_2 Brayton cycle is investigated to prevent the risk of decomposition of organic working fluid and provide power.
- A novel dual-pressure ORC system is developed to cascading utilize the waste heat in exhaust gas and jacket water and provide large amounts of power output.
- An ejector refrigeration cycle driven by jacket water is designed to provide refrigeration and fully utilize the jacket water waste heat.

2. System description

The combined cooling and power system is shown in Fig. 1. The system integrates a dual-pressure organic Rankine cycle with a CO_2 Brayton cycle and an ejector refrigeration, which can produce power and refrigeration simultaneously. High-temperature gas heat from the ICE enters the gas heater to provide heat for the CBC. In the CBC, compressor compresses the CO_2 to a supercritical state. The high-pressure CO_2 flows into the gas heater to absorb heat. Then CO_2 with high temperature and high pressure expands through the BC turbine to produce power.

After expanding in the BC turbine, the high-temperature exhaust CO_2 flows into vapor generator 2 to heat the organic working fluid. High-pressure side organic working fluid heated by the CO_2 then flows into the ORC turbine to produce power. Meanwhile low-pressure side organic working fluid absorbs heat from the secondary engine exhaust gas in vapor generator 1 and then enters ORC turbine to produce power.

Exhaust vapor from the ORC turbine is cooled by condenser 1 to liquid state and pressured by pump 1. Jacket water with large mass flow rate is used to preheat the organic working fluid in the preheater. The preheated organic working fluid then separates. One part of the fluid is pumped by pump 3 to the vapor generator 1 to cycle in the low-pressure side. The other part is pumped by pump 2 to the vapor generator 2 to cycle in the high-pressure side.

The jacket water then flows into vapor generator 3 to provide heat for the ejector refrigeration cycle. After the condensation process in condenser 2, liquid working fluid is divided into two separated parts. One part of the fluid is pumped to the vapor generator 3 to absorb heat from jacket water and then becomes superheated vapor. The other part of the working fluid flows through the throttle valve to become low-pressure vapor-liquid mixture. The low-pressure mixture enters the evaporator to produce cooling capacity when absorbing heat from the environment and become low-pressure vapor. After that, the superheated vapor mixes with the low-pressure vapor in the ejector. The mixed working fluid enters the condenser 2 to be condensed to liquid.

R245fa is selected as the working fluid for the organic Rankine cycle and the ejector refrigeration cycle because of the great thermodynamic performance [33] and the low environment effects [34].

3. System model

Several assumptions are made to simplify the simulation of the system, which are: (1) the system keeps a steady state; (2) the heat and frication in the system are not considered; (3) the pressure losses in the vapor generators, preheater, evaporator, condensers and pipes are neglected; (4) the gas temperature at the outlet of the vapor generator 1 is higher than 110 ℃[35], considering the low gas dew point temperature; (5) the working fluids at the outlet of the condensers and the preheater are saturated liquids, and the evaporator outlet state is saturated vapor; (6) the process through the throttle valve is isenthalpic.

3.1.Energy model

The net power of the CO_2 Brayton cycle is expressed as:

$$W_{\mathrm{BC}} = W_{\mathrm{Bt}} - W_{\mathrm{comp}} \tag{1}$$

The net power of the DORC is given as:

$$W_{\mathrm{ORC}} = W_{\mathrm{Ot}} - W_{\mathrm{p1}} - W_{\mathrm{p2}} - W_{\mathrm{p3}} \tag{2}$$

The cooling capacity of the ERC is given as:

$$Q_{\mathrm{cool}} = M_{\mathrm{cool}} \cdot (h_{21} - h_{20}) \tag{3}$$

The net power output of the whole system is calculated as:

$$W_{\mathrm{net}} = W_{\mathrm{ORC}} + W_{\mathrm{BC}} - W_{\mathrm{p4}} \tag{4}$$

The thermal efficiency of the system is given as:

$$\eta_{\mathrm{th}} = \frac{W_{\mathrm{net}} + Q_{\mathrm{cool}}}{M_{\mathrm{g1}} \cdot (h_{\mathrm{g1}} - h_{\mathrm{g3}}) + M_{\mathrm{w1}} \cdot (h_{\mathrm{w1}} - h_{\mathrm{w3}})} \tag{5}$$

The detailed energy model equations of each component are list in Table 1. Note that there are two expanding processes in the ORC turbine. The high-pressure vapor expands in the turbine and then mixes with the vapor from vapor generator 1. After that, the mixed vapor expands in the turbine for the second time.

3.2.Exergy model

The energy model of the system is based on the first law of thermodynamics. From the viewpoint of the first law, it is equivalent for work and heat. Nevertheless, according to the second law of the thermodynamics, the irreversibility of work and heat is different. The exergy is used to quantifies the difference between them. The exergy model of the system is based on a dead state (the ambient condition in this study). Definition of exergy is given as:

$$e = (h - h_0) - T_0 \cdot (s - s_0) \tag{6}$$

where h_0, T_0 and s_0 are the parameters under the ambient conditions.

The exergy flow rate in this study is given by:

$$E = M \cdot e \tag{7}$$

In this study, all the components in the system are associated directly or indirectly with fuel of other heat sources, such as exhaust as and jacket water. The heat sources provide exergy for the components to operate. For each component, there is an exergy balance equation, being expressed as [36]:

$$E_{\mathrm{F}} = E_{\mathrm{P}} + E_{\mathrm{D}} + E_{\mathrm{L}} \tag{8}$$

where E_F, E_P, E_D, E_L donate the rate of exergy for the component fuel, the rate of exergy for component product, the rate of component exergy destruction and the rate of component exergy loss, respectively.

The details of the exergy balance equations for each component are listed in Table 1.

The exergy efficiency represents the degree of the utilization of the waste heat in the system, being expressed as:

$$\eta_{ex} = \frac{W_{net} + E_{cool}}{E_{g1} - E_{g3} + E_{w1} - E_{w3}} \tag{9}$$

where E_{cool} is the exergy rate of the cooling process, being expressed as:

$$E_{cool} = E_{25} - E_{24} \tag{10}$$

3.3.Capital cost calculation

A method of modeling the capital costs of main components is used in this study. According to Ref. [37], the bare module cost of the components is calculated as the basic cost. The basic cost of the components includes the direct project cost (such as component cost, material cost of the installation, etc.) and the indirect project cost (like the taxes, insurance engineering expenses, etc.). The bare module cost of the components is calculated under basic conditions. For deviations from the based conditions, multiplying factors (the specific component type, the specific system pressure and the specific material of construction) are added in the calculation to correct the results. In the following text, equations from Eq. (11) to Eq. (21) are proposed in Ref. [37].

Axial turbines (BC turbine and ORC turbine) are used in this study. The bare module cost equation of the turbine is:

$$\log_{10} C^0_{\mathrm{turb}} = K_{1,\mathrm{turb}} + K_{2,\mathrm{turb}} \cdot \log_{10} W + K_{3,\mathrm{turb}} \cdot (\log_{10} W)^2 \tag{11}$$

where $K_{\mathrm{i,\ turb}}$ are constants corresponding to the turbine type; and W is the power output of the turbine.

Turbines used in this study are made of carbon steel (CS) and operate under high pressure. Thus, a multiplying factor is used to correct the result. The capital cost of the turbine is given as:

$$C_{\mathrm{turb}} = F_{\mathrm{BM,turb}} \cdot C^0_{\mathrm{turb}} \tag{12}$$

where $F_{\mathrm{BM,turb}}$ is the multiplying factor corresponding to the working conditions of the turbine.

Reciprocating pumps are used in this study. The bare module cost equation of the pumps is given as:

$$\log_{10} C^0_{\mathrm{pump}} = K_{1,\mathrm{pump}} + K_{2,\mathrm{pump}} \cdot \log_{10} W + K_{3,\mathrm{pump}} \cdot (\log_{10} W)^2 \tag{13}$$

where $K_{\mathrm{i,\ pump}}$ are the constants corresponding to the pump type; and W is the power input of the pump.

Pumps used in this study are made of stainless steel (SS) and work under high pressure. Thus, multiplying factors are used to correct the bare module cost. The capital cost of the pump is given as:

$$C_{\mathrm{pump}} = \left(B_{1,\mathrm{pump}} + B_{2,\mathrm{pump}} \cdot F_{\mathrm{M,pump}} \cdot F_{\mathrm{P,pump}}\right) \cdot C^0_{\mathrm{pump}} \tag{14}$$

where $B_{\mathrm{i,\,pump}}$ are the constants corresponding to the type of the pump; $F_{\mathrm{M,pump}}$ is the material factor of the pump and $F_{\mathrm{P,pump}}$ is the pressure factor of the pump. The equation of the pressure factor is given as:

$$\log_{10} F_{\mathrm{P,pump}} = C_{1,\mathrm{pump}} + C_{2,\mathrm{pump}} \cdot \log_{10} P_{\mathrm{pump}} + C_{3,\mathrm{pump}} \cdot (\log_{10} P_{\mathrm{pump}})^2 \tag{15}$$

where $C_{\mathrm{i,\,pump}}$ are the constants corresponding to the type of the pump; and P_{pump} is the pressure of the pump under working conditions.

Axial compressor is used in this study. The bare module cost equation of the compressor is given as:

$$\log_{10} C^0_{\mathrm{comp}} = K_{1,\mathrm{comp}} + K_{2,\mathrm{comp}} \cdot \log_{10} W + K_{3,\mathrm{comp}} \cdot (\log_{10} W)^2 \tag{16}$$

where $K_{\mathrm{i,comp}}$ are the constants corresponding to the type of the compressor; W is the power input of the compressor.

The compressor is made of carbon steel (CS) and works under high pressure. Correction equation of the bare module cost is given as:

$$C_{\mathrm{comp}} = F_{\mathrm{BM,comp}} \cdot C^0_{\mathrm{comp}} \tag{17}$$

where $F_{\mathrm{BM,comp}}$ is the constant corresponding to the type of the compressor.

Shell-and-tube heat exchangers (gas heater, vapor generators, precooler, preheater, evaporator and condensers) are used in this study. The bare module cost equation of the heat exchanger is given as:

$$\log_{10} C^0_{\mathrm{he}} = K_{1,\mathrm{he}} + K_{2,\mathrm{he}} \cdot \log_{10} A + K_{3,\mathrm{he}} \cdot (\log_{10} A)^2 \tag{18}$$

where $K_{\mathrm{i,he}}$ are the constants corresponding to the type of the heat exchanger; A is the heat transfer area of the heat exchanger. The calculation of the heat exchanger areas is presented in Appendix A.

Heat exchangers used in this study are made of carbon steel (CS) and work under different pressure. Multiplying factors are needed to correct the results, the equation is given as:

$$C_{\mathrm{he}} = \left(B_{1,\mathrm{he}} + B_{2,\mathrm{he}} \cdot F_{\mathrm{M,he}} \cdot F_{\mathrm{P,he}}\right) \cdot C_{\mathrm{he}}^{0} \tag{19}$$

where $B_{\mathrm{i,he}}$ are the constants corresponding to the type of the heat exchanger. $F_{\mathrm{M,he}}$ and $F_{\mathrm{P,he}}$ are the material factor and pressure factor, respectively. The pressure factor is obtained from the following equation:

$$\log_{10} F_{\mathrm{P,he}} = C_{1,\mathrm{he}} + C_{2,\mathrm{he}} \cdot \log_{10} P_{\mathrm{he}} + C_{3,\mathrm{he}} \cdot (\log_{10} P_{\mathrm{he}})^2 \tag{20}$$

where $C_{\mathrm{i,he}}$ are the constants corresponding to the type of the heat exchanger; P_{he} is the designed working pressure for the heat exchanger.

The values of the constants mentioned above for the main components are listed in Appendix B.

The calculation of the bare module cost depends on past records or published correlations for price information. It is necessary to update the costs because of the inflation. This can be achieved by the following equation:

$$C_2 = C_1 \cdot \left(\frac{I_2}{I_1}\right) \tag{21}$$

where C is the purchased cost and I is the cost index. The subscript 1 refers to base time when cost is known and subscript 2 refers to time when cost is desired. The *CEPCI* (Chemical Engineering Plant Cost Index) is employed to calculate the inflation. The values of $CEPCI_{2016}$ and $CEPCI_{\mathrm{ref},2001}$ are 541.7 and 397, respectively [38].

3.4.Exergoeconomic model

Exergoeconomic is a branch of engineering which combines the thermodynamic analysis and economic principles. Thermodynamic performance and economic cost of the system are all taken into consideration.

To find the relationship between the present value of the expenditure and the equivalent annually levelized costs, the capital recovery factor (CRF) is employed, being expressed as [36]:

$$Z_{\mathrm{i}} = CRF \cdot C_{\mathrm{i}} \tag{22}$$

$$CRF = \frac{i_{\mathrm{eff}} \cdot \left(1 + i_{\mathrm{eff}}\right)^{n}}{(1 + i_{\mathrm{eff}})^{n} - 1} \tag{23}$$

where i_{eff} is the effective discount rate with a value of 0.05 [39]; and n is the lifetime of the CCP system, being assumed as 30 years [40].

In order to calculate the equivalent annually levelized costs, the annual working time of the system is assumed as 8000 h [41]. Then the annual exergy rates and annual power output or consumption are obtained.

In a steady system, there are a number of entering and outing working fluid streams and heat and work interactions with the surroundings. In exergoeconomic analysis, each flowing stream is associated with a levelized exergy cost. The equations to calculate the cost of the stream product are given as:

$$C_{\mathrm{in}} = c_{\mathrm{in}} \cdot E_{\mathrm{y,in}} \tag{24}$$

$$C_{\mathrm{out}} = c_{\mathrm{out}} \cdot E_{\mathrm{y,out}} \tag{25}$$

$$C_{\mathrm{work}} = c_{\mathrm{work}} \cdot W_{\mathrm{y}} \tag{26}$$

$$C_{\mathrm{heat}} = c_{\mathrm{heat}} \cdot E_{\mathrm{y,heat}} \tag{27}$$

where c denotes levelized exergy cost of the streams; $E_{\mathrm{y,in}}$ and $E_{\mathrm{y,out}}$ are the exergy transfer rate of the stream flowing in and out of a component; W_{y} and $E_{\mathrm{y,heat}}$ are the power and the heat transfer rate of the components considering the annual working time.

The cost balance equation applied to the kth system component is given as:

$$\sum_{\mathrm{out}} C_{\mathrm{out,k}} + C_{\mathrm{w,k}} = C_{\mathrm{heat,k}} + \sum_{\mathrm{in}} C_{\mathrm{in,k}} + Z_{\mathrm{k}} \tag{28}$$

Details of the cost balance equation are listed in Table 2.

The levelized exergy cost for system product is chosen to indicate the exergoeconomic performance, being expressed as [42,43]:

$$c_{\mathrm{product}} = c_{\mathrm{capital}} + c_{\mathrm{fuel}} \tag{29}$$

where c_{capital} is the capital-cost-related part of the levelized exergy cost for the system product, being expressed as:

$$c_{\mathrm{capital}} = \frac{Z_{\mathrm{total}}}{W_{\mathrm{net}} + E_{\mathrm{cool}}} \tag{30}$$

where c_{fuel} is the fuel-cost-related part of the levelized exergy cost for the system product, being expressed as:

$$c_{\mathrm{fuel}} = \frac{c_{\mathrm{Bt}} \cdot W_{\mathrm{y,comp}} + c_{\mathrm{Ot}} \cdot W_{\mathrm{y,pump1}} + c_{\mathrm{Ot}} \cdot W_{\mathrm{y,pump2}} + c_{\mathrm{Ot}} \cdot W_{\mathrm{y,pump3}} + c_{\mathrm{Ot}} \cdot W_{\mathrm{y,pump4}}}{W_{\mathrm{net}} + E_{\mathrm{cool}}} \tag{31}$$

where c_{Bt} and c_{Ot} are the levelized exergy cost for the BC turbine power output and the ORC turbine power output, which are calculated in Table 3. Likewise, they can be expressed as the capital-cost-related part and the fuel-cost-related part, given by Eq. (32) and Eq. (33).

$$c_{\mathrm{Bt}} = \frac{Z_{\mathrm{Bt}}}{W_{\mathrm{y,Bt}}} + \frac{c_3 \cdot \left(E_{\mathrm{y,3}} - E_{\mathrm{y,4}}\right)}{W_{\mathrm{y,Bt}}} \tag{32}$$

$$c_{\mathrm{Ot}} = \frac{Z_{\mathrm{Ot}}}{W_{\mathrm{y,Ot}}} + \frac{c_{10} \cdot \left(E_{\mathrm{y,10}} + E_{\mathrm{y,11}} - E_{\mathrm{y,12}}\right)}{W_{\mathrm{y,Ot}}} \tag{33}$$

In addition, the levelized exergy cost for the condensers and the precooler is equal to zero, being given by:

$$c_{26}=c_{28}=c_{30}=0 \tag{34}$$

The levelized exergy cost for the exhaust gas as well as the jacket water is zero, being expressed as:

$$c_{g1}=c_{w1}=0 \tag{35}$$

3.5.Internal combustion engine

In this study, the engine selected [7] is a 12-cylinder 4-stroke supercharged engine. The main designed parameters of the engine are listed in Table 3. The composition of the engine exhaust gas is presented in Table 4. The thermal load of the engine exhaust gas is about 1700 kW and 1000 kW can be obtained from the engine jacket water.

3.6.Simulation conditions for the system

The thermodynamic parameters of the working fluid are calculated under the environment of MATLAB with the help of REFPROP 9.1 [44]. The basic conditions of simulation for the CCP system are listed in Table 5.

Seven key parameters : BC turbine inlet temperature ($T_{\mathrm{Bt,in}}$), BC turbine inlet pressure ($P_{\mathrm{Bt,\,in}}$), inlet temperature at the high-pressure side of ORC turbine ($T_{\mathrm{Ot,\,in,\,h}}$), inlet pressure at the high-pressure side of ORC turbine ($P_{\mathrm{Ot,\,in,\,h}}$), inlet temperature at the low-pressure side of ORC turbine ($T_{Ot, in, l}$), inlet pressure at the low-pressure side of ORC turbine ($P_{Ot, in, l}$) and the ejector primary inlet pressure ($P_{ej, in}$), are chosen to analyze the thermodynamic and exergoeconomic performance of the system. When one parameter is investigated to analyze the system performance, other parameters are maintained constants based on the conditions in Table 5.

In the thermodynamic aspect, the net power output of the CO_2 Brayton cycle (W_{BC}), net power output of the DORC (W_{ORC}), net power of the whole system (W_{net}), cooling capacity of the system (Q_{cool}) and the exergy efficiency of the system (η_{exergy}) are selected to reflect the system performance. Levelized exergy cost for the BC turbine power output (c_{Bt}), levelized exergy cost for the ORC turbine power output (c_{Ot}), levelized exergy cost the system product ($c_{product}$) and the system capital cost ($z_{capital}$) are chosen to represent the exergoeconomic performance.

4. Results and discussion

The influence of the BC turbine inlet temperature ($T_{Bt,in}$) on the output and the exergy efficiency of the system are shown in Fig. 2. The net power output of the CBC increases with the rise of $T_{Bt,in}$. That can be explained by the large decrease of the compressor power consumption. With the increase of the CO_2 temperature at the BC turbine inlet, the mass flow rate of CO_2 decreases, leading to the decrease of the compressor power consumption. Although the drop of CO_2 mass flow rate would cut down the BC turbine power output, the decrease quantity of compressor power consumption is larger than the decrease of the BC turbine power output. Thus, the large decrease of the compressor power consumption determines the increase trend of the CBC net power output.

It is presented that the net power output of the DORC increases with the rise of the BC turbine inlet temperature. Since the residual heat in exhaust CO_2 acts as the heat source for the high-pressure side of DORC, the temperature rise of the exhaust CO_2, caused by the rise of $T_{\mathrm{Bt,in}}$, would offer more heat for the bottom cycle, which causes the increase of the mass flow rate of the organic working fluid in the high-pressure side of DORC . Hence, the power output of the ORC turbine increases, leading to the increase of the net power output of the DORC.

With the increase of $T_{\mathrm{Bt,in}}$, the cooling capacity of the ERC decreases, as shown in Fig. 2. The increase of the organic working fluid mass flow rate in DORC would absorb more heat from jacket water, resulting in the decrease of energy available for the ERC. As a result, less secondary flow working fluid from the evaporator is entrained to the ejector, resulting the decrease of the cooling capacity of the CCP system.

The increase of the CBC net power output and the DORC net power output account for the increase of the net power output of the whole CCP system. Though the cooling capacity of the ERC is large, it produces only a small amount of exergy. The decrease of the exergy output caused by the cooling capacity drop can be made up by the increase of the power exergy output. Thus, the exergy efficiency of the system increases.

The influences of the BC turbine inlet temperature on the levelized exergy cost and the system capital cost of the system are shown in Fig. 3. The levelized exergy cost for the BC turbine power output (c_{Bt}) drops with the rise of the BC turbine inlet temperature ($T_{Bt,in}$). That can be explained by the decrease of the capital-cost-related part of c_{Bt}. The capital-cost-related part of c_{Bt} decreases with the decrease of cost of compressor, which is cut down by the drop of the compressor power consumption. The increase of the ORC turbine power output causes the decrease of both the capital-cost related part and the fuel-cost-related part of c_{Ot}, resulting in the decrease of c_{Ot}.

The system capital cost ($z_{capital}$) rises with the rise of $T_{Bt,in}$. The large increase of the ORC turbine power output increases the cost of the ORC turbine. Moreover, the increase of the mass flow rate of the organic working fluid in the DORC causes the increase of cost for the vapor generator 2 and the preheater. Though the cost of compressor decreases, it can't change the ascending trend of the total system capital.

It can be obtained in Fig. 3 that the levelized exergy cost for the system product ($c_{product}$) decreases with the rise of $T_{Bt,in}$. The decline in levelized exergy cost for the BC turbine and ORC turbine power output, according to Eq. (31), would cause the decrease of the fuel-cost related part of $c_{product}$. Though the increase of $z_{capital}$ would cut down the capital-cost-related part of $c_{product}$, the impact of levelized exergy cost for the BC turbine and ORC turbine is greater, which leads to the descending trend of $c_{product}$.

The influence of the BC turbine inlet pressure ($P_{Bt, in}$) on the output and the exergy efficiency of the system are shown in Fig. 4. The net power output of the CBC increases with the increase of $P_{Bt, in}$, which can be explained by the rise of enthalpy drop of the CO_2 in the BC turbine. Though the rise of $P_{Bt, in}$ requires more compressor power consumption, the increase of the BC turbine power output is larger in quantity than the consumption, which leads to the increase of the CBC net power output.

The net power output of the DORC decreases with the rise of $P_{Bt, in}$. On the one hand, the temperature of the exhaust CO_2 at the BC turbine outlet decreases with the increase of $P_{Bt, in}$. Thus, less heat is offered to the high-pressure cycle of DORC, resulting in the decrease of the high-pressure cycle power output. On the other hand, the increase of $P_{Bt, in}$ causes the increase of the compressor power consumption, which results in the rise of the CO_2 temperature at the compressor outlet. Thus, less heat is released in the gas heater and more heat is provided to the low-pressure cycle of DORC, which leads to the increase of the low-pressure cycle power output. However, the increase of the power output in low-pressure side is smaller than the decrease of the power output in the high-pressure side. Thus, the net power of the DORC decreases slightly.

The cooling capacity of the system increases with the increase of $P_{Bt, in}$. Just like the variation of the power output, the decrease of the mass flow rate in the high-pressure side of DORC is larger than the increase of mass flow rate in the low-pressure side. Therefore, the total mass flow rate in the DORC decreases, resulting in the reduction of heat provided for the ejector refrigeration cycle. Thus, the cooling capacity of the ERC decreases.

The net power output of the whole system increases with the increase of the BC turbine inlet pressure. Though the net power output of the DORC decreases, the increase of CBC net power output is much larger. Thus, the net power output of the CCP system increases with the increase of $P_{\mathrm{Bt,\,in}}$. The exergy efficiency of the system likewise has the same rising trend.

The influences of the BC turbine inlet pressure ($P_{\mathrm{Bt,\,in}}$) on the levelized exergy cost and the system capital cost of the system are depicted in Fig. 5. The levelized exergy cost for the BC turbine output c_{Bt} increases with the rise of the $P_{\mathrm{Bt,\,in}}$, which can be explained by the variations of the capital-cost-related part and the fuel-cost-related part. The increase of $P_{\mathrm{Bt,\,in}}$ causes the increase of cost for both the BC turbine and the compressor, which lead to the rise of the two related parts.

The levelized exergy cost for the ORC turbine product (c_{Ot}) increases with the rise of $P_{\mathrm{Bt,in}}$. The decrease of the mass flow rate in the DORC causes that less exergy is produced in vapor generator 2, causing the increase of the fuel-related part of c_{Ot}. Therefore, the levelized exergy cost for the ORC turbine (c_{Ot}) increases.

The system capital cost (z_{capital}) increases with the rise of ($P_{\mathrm{Bt,\,in}}$). The increase of the mass flow rate in the ERC causes the rise of capital cost for the evaporator and vapor generator 3, which combined with the rise of the BC turbine cost and compressor cost accounts for the system capital cost rise.

The levelized exergy cost for the system product decreases with the rise of $P_{\mathrm{Bt,\,in}}$ as presented in Fig. 5. According to Eq. (31), the rise of the c_{Ot}, c_{Bt} would cause the rise of the fuel-cost-related part of c_{product}. However, because of the large increase of the system net power output, the capital-cost-related part and the fuel-cost-related part decrease actually, which determines the decrease of c_{product}.

The influence of inlet temperature at the high-pressure side of ORC turbine ($T_{Ot, in, h}$) on the output and the exergy efficiency of the system are shown in Fig. 6. The net power output of the CBC remains unchanged since thermal parameters in dual-pressure ORC are irrelevant to the thermodynamic performance of the CBC.

The net power output of the DORC decreases with the increase of $T_{Ot, in, h}$. Though the increase of the vapor temperature could lead to the rise of the enthalpy drop in the ORC turbine, it would also cause the decrease of the mass flow rate in the high-pressure side, whose impact is greater than that of the enthalpy drop. Therefore, the power output of the DORC decreases.

The cooling capacity of the ejector refrigeration cycle increases with the rise of $T_{Ot, in, h}$. More heat is provided for the ERC because of the decrease of the mass flow rate in the DORC, leading to the increase of the mass flow rate in vapor generator 3. Thus, more secondary flow from the evaporator is entrained into the ejector, resulting in the increase of the cooling capacity.

The net power output of the CCP system decreases with the rise of $T_{Ot, in, h}$. The unchanged CBC power output and the drop of the DORC power output determine the decrease of the net power output of the CCP system. The exergy efficiency of the system as well drops with the increase of the increase of $T_{Ot, in, h}$.

The influences of inlet temperature at the high-pressure side of ORC turbine on the levelized exergy cost and the system capital cost of the system are presented in Fig. 7. The levelized exergy cost for the ORC turbine output (c_{Ot}) increases with the increase of $T_{Ot, in, h}$. The reason is that the two related parts of c_{Ot} increase with the drop of the

ORC turbine power output.

The levelized exergy cost for the BC turbine power output (c_{Bt}) increases with the rise the $T_{Ot, in, h}$. Since the decrease of the mass flow rate in the high-pressure side of DORC, the exergy generated in the vapor generator 2 decreases, causing the increase of the levelized exergy cost of the vapor. Thus, the increase levelized exergy cost of the vapor, which is heated by the BC turbine residual heat, causes the increase of the levelized exergy cost for the exhaust CO_2. According to Eq. (32), the fuel-cost-related part of c_{Bt} increases, leading to the increase of c_{Bt}.

The system capital cost ($z_{capital}$) decreases with the increase of $T_{Ot, in, h}$. The decrease of the DORC power output causes the drop of the ORC turbine cost, which leads to the descending trend of $z_{capital}$.

The levelized exergy cost for the system product ($c_{product}$) increases with the rise of $T_{Ot, in, h}$, as shown in Fig. 7. The increase of the levelized exergy cost for the BC turbine and ORC turbine power output cause the rise of fuel-cost-related part of $c_{product}$. Meanwhile, the large decrease of the net power of the CCP system causes the increase of the capital-cost-related part. The two increase parts determine the rise of $c_{product}$.

The influences of the inlet pressure at the high-pressure side of ORC turbine ($P_{Ot, in, h}$) on the output and exergy efficiency of the system are presented in Fig. 8. The net power of the CBC keeps unchanged because of the unchanged thermal parameters in the cycle.

The net power output of the DORC increase with the rise of $P_{Ot, in, h}$. The increase of the evaporation pressure cuts down the latent heat of the organic working fluid, which causes the increase of the mass flow rate in the high-pressure side of DORC. As a result, the net power output of the ORC turbine increases, leading to the increase of the net power output of the DORC.

Considering the increase of the DORC net power output and the unchanged CBC net power output, the net power output of the whole system increases. Also, the exergy efficiency of the system increases.

The increase of the mass flow rate in the DORC absorbs more heat from the jacket water in the preheater. Thus, less heat is released in the vapor generator 3, causing the decrease of the mass flow rate of the working fluid in the ERC. As a result, the cooling capacity of the system decreases.

The influence of the inlet pressure at the high-pressure side of the ORC turbine ($P_{\mathrm{Ot,\ in,\ h}}$) on the levelized exergy cost and system capital cost of the system are presented in Fig. 9. The large increase of the ORC turbine power output accounts for the decrease of the levelized exergy cost for the ORC turbine power output (c_{Ot}). The increase of the mass flow rate in the high-pressure side of DORC means that more exergy in the vapor is generated by the vapor generator 2, which leads to the decrease of its levelized exergy cost. Thus, the levelized exergy cost for the BC turbine exhaust CO_2, which provides heat for the vapor, decreases with the vapor levelized exergy cost. Moreover, the drop of the CO_2 levelized exergy cost causes the decrease of the fuel-cost-related part of c_{Bt}, which further results in the decrease of c_{Bt}.

The increase of the ORC turbine power output and the increase of mass flow rate in the DORC cause the increase of cost for the turbine and the vapor generator 2, leading to the rise of the system capital cost.

The levelized exergy cost for the system product ($c_{product}$) decreases with the increase of $P_{Ot, in, h}$. The decrease of c_{Ot} and c_{Bt} account for the decrease of the fuel-cost-related part of the levelized exergy for the system product. The impact of c_{Ot} and c_{Bt} is greater than that of the system capital cost which would result in the increase of the capital-cost-related part of $c_{product}$. Thus, the levelized exergy cost of the system product ($c_{product}$) shows a descending trend.

The influences of the inlet temperature at the low-pressure side of ORC turbine ($T_{Ot, in, l}$) on the output and the exergy efficiency of the system are presented in Fig. 10. Parameters changes in the DORC are irrelevant to the thermodynamic performance of the CBC. Thus, the net power of the CBC remains unchanged.

The net power output of the DORC decreases with the increase of $T_{Ot, in, l}$. The increase of the inlet temperature causes the decrease of the mass flow rate in the low-pressure side of the DORC, leading to the decrease of the DORC net power output.

Considering the decrease of the DORC net power output and the unchanged CBC net power output, the net power output of the whole system deceases. Likewise, the exergy efficiency of the system decreases.

The cooling capacity of the ejector refrigeration cycle increases with the increase of $T_{Ot, in, l}$. The decrease of the mass flow rate in the low-pressure side means that more heat is offered to the ERC. Thus, the mass flow rate of the working fluid in the vapor generator 3 increases and more working fluid is entrained to the ejector from the evaporator, which leads to the increase of the refrigeration cycle.

The influence of inlet temperature at the low-pressure side of the ORC turbine ($T_{Ot, in, l}$) on the levelized exergy cost and system capital cost of the system are presented in Fig. 11. The levelized cost for the BC turbine power output increase with the increase of $T_{Ot, in, l}$. The decrease of the mass flow rate in the vapor generator 1 leads to the drop of the vapor exergy output, which results in the increase of the levelized exergy cost for the vapor. The levelized exergy cost for vapor in vapor generator 2, which is the equal to that of the vapor in vapor generator 1, increases as a result, causing the increase of the levelized exergy cost of the exhaust CO_2 after the BC turbine. Thus, the fuel-cost-related part of c_{Bt} increases, resulting in the rise of c_{Bt}.

The levelized exergy cost for the ORC turbine (c_{Ot}) increases with the increase of $T_{Ot, in, l}$. That can be explained by the increase of the levelized exergy cost of the ORC low-pressure inlet vapor and the decrease of the power output of the ORC turbine power output. Both the fuel-cost-related part and the capital-cost-related part of c_{Ot} increases.

The decrease of the mass flow rate and the ORC turbine power output cause the decrease of the vapor generator 1 cost and the turbine cost. Thus, the capital cost of the system decreases.

The levelized exergy cost for the system product increases with the increase of $T_{Ot, in, l}$. The increase of c_{Bt} and c_{Ot} cause the increase of the fuel-cost-related part of the levelized exergy cost for the system product. Though of, the decease of the system capital cost causes the decrease of the capital-cost-related part, its effect is less important. Thus, the increase of the fuel-cost-related part determines the increase of the levelized exergy cost for the system product.

The influences of the inlet temperature of the low-pressure side of the ORC turbine ($P_{Ot, in, l}$) on the output of the exergy efficiency of the system are shown in Fig. 12. The net power of the CBC keeps unchanged with the increase of the increase of the low evaporation pressure. The reason is that the thermodynamic of the CBC is irrelevant to the thermal parameters in DORC.

The net power output of the DORC increases with the rise of $P_{Ot, in, l}$. The increase of enthalpy drop of the organic working fluid in the low-pressure side, which is caused by the rise of $P_{Ot, in, l}$, results in the increase of the power output of the low-pressure side. Though mass flow rate in the low-pressure side would decrease, its impact is less important than that of the enthalpy drop. Thus, the net power output of DORC increases.

The unchanged CBC power output and the increase of the DORC power accounts for the increase of the system net power output and exergy efficiency of the system.

The cooling capacity increases slightly with the increase of $P_{Ot, in, l}$. Because of the decrease of the mass flow rate in DORC, less heat is released in the preheater and more heat is provided in vapor generator 3. Thus, the mass flow rate of the working fluid in the ERC increases, resulting in the slight increase of the cooling capacity.

The influences of inlet pressure at the low-pressure side of the ORC turbine ($P_{Ot, in, l}$) on the levelized exergy cost and system capital cost of the system are shown in Fig. 13. The levelized exergy cost for the ORC turbine power output decreases with the increase of $P_{\mathrm{Ot,\,in,\,l}}$. That can be explained by the decrease of the vapor generator 1 cost, caused by the decrease of the mass flow rate in DORC, and the increase of the DORC power output. Both the capital-cost-related part and the fuel-cost-related part of c_{Ot} decrease.

The levelized exergy cost for the BC turbine power output decreases with of $P_{\mathrm{Ot,\,in,\,l}}$. The decrease of the c_{Ot} causes the drop of levelized exergy cost for the vapor in vapor generator 2, which is heated by the residual heat in the BC turbine exhaust CO_2. Thus, the levelized exergy cost of the exhaust CO_2 decreases, which further leads to the drop of the fuel-cost-related part of c_{Bt}. Therefore, the levelized exergy cost for the BC turbine power output (c_{Bt}) decreases, as shown in Fig. 13.

The increase of the ORC turbine power output causes the increase of the ORC turbine cost. Meanwhile, the increase of the cooling capacity causes the increase of the heat transfer area in the evaporator which requires the rise of the evaporator cost. Thus, the capacity cost of the system increases.

The levelized exergy cost for the system product decreases with the increase of $P_{\mathrm{Ot,\,in,\,l}}$. The decrease of the levelized exergy cost for the BC turbine power output and ORC turbine power cause the decrease of the fuel-cost-related part of the system levelized exergy cost, which determined the decrease of the levelized exergy cost for the system product.

The influence of ejector primary inlet pressure ($P_{\mathrm{ej,\,in}}$) on the output and the exergy efficiency of the system are shown in Fig. 14. Thermal parameter changes in the ERC can't affect the thermodynamic performance of the CBC and DORC. Thus, the net power output of the two cycles remain unchanged. With the increase of the ejector primary inlet pressure, the power consumption of pump 4 increases, leading to the slight decrease of the power output of the whole system.

The increase of the ejector primary inlet pressure causes the increase of the entrainment ratio of the ejector. Thus, more secondary flow is entrained to the ejector from the evaporation, leading to the increase of the cooling capacity.

With the increase of the ejector primary inlet pressure, the power consumption of pump 4 increases gradually. At first, the exergy loss in pump 4 is smaller than the exergy produced by the cooling capacity. Then, with the increase of the pump power consumption, the exergy loss in pump 4 becomes larger than the cooling exergy increase. Thus, the exergy efficiency for the system increases at first and then decreases with the increase of the ejector primary inlet pressure.

The influence of the ejector primary inlet pressure on the levelized exergy cost and the system capital cost of the system are presented in Fig. 15. The increase of the ejector primary inlet pressure can't affect the power output of the BC turbine and the ORC turbine. Thus, the levelized exergy cost for the BC turbine and the ORC power output remain unchanged.

The increase of the pump power consumption results in the increase of the pump 4 cost. The increase of the mass flow rate in the evaporator causes the increase of the evaporator cost. Thus, the system capital cost increases, which leads to the increase of the capital-cost-related part of c_{product}. As a result, the levelized exergy cost for the system increases.

The parametric analysis reveals the potential of optimization for the CCP system. With the increase of the BC turbine inlet temperature, the net power output of the system increases while the cooling capacity decreases. With the increase of the inlet temperature at the high-pressure side of ORC turbine, the net power output of the system decreases while the cooling capacity increases. In this study, seven key parameters (BC turbine inlet temperature, BC turbine inlet pressure, inlet temperature at the high-pressure side of ORC turbine, inlet pressure at the high-pressure side of ORC turbine, inlet temperature at the low-pressure side of ORC turbine, inlet pressure at the low-pressure side of ORC turbine and the ejector primary inlet pressure) are chosen as the variables to optimize the system. The ranges of these parameters are listed in Table 6.

Considering that the levelized exergy cost reflects the thermodynamic and the exergoeconomic aspect of the system, the levelized exergy cost for the system product is selected as the objective function and genetic algorithm is selected to conduct the single-objective optimization.

Genetic algorithm (GA) is an optimization method based on the natural biological evaluation. [45] It simulates the natural genetic rules and searches the optimization result in all the generation. The control parameters of the GA are listed in Table 7.

The optimization results of GA are listed in Table 8. It can be obtained that the minimum levelized exergy cost for the system product c_{product} is 53.25 \$(MWh)$^{-1}$. The net power output, exergy efficiency of the CCP system are 374.37 kW, 37.31 % respectively. The inlet pressure at the high-pressure side of ORC turbine is 1.85 MPa.

Meanwhile, it can be evidenced from Fig. 8 and 9 that the highest output power (about 374.37 kW), exergy efficiency (about 37.31 %) and the lowest levelized exergy cost (about 53.25 \$(MWh)$^{-1}$) at the highest inlet pressure at the high-pressure side ORC turbine (about 1.85 MPa). The results shown in Fig. 8 and 9 are close to the optimization results. The inlet pressure at the high-pressure side ORC turbine is varied while other six parameters are kept as constants in Fig. 8 and 9. Thus, inlet pressure at the high-pressure side ORC turbine plays a more important role than other six parameters when determining the performance of the system. When the inlet pressure at the high-pressure side ORC turbine is close to the highest permitted pressure, the system performance is close to the optimization performance.

Fig. 16 shows the exergy destruction of different components of the system under the optimization conditions. The largest exergy destruction takes place in the ORC turbine (41.26 %), which is mainly caused by the mixing of the high-pressure vapor and the low-pressure vapor. Gas heater contributes 13.44 % of the total exergy destruction. Three vapor generators take up 4.13 %, 11.67 % and 3.73 % of the exergy destruction, respectively. The exergy destruction for the ejector is 5.61 %, which is also caused by the working fluid mixing. For BC turbine, condenser 1, precooler and preheater, the exergy destruction are 3.31 %, 4.64 %, 3.69 % and 3.65 %, respectively. Other components contribute to the rest 4.87 % of the exergy destruction.

5. Conclusion

In this paper, a combined cooling and power system is developed. Seven parameters are selected to analyze the thermodynamic and exergoeconomic performance of the system. Single-objective optimization is carried out with the help of GA. The conclusions of the study are presented as follows:

(1) In the CBC, the increase of $T_{\mathrm{Bt,in}}$ and $P_{\mathrm{Bt,\,in}}$ contribute to the increase of the system exergy efficiency and the decrease of the levelized exergy cost for the system product.

(2) In the DORC, the increase of $T_{\mathrm{Ot,\,in}}$ and $T_{\mathrm{Ot,\,in,\,l}}$ would cause the decrease of the system exergy efficiency and the increase of the levelized exergy cost for the system product. Meanwhile, the increase of $P_{\mathrm{Ot,\,in,\,h}}$ and $P_{\mathrm{Ot,\,in,\,l}}$ would result in the increase of the exergy efficiency and the decrease of the levelized exergy cost.

(3) In the ERC, the increase of $P_{\mathrm{ej,\,in}}$ would cause the increase of the refrigeration capacity and the decrease of the system net power output.

(4) Single -objective optimization results show that the minimum levelized exergy cost for the system product is obtain as 53.25 (MWh)^{-1}$ with net power output of 374.37 kW, cooling capacity of 188.63 kW and system exergy efficiency of 37.31 %.

Acknowledgement

The authors gratefully acknowledge the financial support by the National Natural Science Foundation of China (Grant No. 51476121)

Appendix A

This section shows the calculation of the heat transfer area in the heat exchangers used in this study.

All the heat exchangers used in this study are shell-and-tube heat exchanger. The thermodynamic properties of the working fluid vary with the heat transfer process. Thus, to calculate the heat transfer area actually, the heat transfer processes are discretized into a lot of small sections. In each section, the heat transfer area is small and the thermodynamic properties are assumed to be constant.

For each section the heat transfer area is calculated as:

$$A_i = Q_i / \left(\Delta T_i \cdot U_i\right) \tag{B1}$$

where ΔT_i is the log-mean temperature difference (LMTD) and U_i is the overall heat transfer coefficient.

$$\frac{1}{U_i} = \frac{1}{\alpha_{t,i}} + \frac{\delta}{\lambda} + \frac{1}{\alpha_{s,i}} \tag{B2}$$

In Eq. (B2) δ and λ represent the thickness of the tube and the thermal conductivity of the tube wall, respectively. $\alpha_{t,i}$ is the convection heat transfer coefficient in the tube side and $\alpha_{s,i}$ is the convection heat transfer coefficient in the shell side.

For different heat transfer process, the convection heat transfer coefficient has different format. We classify the heat transfer processes into single-phase heat transfer process and two-phase heat transfer process. In gas heater, precooler and the preheater, single-phase heat transfer process happens. In evaporator, two-phase heat transfer process occurs. In vapor generators and the condensers, both the single-phase and the two-phase heat transfer process happen.

In the single-phase heat transfer process, the convection heat transfer coefficient in the tube side and the shell side are expressed as [46]:

$$\alpha_{\mathrm{t,i}} = \frac{\lambda \cdot Nu}{D_{\mathrm{i}}} \tag{B3}$$

$$\alpha_{\mathrm{s,i}} = 0.36\left(\frac{\lambda}{D_{\mathrm{es}}}\right)\cdot\left(\frac{D_{\mathrm{es}}\cdot G_{\mathrm{s}}}{\mu}\right)^{0.55}\cdot \mathrm{Pr}^{\frac{1}{3}}\cdot\left(\frac{\mu}{\mu_{\mathrm{w}}}\right)^{0.14} \tag{B4}$$

In Eq. (B3), the Nusselt number is calculated as [47,48]:

$$Nu = \left[\frac{(f/8)\cdot \mathrm{Re}\cdot \mathrm{Pr}}{12.7(f/8)^{0.5}\cdot\left(\mathrm{Pr}^{2/3}-1\right)+1.07}\right],\ for\ \mathrm{Re}<10^4 \tag{B5}$$

$$Nu = \left[\frac{(f/8)\cdot (\mathrm{Re}-1000)\cdot \mathrm{Pr}}{12.7(f/8)^{0.5}\cdot\left(\mathrm{Pr}^{2/3}-1\right)+1.07}\right],\ for\ 10^4<\mathrm{Re}<5\times 10^6 \tag{B6}$$

where f is the Darcy friction factor, Re is the Reynolds and Pr is the Prandtl number.

In Eq. (B4), D_{es} is the equivalent diameter of the shell, being expressed as:

$$D_{\mathrm{es}} = \frac{1.10\mathrm{Pt}^2}{D_{\mathrm{out,i}}} - D_{\mathrm{out,i}} \tag{B7}$$

where Pt is the center distance between the tubes.

Evaporation and condensation are two different two-phase heat transfer processes. In this study, the cold organic working fluid flows in the tubes of the heat exchangers. The convection heat transfer coefficient of evaporation and condensation are expressed as [49,50]:

$$\alpha_{\mathrm{ev,i}} = 0.023\left[\frac{G(1-x)}{\mu_{\mathrm{l}}}\right]^{0.8}\cdot \mathrm{Pr}_{\mathrm{l}}^{0.4}\cdot\frac{\lambda_{\mathrm{l}}}{d}\cdot\left[1+3000Bo^{0.86}+1.12\left(\frac{x}{1-x}\right)^{0.75}\cdot\left(\frac{\rho_{\mathrm{l}}}{\rho_{\mathrm{v}}}\right)^{0.41}\right] \tag{B8}$$

$$\alpha_{\mathrm{cond,i}} = 0.023\left[\frac{G(1-x)}{\mu_{\mathrm{l}}}\right]^{0.8}\cdot \mathrm{Pr}_{\mathrm{l}}^{0.4}\cdot\frac{\lambda_{\mathrm{l}}}{d}\cdot\left[(1-x)^{0.8}+\frac{3.8x^{0.76}(1-x)0.04}{P_r^{0.38}}\right] \tag{B9}$$

In Eq. (B9), P_r is the reduced pressure. In Eq. (B8) Bo is the boiling number, being expressed as:

$$Bo = \frac{q_{\mathrm{m}}}{G \cdot r_{\mathrm{f}}} \tag{B10}$$

Appendix B

The constants for component capital cost calculation are list in Table B1.

Reference

[1] Abdul-Wahhab H, Al-Kayiem H, Aziz A, Nasif M. Survey of invest fuel magnetization in developing internal combustion engine characteristics. Renew Sustain Energy Rev 2017; 79:1392-99.

[2] Heywood J. B. Internal combustion engine fundamentals. New York: McGraw-Hill; 1988.

[3] Chao H, Chao L, Hong G, Hui X, You L, Shuang W. The optimal evaporation temperature and working fluids for subcritical Organic Rankine Cycle. Energy 2012; 38: 136-143.

[4] Tian H, Shu G, Wei H, Liang X, Liu L. Fluids and parameters optimization for the organic Rankine cycles (ORCs) used in exhaust heat recovery of Internal Combustion Engine (ICE). Energy 2012; 47: 125-136.

[5] Rijpkema J, Munch K, Andersson S. Thermodynamic potential of twelve working fluids in Rankine and flash cycles for waste heat recovery in heavy duty diesel engines. Energy 2018; 160:996-1007.

[6] Su X, Shedd T A. Towards working fluid properties and selection of Rankine cycle based waste heat recovery (WHR) systems for internal combustion engines – A

fundamental analysis. Appl Therm Eng 2018; 142:502-10.

[7] Vaja I, Gambarotta A. Internal Combustion Engine (ICE) bottoming with Organic Rankine Cycles (ORCs). Energy 2010; 35(2):1084-93.

[8] Kim M, Shin G, Kim G, Cho B. Single-loop organic Rankine cycle for engine waste heat recovery using both low-and high-temperature heat sources. Energy 2016; 96:482-94.

[9] Ringer J, Seifert M, Guyotot V, Hübner W. Rankine cycle for waste heat recovery of IC engines. SAE. 2009. 2009-01-0174.

[10] Wang X, Shu G, Tian H, Liu P, Jing D, Li X. Dynamic analysis of the dual-loop Organic Rankine Cycle for waste heat recovery of a natural gas engine. Energy Convers Manage 2017; 148:724-736.

[11] Wang E, Yu Z, Zhang H, Yang F. A regenerative supercritical dual-loop organic Rankine cycle system for energy recovery from the waste heat of internal combustion engines. Appl Energy 2017; 190:574-90.

[12] Huang H, Zhu J, Deng W, Ouyang T, Yan B, Yang X. Influence of exhaust heat distribution on the performance of dual-loop organic Rankine Cycle (DORC) for waste heat recovery. Energy 2018; 151:54-65.

[13] Rajabloo T, Bonalumi D, Lora P. Effect of a partial thermal decomposition of the working fluid on the performances of ORC power plants. Energy 2017; 133:1013-26.

[14] Shi L, Shu G, Tian H, Deng S. A review of modified Organic Rankine cycles (ORCs) for internal combustion engine waste heat recovery (ICE-WHR). Renew Sustain Energy Rev 2018; 92:95-110.

[15] EI-Harbawi M, Shaaran S, Ahmad F, Wahi M, Abdul A, Larid D, Yin C. Estimating the flammability of vapours above refinery wasterwater laden with hydrocarbon mixtures. Fire Safety J 2012; 51:61-67.

[16] Wang X, Tian H, Shu G. Part-load performance prediction and operation strategy design of organic Rankine cycles with a medium cycle used for recovering waste heat from gaseous fuel engines. Energies 2016; 9: 527.

[17] Miller E, Hendricks T, Wang H, Peterson R. Integrated dual-cycle energy recovery using thermoelectric conversion and an organic Rankine bottoming cycle. Proceedings of the Institution of Mechanical Engineers, Part A: J Power Energy 2011; 225:33-43.

[18] Shu G, Wang X, Tian H. Theoretical analysis and comparison of Rankine cycle and different organic Rankine cycles as waste heat recovery system for a large gaseous fuel internal combustion engine. Appl Therm Eng 2016; 108:525-37.

[19] Yu G, Shu G, Tian H, Huo Y, Zhu W. Experimental investigations on a cascaded steam-/organic-Rankine-cycle (RC/ORC) system for waste heat recovery (WHR) from diesel engine. Energy Convers Manage 2016; 129:43-51.

[20] Zhang C, Shu G, Tian H, Wei H, Liang X. Comparative study of alternative ORC-based combined power systems to exploit high temperature waste heat. Energy Convers Manage 2015; 89:541-54.

[21] Galindo J, Guardiola C, Dolz V, Kleut P. Further analysis of a compression-expansion machine for a Brayton Waste Heat Recovery cycle on an IC engine. Applied Thermal Engineering 2018; 128: 345-356.

[22] Ma J, Liu L, Zhu T, Zhang T. Cascade utilization of exhaust gas and jacket water waste heat from an Internal Combustion Engine by a single loop Organic Rankine Cycle system. Appl Therm Eng 2016; 107:218-26.

[23] Zhang H G, Wang E H, Fan B Y. A performance analysis of a novel system of a dual loop bottoming organic Rankine cycle (ORC) with a light-duty diesel engine. Applied Energy 2013;102: 1504-1513.

[24] Yang F, Cho H, Zhang H, Zhang J. Thermoeconomic multi-objective optimization of a dual loop organic Rankine cycle (ORC) for CNG engine waste heat recovery. Applied Energy 2017; 205: 1100-1118.

[25] Song J, Gu C. Parametric analysis of a dual loop Organic Rankine cycle (ORC) system for engine waste heat recovery. 2015; 105:995-1005.

[26] Yu G, Shu G, Tian H, Wei H, Liu L. Simulation and thermodynamic analysis of a bottoming Organic Rankine Cycle (ORC) of diesel engine (DE). Energy 2013; 51:281-90.

[27] Li Fan, Sun Bo, Zhang C, Zhang L. Operation optimization for combined cooling, heating, and power system with condensation heat recovery. Appl Energy 2018; 230:305-16.

[28] Yari Mortaza, Ariyanfar Leyli, Aghdam EA. Analysis and performance assessment of a novel ORC based multigeneration system for power, distilled water and heat. Renew Energy 2018; 119:262-81.

[29] Bai Z, Liu T, Liu Q, Lei J, Gong L, Jin H. Performance investigation of a new cooling, heating and power system with methanol decomposition based chemical

recuperation process. Appl Energy 2018; 229: 1152-63.

[30] Chen Y, Han W, Jin H. Investigation of an ammonia-water combined power and cooling system driven by the jacket water and exhaust gas heat of an internal combustion engine. International Journal of Refrigeration 2017; 82: 174-188.

[31] Salek F, Moghaddam A, Naserian M. Thermodynamic analysis of diesel engine coupled with ORC and absorption refrigeration cycle. Energy Conversion and Management 2017; 140: 240-246.

[32] Wang J, Dai Y, Sun Z. A theoretical study on a novel combined power and ejector refrigeration cycle. Int J Refrig 2009; 32(6):1186-94.

[33] Dai Y, Wang J, Gao L. Parametric optimization and comparative study of organic Rankine cycle (ORC) for low grade waste heat recovery. Energy Convers Manage 2009; 50:576-82.

[34] Shu G, Zhao M, Tian H, Huo Y, Zhu W. Experimental comparison of R123 and R245fa as working fluids for waste heat recovery from heavy-duty diesel engine. Energy 2016; 115:756-69.

[35] Zhang J, Zhang H, Yang K, Yang F, Wang Z, Zhao G, Liu H, Wang E, Yao B. Performance analysis of regenerative organic Rankine cycle (RORC) using the pure working fluid and the zeotropic mixture over the whole operating range of a diesel engine. Energy Convers Manage 2014; 84:282-94.

[36] Bejan A, Tsatsaronis G, Moran M. Thermal design and optimization. New York: John Wiley & Sons; 1996.

[37] Turton R, Bailie RC, Whiting WB, Shaeiwitz JA. Analysis, synthesis, and design

of chemical processes. 3rd ed. Upper Saddle River, N.J: Prentice Hall; 2009.

[38] Li J, Ge Z, Liu Q, Duan Y, Yang Z. Thermo-economic performance analyses and comparison of two turbine layouts for organic Rankine cycles with dual-pressure evaporation. Energy Conversion and Management, 2018; 164: 603-614.

[39] Sheng Z, Huai W, Tao G. Performance comparison and parametric optimization of subcritical organic Rankine cycle (ORC) and transcritical power cycle system for low-temperature geothermal power generation. Appl Energy 2011;88(8):2740-54.

[40] Tempesti D, Fiaschi D. Thermo-economic assessment of a micro CHP system fueled by geothermal and solar energy. Energy 2013; 58: 45-51.

[41] Velez F, Segovia JJ, Martin MC, Antonlin G, Chejne F, Quijano A. A technical, economical and market review of organic Rankine cycles for the conversion of low-grade heat for power generation. Renew Sustain Energy Rev 2012; 16:4175-89.

[42] Akbari D, Mahmoudi M. Thermoeconomic analysis & optimization of the combined supercritical CO2 (carbon dioxide) recompression Brayton/ organic Rankine cycle. Energy 2014; 78:501-12.

[43] Zare V, Mahmoudi M, Yari M. An exergoeconomic investigation of waste heat recovery from the Gas Turbine-Modular Helium Reactor (GT-MHR) employing an ammonia–water power/cooling cycle. Energy 2013;61. 397-409.

[44] Lemmon EW, Huber ML, McLinden MO. NIST standard reference database 23, reference fluid thermodynamic and transport properties (REFPROP). Version 9.1. National Institute of Standards and Technology; 2010

[45] Wang J, Dai Y, Gao L. Parametric analysis and optimization for a combined

power and refrigeration cycle. Appl Energy 2008;85(11):1071-85.

[46] Kern DQ. Process heat transfer. New York: McGraw-Hill; 1950

[47] Kandylas IP, Stamatelos AM. Engine exhaust system design based on heat transfer computation. Energy Convers Manage 1999; 40:1057-72.

[48] Incropera FP, DeWitt DP. Fundamentals of heat and mass transfer. New York: Wiley; 2002

[49] Gungor KE, Winterton RHS. Simplified general correlation for saturated flow boiling and comparisons of correlations with data. Chem Eng Res and Des, 1987; 65:148-56.

[50] Shah MM. A general correlation for heat transfer during film condensation inside pipes. Int J Heat Mass Transf 1979; 22:547-56.

Figure captions

Fig. 1. Schematic diagram of the CCP system

Fig. 2. Influences of BC turbine inlet temperature on the output and the exergy efficiency of the system.

Fig. 3. Influences of BC turbine inlet temperature on the levelized exergy cost and the system capital cost of the system.

Fig. 4. Influences of BC turbine inlet pressure on the output and the exergy efficiency of the system.

Fig. 5. Influences of BC turbine inlet pressure on the levelized exergy cost and the system capital cost of the system.

Fig. 6. Influences of inlet temperature at the high-pressure side of ORC turbine on the output and the exergy efficiency of the system.

Fig. 7. Influences of inlet temperature at the high-pressure side of ORC turbine on the levelized exergy cost and the system capital cost of the system.

Fig. 8. Influences of inlet pressure at the high-pressure side of ORC turbine on the output and the exergy efficiency of the system.

Fig. 9. Influences of inlet pressure at the high-pressure side of ORC turbine on the levelized exergy cost and the system capital cost of the system.

Fig. 10. Influences of inlet temperature at the low-pressure side of ORC turbine on the output and the exergy efficiency of the system.

Fig. 11. Influences of inlet temperature at the low-pressure side of ORC turbine on the levelized exergy cost and system capital cost of the system.

Fig. 12. Influences of inlet pressure at the low-pressure side of ORC turbine on the output and the exergy efficiency of the system.

Fig. 13. Influences of inlet pressure at the low-pressure side of ORC turbine on the levelized exergy cost and system capital cost of the system.

Fig. 14. Influences of ejector primary inlet pressure on the output and the exergy efficiency of the system.

Fig. 15. Influences of ejector primary inlet pressure on the levelized exergy cost and the system capital cost of the system.

Fig. 16. Exergy destruction of different components

Table 1 Energy and exergy models for each component in CCP system

Component	Energy equation	E_F	E_P	E_D	E_L
Gas heater	$M_{g1}\cdot(h_{g1}-h_{g2})=M_2\cdot(h_3-h_2)$	$E_{g1}-E_{g2}$	E_3-E_2	$E_{g1}+E_2-E_3-E_{g2}$	/
BC turbine	$W_{Bt}=M_3\cdot(h_3-h_4)=M_3\cdot(h_3-h_{4s})\cdot\eta_{Bt}$	E_3-E_4	W_{Bt}	$E_3-E_4-W_{Bt}$	/
Vapor generator 2	$M_4\cdot(h_4-h_5)=M_9\cdot(h_{10}-h_9)$	E_4-E_5	$E_{10}-E_9$	$E_4+E_9-E_5-E_{10}$	/
Precooler	$M_1\cdot(h_5-h_1)=M_{26}\cdot(h_{27}-h_{26})$	/	/	$E_5+E_{26}-E_1-E_{27}$	$E_{27}-E_{26}$
Compressor	$W_{comp}=M_1\cdot(h_2-h_1)=M_1\cdot(h_{2s}-h_1)/\eta_{comp}$	W_{comp}	E_2-E_1	$E_1-E_2+W_{comp}$	/
Vapor generator 1	$M_{g2}\cdot(h_{g2}-h_{g3})=M_8\cdot(h_{11}-h_8)$	$E_{g2}-E_{g1}$	$E_{11}-E_8$	$E_{g2}+E_8-E_{11}-E_{g3}$	/
ORC turbine	$W_{Ot}=M_{10}\cdot(h_{10}-h_{12})+M_{11}\cdot(h_{11}-h_{12})$	$E_{10}+E_{11}-E_{12}$	W_{Ot}	$E_{10}+E_{11}-E_{12}-W_{Ot}$	/
Condenser 1	$M_{12}\cdot(h_{12}-h_{13})=M_{28}\cdot(h_{29}-h_{28})$	/	/	$E_{12}+E_{28}-E_{13}-E_{29}$	$E_{29}-E_{28}$
Pump 1	$W_{p1}=M_{13}\cdot(h_{14}-h_{13})=M_{13}\cdot(h_{14s}-h_{13})/\eta_{p1}$	W_{p1}	$E_{14}-E_{13}$	$E_{13}-E_{14}+W_{p1}$	/
Preheater	$M_{15}\cdot(h_{15}-h_{14})=M_{w1}\cdot(h_{w1}-h_{w2})$	$E_{w1}-E_{w2}$	$E_{15}-E_{14}$	$E_{w1}+E_{14}-E_{15}-E_{w2}$	/
Pump 2	$W_{p2}=M_7\cdot(h_9-h_7)=M_7\cdot(h_{9s}-h_7)/\eta_{p2}$	W_{p2}	E_9-E_7	$E_7-E_9+W_{p2}$	/
Pump 3	$W_{p3}=M_6\cdot(h_8-h_6)=M_6\cdot(h_{8s}-h_6)/\eta_{p3}$	W_{p3}	E_8-E_6	$E_6-E_8+W_{p3}$	/
Vapor generator 3	$M_{23}\cdot(h_{23}-h_{22})=M_{w2}\cdot(h_{w2}-h_{w3})$	$E_{w2}-E_{w3}$	$E_{23}-E_{22}$	$E_{w2}+E_{22}-E_{23}-E_{w3}$	/
Condenser 2	$M_{16}\cdot(h_{16}-h_{17})=M_{30}\cdot(h_{31}-h_{30})$	/	/	$E_{16}+E_{30}-E_{17}-E_{31}$	$E_{31}-E_{30}$
Valve	$h_{19}=h_{20}$	/	/	$E_{19}-E_{20}$	/
Pump 4	$W_{p4}=M_{22}\cdot(h_{22}-h_{18})=M_{22}\cdot(h_{22s}-h_{18})/\eta_{p4}$	W_{p4}	$E_{22}-E_{18}$	$E_{18}-E_{22}+W_{p4}$	/
Ejector	$M_{16}\cdot h_{16}=M_{23}\cdot h_{23}+M_{21}\cdot h_{21}$	$E_{23}+E_{21}$	E_{16}	$E_{23}+E_{21}-E_{16}$	/
Evaporator	$M_{20}\cdot(h_{21}-h_{20})=M_{24}\cdot(h_{24}-h_{25})$	$E_{20}-E_{21}$	$E_{25}-E_{24}$	$E_{20}+E_{24}-E_{21}-E_{25}$	/

Table 2 Cost balance and auxiliary relation [30] for each component of CCP system

Component	Cost balance	Auxiliary relation

Gas heater	$c_{g2} \cdot E_{y,g2} + c_3 \cdot E_{y,3} = c_{g1} \cdot E_{y,g1} + c_2 \cdot E_{y,2} + Z_{gh}$	$c_{g1}=c_{g2}=0$
Vapor generator 2	$c_5 \cdot E_{y,5} + c_{10} \cdot E_{y,10} = c_4 \cdot E_{y,4} + c_9 \cdot E_{y,9} + Z_{vg,2}$	$c_4=c_5$
BC turbine	$c_4 \cdot E_{y,4} + c_{Bt} \cdot W_{y,Bt} = c_3 \cdot E_{y,3} + Z_{Bt}$	$c_4=c_3$
Precooler	$c_1 \cdot E_{y,1} + c_{26} \cdot E_{y,26} = c_5 \cdot E_{y,5} + c_{27} \cdot E_{y,27} + Z_{prec}$	$c_1=c_5$
Compressor	$c_2 \cdot E_{y,2} = c_1 \cdot E_{y,1} + c_{elec,1} \cdot W_{y,comp} + Z_{comp}$	$c_{elec,1}=c_{Bt}$
Vapor generator 1	$c_{g3} \cdot E_{y,g3} + c_{11} \cdot E_{y,11} = c_{g2} \cdot E_{y,g2} + c_8 \cdot E_{y,8} + Z_{vg,1}$	$c_{g2}=c_{g3}$
ORC turbine	$c_{12} \cdot E_{y,12} + c_{Ot} \cdot W_{y,Ot} = c_{11} \cdot E_{y,11} + c_{10} \cdot E_{y,10} + Z_{Ot}$	$c_{10}=c_{11}=c_{12}$
Pump 1	$c_{14} \cdot E_{y,14} = c_{13} \cdot E_{y,13} + c_{elec,3} \cdot W_{y,pump1} + Z_{pump1}$	$c_{elec,3}=c_{Ot}$
Condenser 1	$c_{13} \cdot E_{y,13} + c_{29} \cdot E_{y,29} = c_{28} \cdot E_{y,28} + c_{12} \cdot E_{y,12} + Z_{cond1}$	$c_{13}=c_{12}$
Preheater	$c_{w2} \cdot E_{y,w2} + c_{15} \cdot E_{y,15} = c_{w1} \cdot E_{y,w1} + c_{14} \cdot E_{y,14} + Z_{preh}$	$c_{w1}=c_{w2}=0$
Pump 2	$c_9 \cdot E_{y,9} = c_7 \cdot E_{y,7} + c_{elec,2} \cdot W_{y,pump2} + Z_{pump2}$	$c_{elec,2}=c_{Ot}$
Pump 3	$c_8 \cdot E_{y,8} = c_6 \cdot E_{y,6} + c_{elec,3} \cdot W_{y,pump3} + Z_{pump3}$	$c_{elec,3}=c_{Ot}$
Vapor generator 3	$c_{w3} \cdot E_{y,w3} + c_{23} \cdot E_{y,23} = c_{w2} \cdot E_{y,w2} + c_{22} \cdot E_{y,22} + Z_{vg,3}$	$c_{w3}=c_{w2}$
Valve	/	$c_{19}=c_{20}$
Pump 4	$c_{22} \cdot E_{y,22} = c_{18} \cdot E_{y,18} + c_{elec,3} \cdot W_{y,pump4} + Z_{pump4}$	$c_{elec,4}=c_{Ot}$
Condenser 2	$c_{17} \cdot E_{y,17} + c_{31} \cdot E_{y,31} = c_{30} \cdot E_{y,30} + c_{16} \cdot E_{y,16} + Z_{cond2}$	$c_{16}=c_{17}$
Ejector	$c_{16} \cdot E_{y,16} = c_{23} \cdot E_{y,23} + c_{21} \cdot E_{y,21}$	/
Evaporator	$c_{21} \cdot E_{y,21} + c_{25} \cdot E_{y,25} = c_{20} \cdot E_{y,20} + c_{24} \cdot E_{y,24} + Z_{ev}$	$c_{20}=c_{21}$

Table 3 Main parameters of the engine [7]

Parameters	Value
Power output (kW)	2928
Rotation (r(min)$^{-1}$)	1000

Exhaust gas temperature (℃)	470
Exhaust gas mass flow rate (kg s^{-1})	4.35
Temperature of jacket water (℃)	90/79
Mass flow rate of jacket water (kg s^{-1})	25

Table 4 Composition of the exhaust gas [7]

Composition	Molecular $(g(mol)^{-1})$	Fraction (%)
O_2	32.00	9.3
CO_2	44.00	9.1
H_2O	18.01	7.4
N_2	28.01	74.2

Table 5 Condition of simulation for the CCP system

Parameter	Value
Ambient temperature (℃)	20
Ambient pressure (MPa)	0.101
Compressor inlet temperature (℃)	35
BC turbine inlet temperature (℃)	400
BC turbine inlet pressure (MPa)	18
BC turbine outlet pressure (MPa)	8
Inlet temperature at the high-pressure side of ORC turbine (℃)	150
Inlet pressure at the high-pressure side of ORC turbine (MPa)	1.6
Inlet temperature at the low-pressure side of ORC turbine (℃)	100
Inlet pressure at the low-pressure side of ORC turbine (MPa)	1.0

Outlet pressure of pump 1 (MPa)	0.9
Ejector primary inlet pressure (MPa)	0.4
Terminal temperature difference at gas heater outlet (℃)	100
Pinch point temperature difference in vapor generator 1 (℃)	30
Pinch point temperature difference in vapor generator 2 (℃)	30
Pinch point temperature difference in vapor generator 3 (℃)	25
Condensation temperature of condenser 1 (℃)	30
Condensation temperature of condenser 2 (℃)	30
Evaporation temperature of evaporator (℃)	5
Isentropic efficiency of BC turbine (%)	80
Isentropic efficiency of ORC turbine (%)	80
Isentropic efficiency of compressor (%)	80
Isentropic efficiency of pump 1 (%)	75
Isentropic efficiency of pump 2 (%)	75
Isentropic efficiency of pump 3 (%)	75
Inlet temperature of cooling water (℃)	20

Table 6 Parameters for GA

Parameter	Operation range
BC turbine inlet temperature (℃)	330-440
BC turbine inlet pressure (MPa)	15-20
Inlet temperature at the high-pressure side of ORC turbine (℃)	130-180
Inlet pressure at the high-pressure side of ORC turbine (MPa)	1.4-2

Inlet temperature at the low-pressure side of ORC turbine (℃)	90-150
Inlet pressure at the low-pressure side of ORC turbine (MPa)	0.9-1.3
Ejector primary inlet pressure (MPa)	0.3-1

Table 7 Control parameters of GA

Tuning parameters	Value
Population size	20
Mutation probability	0.01
Crossover probability	0.8
Stop generation	200

Table 8 Single-objective optimization results

Parameter	Value
BC turbine inlet temperature (℃)	425.46
BC turbine inlet pressure (MPa)	20.00
Inlet temperature at the high-pressure side of ORC turbine (℃)	144.32
Inlet pressure at the high-pressure side of ORC turbine (MPa)	1.85
Inlet temperature at the low-pressure side of ORC turbine (℃)	100.03
Inlet pressure at the low-pressure side of ORC turbine (MPa)	1.26
Ejector primary inlet pressure (MPa)	0.54
Net power output (kW)	374.37
Cooling capacity (kW)	188.63
Exergy efficiency (%)	37.31
Levelized exergy cost ($ (MWh)$^{-1}$)	53.25

Table B1 Constants for component costs [37]

Constant	Value	Constant	Value	Constant	Value
$B_{1,\mathrm{he}}$	1.63	$K_{3,\mathrm{pump}}$	0.1538	$C_{3,\mathrm{he}}$	0.08183
$B_{2,\mathrm{he}}$	1.66	$K_{1,\mathrm{turb}}$	2.7051	$C_{1,\mathrm{pump}}$	-0.3635
$B_{1,\mathrm{pump}}$	1.89	$K_{2,\mathrm{turb}}$	1.4398	$C_{2,\mathrm{pump}}$	0.3957
$B_{2,\mathrm{pump}}$	1.35	$K_{3,\mathrm{turb}}$	-0.1776	$C_{3,\mathrm{pump}}$	-0.0026
$K_{1,\mathrm{he}}$	4.3247	$K_{1,\mathrm{comp}}$	2.2897	$F_{\mathrm{M,he}}$	1.0
$K_{2,\mathrm{he}}$	-0.3030	$K_{2,\mathrm{comp}}$	1.3604	$F_{\mathrm{BM,turb}}$	3.5
$K_{3,\mathrm{he}}$	0.1634	$K_{3,\mathrm{comp}}$	-0.1027	$F_{\mathrm{BM,comp}}$	2.7
$K_{1,\mathrm{pump}}$	3.3892	$C_{1,\mathrm{he}}$	0.03881	$F_{\mathrm{M,pump}}$	2.2
$K_{2,\mathrm{pump}}$	0.0536	$C_{2,\mathrm{he}}$	-0.11272		

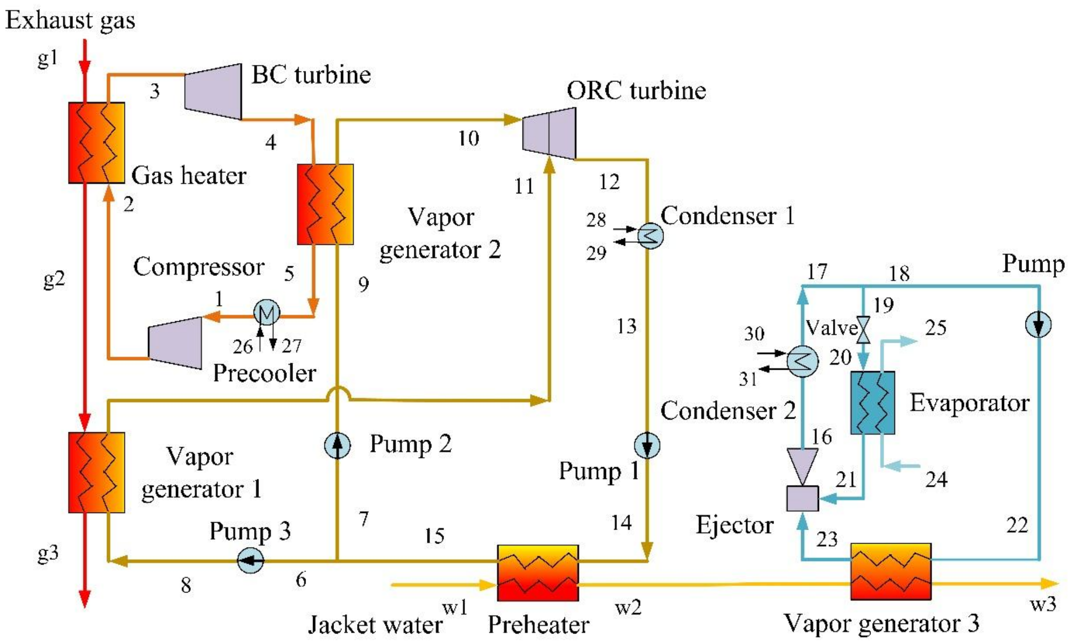

Fig. 1. Schematic diagram of the CCP system

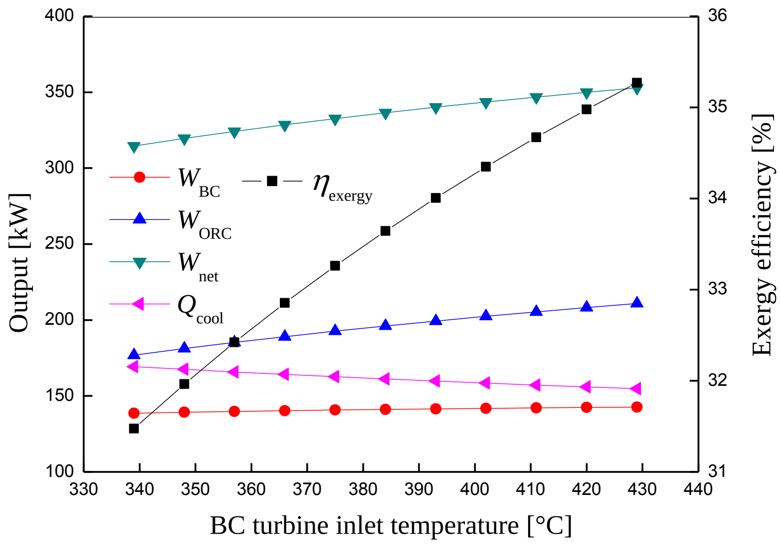

Fig. 2. Influences of BC turbine inlet temperature on the output and the exergy efficiency of the system.

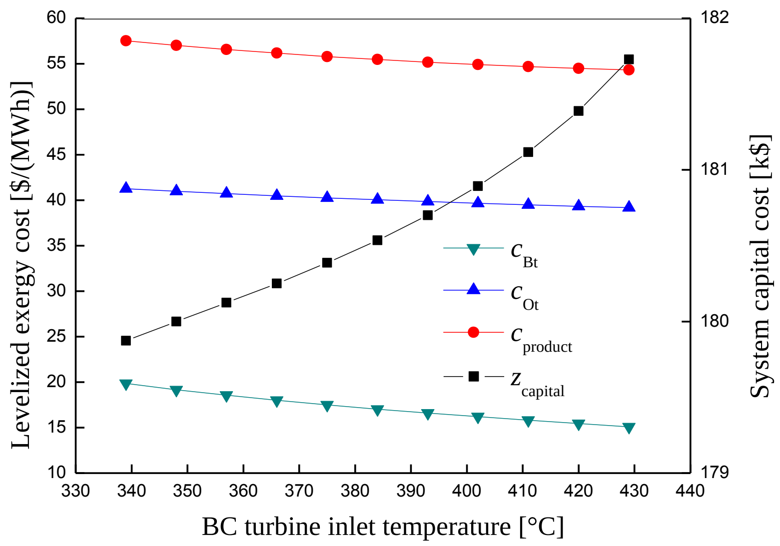

Fig. 3. Influences of BC turbine inlet temperature on the levelized exergy cost and the system capital cost of the system.

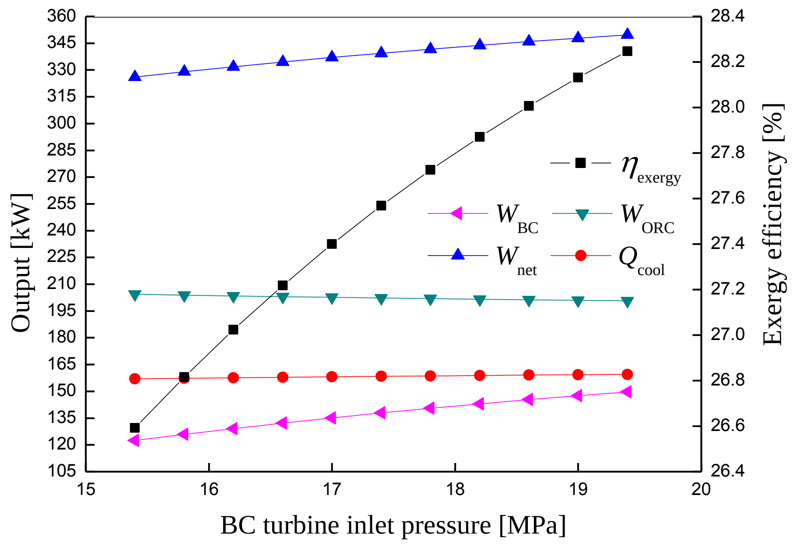

Fig. 4. Influences of BC turbine inlet pressure on the output and the exergy efficiency of the system.

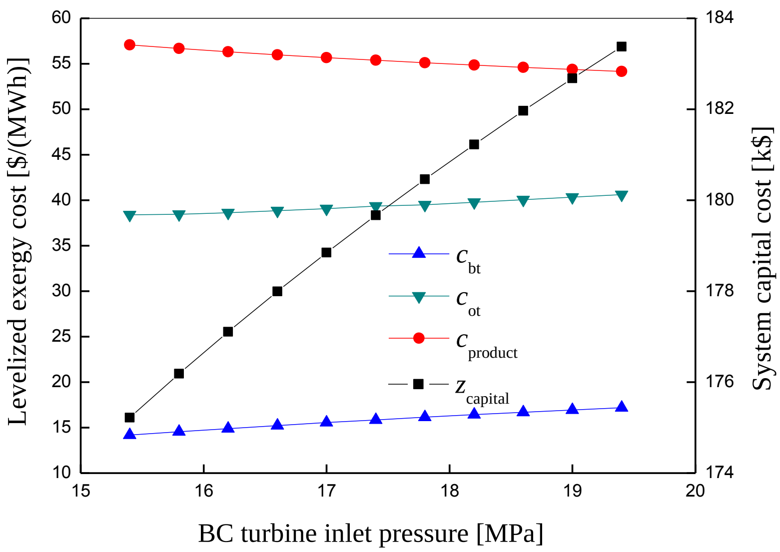

Fig. 5. Influences of BC turbine inlet pressure on the levelized exergy cost and the system capital cost of the system.

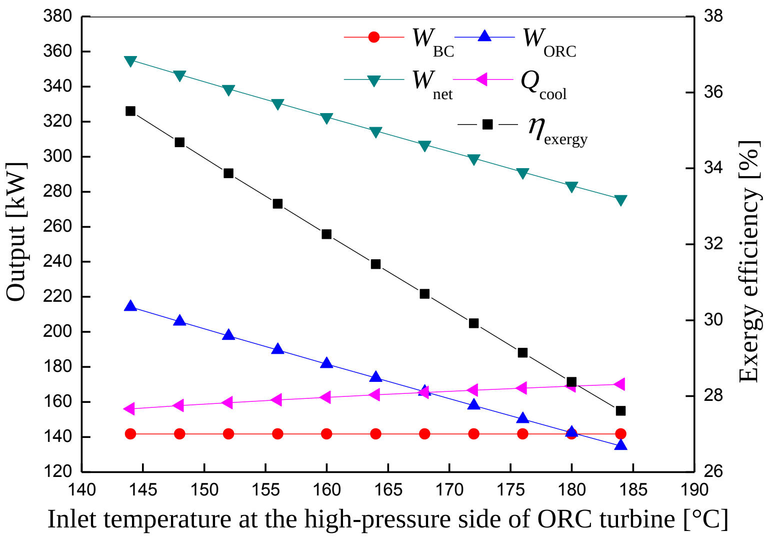

Fig. 6. Influences of inlet temperature at the high-pressure side of ORC turbine on the output and the exergy efficiency of the system.

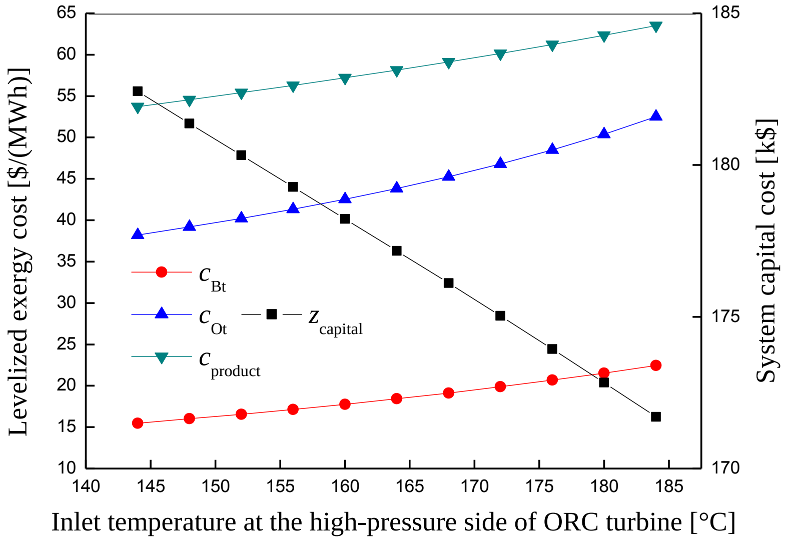

Fig. 7. Influences of inlet temperature at the high-pressure side of ORC turbine on the levelized exergy cost and the system capital cost of the system.

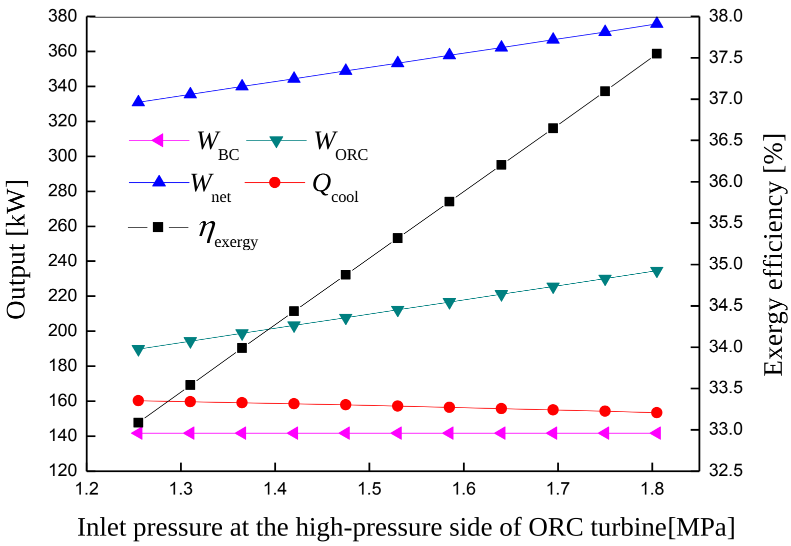

Fig. 8. Influences of inlet pressure at the high-pressure side of ORC turbine on the output and the exergy efficiency of the system.

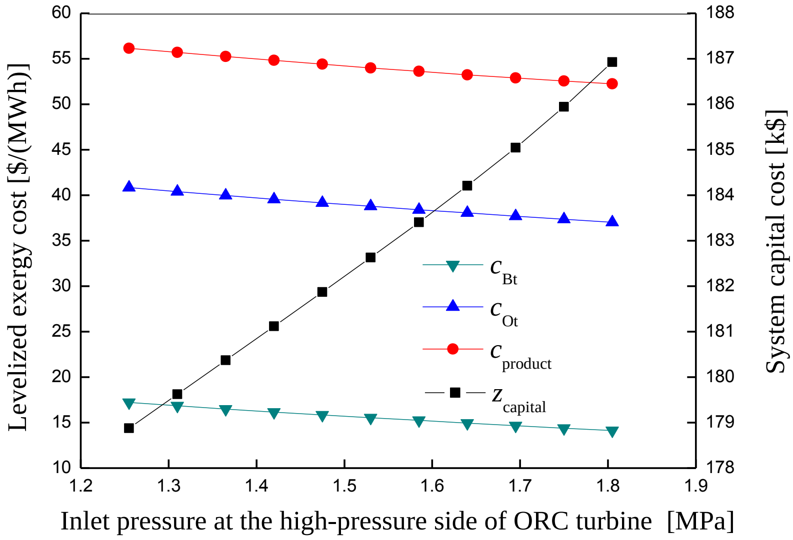

Fig. 9. Influences of inlet pressure at the high-pressure side of ORC turbine on the levelized exergy cost and the system capital cost of the system.

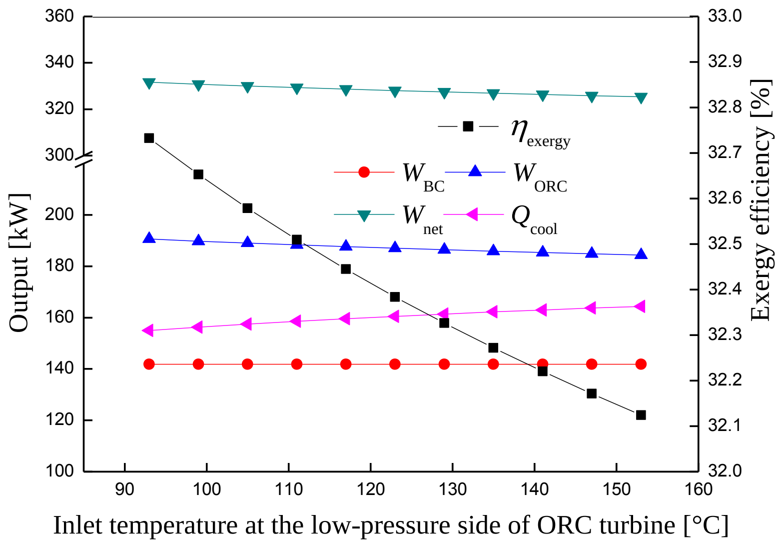

Fig. 10. Influences of inlet temperature at the low-pressure side of ORC turbine on the output and the exergy efficiency of the system.

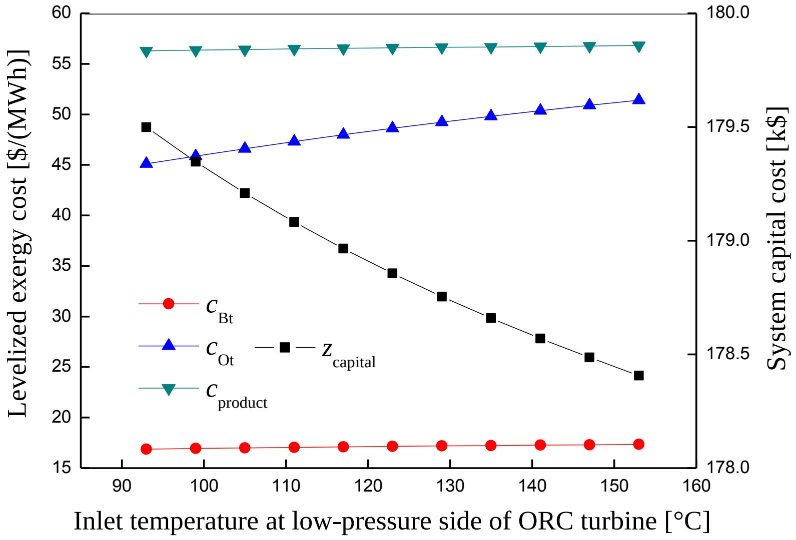

Fig. 11. Influences of inlet temperature at the low-pressure side of ORC turbine on the levelized exergy cost and system capital cost of the system.

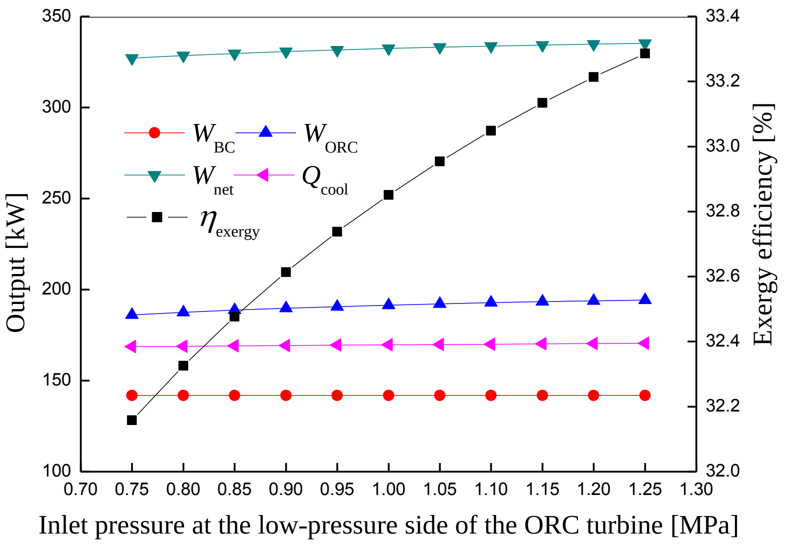

Fig. 12. Influences of inlet pressure at the low-pressure side of ORC turbine on the output and the exergy efficiency of the system.

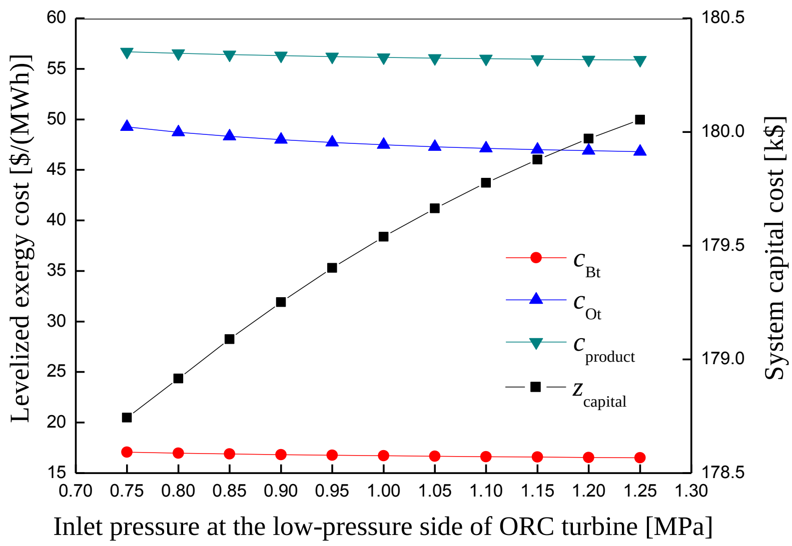

Fig. 13. Influences of the inlet pressure at the low-pressure side of ORC turbine on the levelized exergy cost and system capital cost of the system.

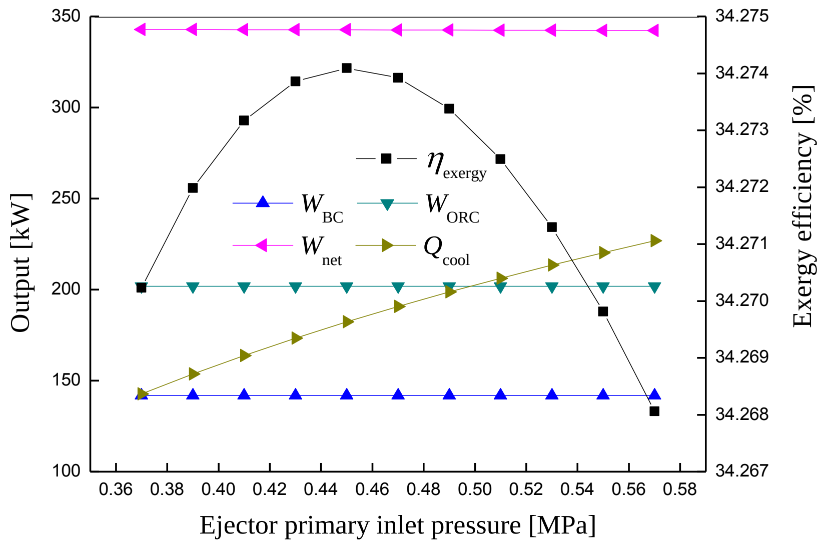

Fig. 14. Influences of ejector primary inlet pressure on the output and the exergy efficiency of the system.

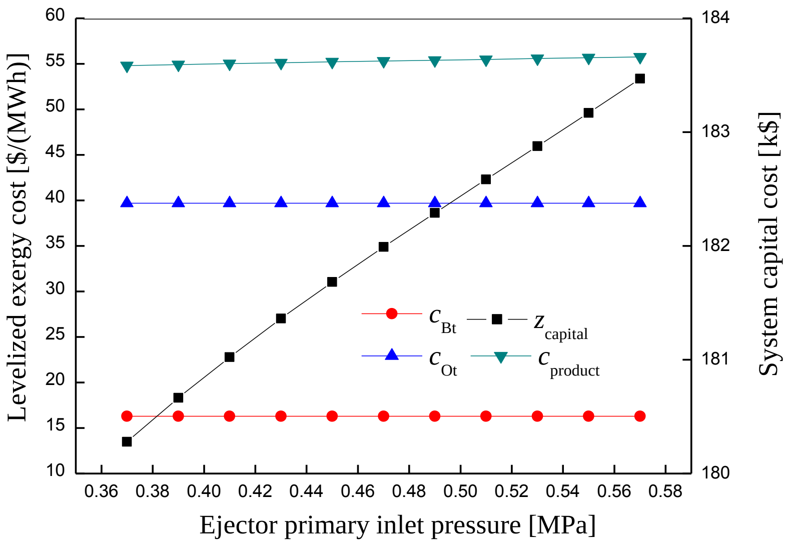

Fig. 15. Influences of ejector primary inlet pressure on the levelized exergy cost and the system capital cost of the system.

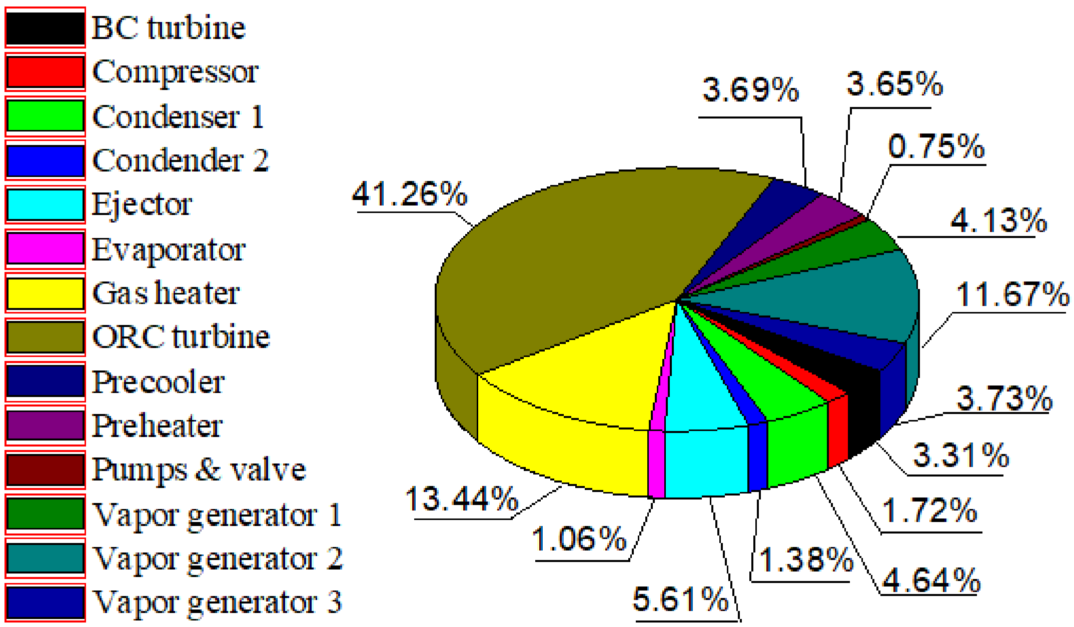

Fig. 16. Exergy destruction of different components

*Detailed Response to Reviewer Comments

Response to Reviewers

Paper No. ECM-D-18-05037, Energy Conversion and Management

Title: Performance analysis and optimization of a combined cooling and power system using low boiling point working fluid driven by engine waste heat

Dear editor & reviewers,

Thank you very much for your review of our paper entitled "Performance analysis and optimization of a combined cooling and power system using low boiling working fluid driven by engine waste heat", and for your comments and recommendations. These commends and recommendations help us to make better modifications and improve the quality of the paper. We have modified the manuscript accordingly in the revised manuscript. Please find below our response and explanations for your comments and questions.

Editor Comments:

1. Avoid lumping references as in [2, 3] and all other. Instead summarize the main contribution of each referenced paper in a separate sentence. How each paper is related to the work presented in the manuscript? What is being challenged or extended?

We thank the editor for the suggestion. We have avoided the reference lumping in the revised manuscript. The lumping parts have been removed in the previous manuscript such as "~~waste heat recovery technology [2,3]~~", "~~by many researchers~~

~~[13-15]~~", "~~avoid the decomposition [17,18]~~", "~~simple layout [27,28],~~".

Research work in references were summarized to descript the present research and existing questions. Ref. [1] descripted the widely use of internal combustion engines. Ref. [2] descripted the low fuel utilization efficiency of internal combustion engines. Ref. [3] descripted the advantages of organic Rankine cycle system. Ref. [4], [5] and [6] descripted the work of selecting suitable organic working fluids for organic Rankine cycle system by three different research groups. Ref. [7] and [8] descripted the configuration improving work in single-loop organic Rankine cycle system for internal combustion engine waste heat recovery. The maximum power output of single-loop organic Rankine cycle was challenged. Ref. [9] pointed out that maximum power output of a single-loop organic Rankine cycle system was lower than that of a dual-loop organic Rankine cycle. Ref. [10], [11] and [12] descripted the configuration improving work in dual-loop organic Rankine cycle system by three different research groups. But thermal stability of the organic working fluids in these systems was neglected. To avoid this issue, Ref. [17], [18] and [19] developed thermoelectric generator and steam Rankine cycle to address the decomposition issue of the high temperature heat transfer. But the energy conversion efficiency of the thermoelectric generator and component size of steam Rankine cycle in the references were challenged. Low thermal efficiency and large component bulk might limit their application. Thus, we provided our solution: a carbon dioxide Brayton cycle. For Ref. [20], the authors didn't analysis the parameter variation of carbon dioxide Brayton cycle and they didn't utilized the energy in the jacket water. Ref. [23], [24] and [25] descripted the utilization of jacket water in the organic Rankine cycle system for internal combustion engine waste heat recovery. But the utilization efficiency of jacket water is low. Thus, we designed a dual-pressure organic Rankine cycle to increase the mass flow rate of the working fluid preheated by jacket water. Ref. [27], [28] and [29] descripted the recent research work about multigeneration system driven by waste heat. They expressed the importance of the multigeneration. Ref. [30] and [31] descripted the combined cooling and power system driven by internal combustion engine. The authors used ammonia absorption refrigeration cycle in the systems to provide refrigeration. But the structure of the ammonia absorption refrigeration cycle is complex and it requires a relatively high driven temperature. Thus, we employed the ejector refrigeration cycle to provide refrigeration and further utilize the jacket water energy.

2. Please avoid having heading after heading with nothing in between, either merge your headings or provide a small paragraph in between.

We thank the editor for this suggestion. Heading after heading was avoided in the revised manuscript.

3. Avoid using abbreviations and acronyms in title, abstract, headings and highlights. The first time you use a chemical formula in the text, please write the full compound name and the formula in parenthesis. Do not use chemical formula in the title, abstract, chapter headings and highlights.

We thank the editor for this suggestion. Abbreviations and acronyms in abstract and headings were removed and rewritten in the revised manuscript. (carbon dioxide) was used to explain CO_2 the first time it appeared in the text in Line 106: “Brayton cycle with CO_2 (carbon dioxide) as working fluid”

4. The first time you use an acronym in the text, please write the full name and the acronym in parenthesis. Do not use acronyms in the title, abstract, chapter headings and highlights.

We thank the editor for this suggestion. We have written a full name of the acronym in parenthesis the first time it appeared in the text in the revised manuscript.

The use of acronym in the text were “internal combustion engine (ICE)” in Line 44; “study of organic Rankine cycle (ORC)” in Line 51; “introduced thermoelectric generator (TEG) technology” in Line 96; “coupled with CO_2 Brayton cycle (CBC)” in Line 108; “Combined cooling and power (CCP) systems” in Line 135; “Ammonia absorption refrigeration cycle (AARC)” in Line 143; “ejector refrigeration cycle (ERC)” in Line 146; “dual-pressure organic Rankine (DORC)” in Line 152; “genetic algorithm (GA)” in Line 164.

5. The introduction should include problem context, literature review and the hypothesis based on the gap analysis of the previously published research.

We thank the editor for this suggestion. Introduction was thoroughly rewritten in the revised manuscript. Problem context, literature review and hypothesis were included in the introduction.

6. The originality of the paper needs to be further clarified.

We thank the editor for this suggestion. Originality of the paper was further clarified in the revised manuscript.

There are three innovative features in this paper:

(1) We investigated a CO_2 Brayton cycle to prevent the risk of the decomposition of organic working fluid and provide power with high efficiency.

Organic Rankine cycles are used by many researchers to recover waste heat from internal combustion engines. Refrigerants are widely used as working in organic Rankine cycles but their decomposition temperatures are relatively low (200-300 ℃). When the high-temperature (above 450 ℃) engine exhaust gas transfers heat with these organic working fluids, there is risk of decomposition of the organic working fluids. Though organic working fluids with high decomposition temperature were investigated researchers, their flammability hindered their further applications. Some high-temperature loops for waste heat recovery were proposed by some researchers such as thermoelectric generator, steam Rankine cycle. But the thermal efficiency of the thermoelectric generator is low and the bulk of components in steam Rankine cycle is large, which might limit their application. Thus, we use a CO_2 Brayton cycle work as a high-temperature loop in the system to prevent the decomposition risks and provide power with high efficiency and compact structure.

(2) We developed a dual-pressure organic Rankine cycle to increase the utilization efficiency of the jacket water energy.

The previous internal combustion engine waste heat recovery systems, energy in jacket water was not fully utilized. In some studies, energy in jacket water was not utilized as all. Jacket water was mainly used to preheat the organic working fluid in the organic Rankine cycle based internal combustion engine waste heat recovery system. But there is mismatch of the mass flow rate of the organic working fluid in the preheater and evaporator. Thus, only a small part of the energy in jacket water was harnessed. We developed a dual-pressure organic Rankine cycle as a bottom cycle after the CO_2 Brayton cycle. Dual-pressure organic Rankine cycle can provide a large amount of power output. Moreover, organic working fluid in both high-pressure and low-pressure are preheated by the jacket water, which increases the utilization rate of the jacket water.

(3) We developed an ejector refrigeration cycle to fully utilize the jacket water waste heat and provide refrigeration.

Combined cooling and power system driven by engine waste heat shows the advantages of high efficiency and multiple energy supply. Ammonia absorption refrigeration cycle are widely used for refrigeration in these systems. But the configuration of it is complex and it requires a high driven temperature. We coupled a ejector refrigeration cycle with the organic Rankine cycle system instead of ammonia absorption refrigeration cycle to provide refrigeration. The ejector refrigeration cycle has a simple structure and requires relatively low driven temperature. Thus, jacket water is used to drive the ejector refrigeration cycle to provide refrigeration and fully utilize the waste heat.

Reviewer #1:

This manuscript introduces the performance analysis and optimization of a combined cooling and power system using low boiling point working fluid driven by engine waste. The novelty and the impact of the present manuscript is limited and the relation to previous works is poor.

Thank the reviewer for pointing out the shortcomings of the paper. We have thoroughly rewritten the introduction section to further clarify the novelty and the relation to previous work of the paper.

There are three innovative features in this paper:

(1) We investigated a CO_2 Brayton cycle to prevent the risk of the decomposition of organic working fluid and provide power with high efficiency.

Organic Rankine cycles are used by many researchers to recover waste heat from internal combustion engines. Refrigerants are widely used as working in organic Rankine cycles but their decomposition temperatures are relatively low (200-300 ℃). When the high-temperature (above 450 ℃) engine exhaust gas transfers heat with these organic working fluids, there are risks of decomposition of the organic working fluids. Though organic working fluids with high decomposition temperature were investigated researchers, their flammability hindered their further applications. Some high-temperature loops for waste heat recovery were proposed by some researchers such as thermoelectric generator, steam Rankine cycle. But the thermal efficiency of the thermoelectric generator is low and the bulk of components in steam Rankine cycle is large, which might limit their application. Thus, we use a CO_2 Brayton cycle work as a high-temperature loop in the system to prevent the decomposition risks and provide power with high efficiency and compact structure.

(2) We developed a dual-pressure organic Rankine cycle to increase the utilization efficiency of the jacket water energy.

The previous internal combustion engine waste heat recovery systems, energy in jacket water was not fully utilized. In some studies, energy in jacket water was not utilized as all. Jacket water was mainly used to preheat the organic working fluid in the organic Rankine cycle based internal combustion engine waste heat recovery system. But there is mismatch of the mass flow rate of the organic working fluid in the preheater and evaporator. Thus, only a small part of the energy in jacket water was harnessed. We developed a dual-pressure organic Rankine cycle as a bottom cycle after the CO_2 Brayton cycle. Dual-pressure organic Rankine cycle can provide a large amount of power output. Moreover, organic working fluid in both high-pressure and low-pressure are preheated by the jacket water, which increases the utilization rate of the jacket water.

(3) We developed an ejector refrigeration cycle to fully utilize the jacket water waste heat and provide refrigeration.

Combined cooling and power system driven by engine waste heat shows the advantages of high efficiency and multiple energy supply. Ammonia absorption refrigeration cycle are widely used for refrigeration in these systems. But the configuration of it is complex and it requires a high driven temperature. We coupled a ejector refrigeration cycle with the organic Rankine cycle system instead of ammonia absorption refrigeration cycle to provide refrigeration. The ejector refrigeration cycle has a simple structure and requires relatively low driven temperature. Thus, jacket water is used to drive the ejector refrigeration cycle to provide refrigeration and fully utilize the waste heat.

About the impact of this paper:

There are two pathways to improve the performance of the organic Rankine cycle system for engine waste heat recovery. One will be selecting organic working fluids which are suitable for the system under certain conditions. Another is to optimize the system configuration to make full use of the waste heat. In this paper, we designed a combined cooling and power system with a novel configuration which prevents the decomposition risk of organic working fluid, fully utilizes the jacket water energy and provides power and refrigeration simultaneously.

About the relation of this paper to previous work:

We have thoroughly rewritten the introduction section of this paper. More recently published papers were added to descript research conditions and existing problems. We carried out our work based on the analysis of previous work.

Reviewer #2:

Corrections mainly involve formatting points, such as English grammar, citation of references, etc.; and insufficient information regarding some equipment used in the research. Concerning the formatting and methodology the points are as follows:

1. In Nomenclature, present separately the Latin symbols, Greek symbols, Acronyms, Subscripts and Superscripts, because of the form that is presented, it is confused; include the acronym TEG - Thermoelectric generator and GA - Genetic Algorithm; if the "K" of K$" is "kilo", must be represented by "k".

Thank the reviewer for the kind suggestion. The Nomenclature section was separated as Latin symbols, Acronyms, Greek symbols and Subscripts in the revised manuscript. TEG and GA were added to the list and "K$" was changed to "k$".

2. In lines 72, 96, 97 and 203, separate the temperature values of its units, for example, 90 ºC (line 72).

In the revised manuscript, temperature values were separated with their units.

In Line 87: "low (200-300 ℃) [13], while the temperature of exhaust gas is above 450 ℃".

3. In line 104 change "to the utilize" by other word.

We have thoroughly rewritten the introduction section and the error was avoided in the revised manuscript.

4. In line 126 put comma between gas and while, and after "But" in line 127.

We have thoroughly rewritten the introduction section and the error was avoided in the revised manuscript.

5. In line 139 and 140 change the word "flew" by "flows".

We have thoroughly rewritten the introduction section and the error was avoided in the revised manuscript.

6. In lines 148, 149 and 150 put "2" of "CO2" as subscript.

We have thoroughly rewritten the introduction section and the error was avoided in the revised manuscript.

7. In line 166 change the word "consumption" by "combustion".

We have thoroughly rewritten the introduction section and the error was avoided in the revised manuscript.

8. In line 174 put comma after "Meanwhile".

We have thoroughly rewritten the introduction section and the error was avoided in the revised manuscript.

9. From line 197 to 206 write "Several assumptions are made to simplify the simulation of the system, which are: (1) the system keeps a steady state; (2) the heat and friction ….are not considered; and so on.

We thank the reviewer for the suggestion. The system assumptions part was rewritten based on the suggestion in the revised manuscript from Line 206 to Line 213 "Several assumptions are made to simplify the simulation of the system, which are: (1) the system keeps a steady state; (2) the heat and frication in the system are not considered; (3) the pressure losses in the vapor generators, preheater, evaporator, condensers and pipes are neglected; (4) the gas temperature at the outlet of the vapor generator 1 is higher than 110 ℃ [35], considering the low gas dew point temperature; (5) the working fluids at the outlet of the condensers and the preheater are saturated liquids, and the evaporator outlet state is saturated vapor; (6) the process through the throttle valve is isenthalpic."

10. In line 228 put a comma after "thermodynamic".

We have rewritten that paragraph in the revised manuscript from Line 230 to Line 235. The error was avoided.

11. Begin the sentence of the line 236 by "In this study, all components in the system …" and remove "in this study" of the end of the sentence.

The sentence was rewritten in the revised manuscript in Line 240 as following: "In this study, all the components in the system are associated directly or indirectly with fuel of other heat sources, such as exhaust as and jacket water.”

12. In line 257 put comma between "expenses" and "etc."

A comma was put between "expenses" and "etc." in the revised manuscript in line 260 as following:

(like the taxes, insurance engineering expenses, etc.)

13. Indicate that equations from 11 to 21 are proposed in [33].

We have indicated in the revised manuscript as following:

Line 264: “In the following text, equations from Eq. (11) to Eq. (21) are proposed in Ref. [37].”

14. In line 265 write "where Ki,turb are the constants corresponding to the turbine type; and W is the power ….''; and in similar manner in lines 276, 282 and 286.

We have rewritten the sentences in the revised manuscript in Line 269 “$K_{i,\ turb}$ are constants corresponding to”, Line 280 “$K_{i,\ pump}$ are the constants corresponding to”, Line 286 “$B_{i,\ pump}$ are the constants corresponding to”, Line 290 “$C_{i,\ pump}$ are the constants corresponding to”, Line 295 “$K_{i,comp}$ are the constants corresponding to”, Line 305 “$K_{i,he}$ are the constants corresponding to”, Line 312 “$B_{i,he}$ are the constants corresponding to” and Line 316 “$C_{i,he}$ are the constants corresponding to”.

15. In lines 297 and 784 I suggest to change the word "Tube-and-shell heat exchangers" to "Shell-and-tube heat exchangers".

It was corrected in the revised manuscript in Lines 301 and 741.

16. Verify in the equation (23) if the exponent of the term in brackets of the numerator is "n - 1".

Thank the reviewer for the kind suggestion. We have verified the equation. It was "n".

17. In line 336 add the word "years" after 30.

It was corrected in the revised manuscript in Line 339 as following: “being assumed as 30 years”

18. In lines 340 and 348 change the word "steams" by "streams"; and in lines 342, 343 and 349 change the word "steam" by "stream".

We have changed the expression in the revised manuscript in Lines 343, 345, 346, 351 and 352 as following:

“In a steady system, there are a number of entering and outing working fluid streams and heat and work interactions with the surroundings. In exergoeconomic analysis, each flowing stream is associated with a levelized exergy cost. The equations to calculate the cost of the stream product are given as:”

“where *c* denotes levelized exergy cost of the streams; $E_{y,in}$ and $E_{y,out}$ are the exergy transfer rate of the stream flowing in and out of a component;”

19. In line 348 remove the space before "where" and verify if the variable "c" is the "levelized exergy cost of the system" or is the "average cost per unit of exergy" according to the Nomenclature.

Thank the reviewer for the kind suggestion. "*c*" is the "levelized exergy cost of the system". We have corrected the error in the Nomenclature and remove the space in Line 351.

20. In line 349 add "of" after out.

We have corrected the error in the revised manuscript in Line 352 as following: “flowing in and out of a component”

21. In line 360 and 363 add the word "where" before "cfuel" and "cBt", respectively; and remove the initial space.

We have corrected the error in the revised manuscript in Lines 364 and 367.

22. In line 365 add "… and the fuel-cost-related part, given by Eq. (32) and (33).

We have corrected the error in the revised manuscript in lines 369 and 370. “capital-cost-related part and the fuel-cost-related part, given by Eq. (32) and Eq. (33).”

23. I suggest that sections 4.1.1, 4.1.2 and 4.2 are inserted at the end of section 3, because they represent materials and methods and not results and discussion.

Thank the reviewer for the kind suggestion. We have put sections 4.1.1, 4.1.2 and 4.2 to the end of section 3 from Line 397 to Line 402.

24. In line 380 remove the word "gas" and maintain only "… supercharger engine."; in line 382 replace "The heat load capacity" by "The thermal load of the …" and deleted "when cooled down to the acid dew temperature".

We have rewritten the sentences in the revised manuscript in Line 380.

“In this study, the engine selected [7] is a 12-cylinder 4-stroke supercharged engine. The main designed parameters of the engine are listed in Table 3. The composition of the engine exhaust gas is presented in Table 4. The thermal load of the engine exhaust gas is about 1700 kW and 1000 kW can be obtained from the engine jacket water.”

25. In line 386 express the seven key parameters by its symbols.

We have added the symbols of the key parameters in the revised manuscript from Line 388 to 392 as following:

“Seven key parameters : BC turbine inlet temperature ($T_{Bt,in}$), BC turbine inlet pressure ($P_{Bt, in}$), inlet temperature at the high-pressure side of ORC turbine ($T_{Ot, in, h}$), inlet pressure at the high-pressure side of ORC turbine ($P_{Ot, in, h}$), inlet temperature at the low-pressure side of ORC turbine ($T_{Ot, in, l}$), inlet pressure at the low-pressure side of ORC turbine ($P_{Ot, in, l}$) and the ejector primary inlet pressure ($P_{ej, in}$),”

26. In lines 392, 393, 395 and 396 express the variables "W", "Q" and "c" in italics.

We have corrected the error in the revised manuscript from Line 396 to Line 402.

“In the thermodynamic aspect, the net power output of the CO_2 Brayton cycle (W_{BC}), net power output of the DORC (W_{ORC}), net power of the whole system (W_{net}), cooling capacity of the system (Q_{cool}) and the exergy efficiency of the system (η_{exergy}) are selected to reflect the system performance. Levelized exergy cost for the BC turbine power output (c_{Bt}), levelized exergy cost for the ORC turbine power output (c_{Ot}), levelized exergy cost the system product ($c_{product}$) and the system capital cost ($z_{capital}$) are chosen to represent the exergoeconomic performance.”

27. Start the Results and discussion section from section 4.2.1.

We have put that section at the beginning of Results and discussion in the revised manuscript from Line 404.

28. In all results shown from Fig. 2 to Fig. 15 only one parameter at a time was varied, while the others were maintained constants? Clear this in the text.

We have explained this in the revised manuscript from Line 393 to Line 395 as following: “When one parameter is investigated to analyze the system performance, other parameters are maintained constants based on the conditions in Table 5.”

29. In line 552 change "The can be explained …" by "This can be explained …".

The sentence was rewritten in the revised manuscript from Line 521 to Line 522 as following: “The reason is that the two related parts of c_{Ot} increase with the drop of the ORC turbine power output.”

30. Seems incomplete to me the sentence of the line 612 "Thus, the capita-cost-related …".

We have rewritten the sentence in the revised manuscript from Line 555 to Line 558 as following: “The impact of c_{Ot} and c_{Bt} is greater than that of the system capital cost which would result in the increase of the capital-cost-related part of $c_{product}$. Thus, the levelized exergy cost of the system product ($c_{product}$) shows a descending trend.”

31. In line 641 remove the word "vapor" after "… vapor generator 2".

We have rewritten the sentence in the revised manuscript from Line 594 to Line 596 as following: “The levelized exergy cost for vapor in vapor generator 2, which is the equal to that of the vapor in vapor generator 1, increases as a result, causing the increase of the levelized exergy cost of the exhaust CO_2 after the BC turbine.”

32. In line 658 add "of" after "Though".

We have added an “of” after “Though” in the revised manuscript in Line 608.

33. In the sentence of line 676 I suggest to write "The cooling capacity (Qcool) increases slightly with the …" because by Figure 12 the increase is very small and,

hence, should also be corrected at the end of line 680.

We have rewritten the sentence in the revised manuscript in Lines 625 and 628.

34. In line 709 add a "t" after "can'".

The error was corrected in the revised manuscript in Line 653.

35. Rewrite the two sentences from line 713 to 715.

We have rewritten the two sentences in the revised manuscript from Line 657 to Line 659 as following:

“The increase of the ejector primary inlet pressure causes the increase of the entrainment ratio of the ejector. Thus, more secondary flow is entrained to the ejector from the evaporation, leading to the increase of the cooling capacity.”

36. In the paragraph from line 751 to line 753 I suggest to refer to Fig. 8 and 9 where are evidenced the highest output power, exergy efficiency and the lowest levelized exergy cost (but not the cooling capacity) at the highest inlet pressure at the high-pressure side ORC turbine.

We thank the reviewer for this kind suggestion. We compared the results of the genetic algorithm optimization results with the parameter trend in Fig. 8 and 9. The value of net power output, exergy efficiency, levelized exergy cost and the inlet pressure at the high-pressure side ORC turbine in the two parts were nearly the same. The inlet pressure at the high-pressure side ORC turbine is varied while other six parameters are kept as constants in Fig. 8 and 9. Thus, the inlet pressure at the high-pressure side ORC turbine plays a more important other six parameters. When the inlet pressure at the high-pressure side ORC turbine is close to the highest permitted pressure, the system performance is close to the optimization performance. Note that: When the inlet pressure at the high-pressure side ORC turbine increases, the pinch point temperature difference in vapor generator 2 decreases. Thus, there would be temperature cross in the vapor generator when inlet pressure at the high-pressure side ORC turbine is larger than critical value. That’s why the optimization results shows that the value of the inlet pressure at the high-pressure side ORC turbine is 1.85 MPa in stead of the maximum value 2 MPa.

We have rewritten the paragraph from Line 698 to Line 707 as following:

“The optimization results of GA are listed in Table 8. It can be obtained that the minimum levelized exergy cost for the system product $c_{product}$ is 53.25 (MWh)^{-1}$. The net power output, exergy efficiency of the CCP system are 374.37 kW, 37.31% respectively. The inlet pressure at the high-pressure side of ORC turbine is 1.85 MPa. Meanwhile, it can be evidenced from Fig. 8 and 9 that the highest output power (about 374.37 kW), exergy efficiency (about 37.31%) and the lowest levelized exergy cost (about 53.25 (MWh)^{-1}$) at the highest inlet pressure at the high-pressure side ORC turbine (about 1.85 MPa). The results shown in Fig. 8 and 9 are close to the optimization results. The inlet pressure at the high-pressure side ORC turbine is varied while other six parameters are kept as constants in Fig. 8 and 9. Thus, inlet pressure at the high-pressure side ORC turbine plays a more important role than other six parameters when determining the performance of the system. When the inlet pressure at the high-pressure side ORC turbine is close to the highest permitted pressure, the system performance is close to the optimization performance.”

37. The sentence of conclusion (2) is very extensive and I suggest ending it in "… for the system product.", beginning the next sentence such as, "Meanwhile, the increase of the ORC …".

We have rewritten the sentence in the revised manuscript in line 727 as following: "In the DORC, the increase of $T_{Ot, in}$ and $T_{Ot, in, l}$ would cause the decrease of the system exergy efficiency and the increase of the levelized exergy cost for the system product. Meanwhile, the increase of $P_{Ot, in, h}$ and $P_{Ot, in, l}$ would result in the increase of the exergy efficiency and the decrease of the levelized exergy cost."

38. In line 810 replace the word "frication" by "friction".

The error was corrected in the revised manuscript in line 767 as following: "the Darcy friction factor,"

39. In the "References" use the abbreviation names of the Journals, such as, Energy Convers Manage and the number of pages as 201-14, instead of using 201-214, for example; in the reference [14] line 863 change the number of the pages to 215-32 to differentiate from reference [12];

Thank the reviewer for the suggestion. We have rewritten the abbreviation names of Journals and the page number in the revised manuscript.

40. in reference [16] correct the names of authors to Rajabloo T, Bonalumi D, Lora P; in reference [17] add at the end of the author names, the author Zhu W; in reference [31] add at the end of the author names, the authors Liu H, Wang E, Yao B; in reference [32] correct the author names to Bejan A, Tsatsaronis G, Moran M and the first name of the publisher to John; in reference [33] add other authors, i.e., Turton

R, Bailie RC, Whiting WB, Shaeiwitz JA;

We have corrected the errors in the revised manuscript in Lines 877, 880, 884 and 885 as following:

[34] Shu G, Zhao M, Tian H, Huo Y, Zhu W. Experimental comparison of R123 and R245fa as working fluids for waste heat recovery from heavy-duty diesel engine. Energy 2016; 115:756-69.

[35] Zhang J, Zhang H, Yang K, Yang F, Wang Z, Zhao G, Liu H, Wang E, Yao B. Performance analysis of regenerative organic Rankine cycle (RORC) using the pure working fluid and the zeotropic mixture over the whole operating range of a diesel engine. Energy Convers Manage 2014; 84:282-94.

[36] Bejan A, Tsatsaronis G, Moran M. Thermal design and optimization. New York: John Wiley & Sons; 1996.

41. What is the reference [35]?

That reference was a website for the *CEPCI*. We have removed it.

42. In table 3 replace the word "Term" by "Parameter" and the same in Table 8; in this table I suggest that the values presented be limited in two digits after comma to standardize all.

We have replaced the expression in Table 5 (Table 3 in the previous manuscript) and Table 8 and in Line 957 and Line 960. The values in Table 8 were limited to two digits.

43. In Table 6 replace "Ranges of the decision variables" by only "Parameters or Variables" and add "Operation" before "Range".

We have replaced the expression in Table 6 in the revised manuscript in Line 958.

44.In Table B1 the source is [33} and not [32].

Thank the reviewer for helping us find the error. It was corrected in the revised manuscript.

Reviewer #3:

The authors have conducted a study that covers a topic of great interest: "Performance analysis and optimization of a combined cooling and power system using low boiling point working fluid driven by engine waste heat". This very important topic deserved a great deal of attention. However, many shortcomings can be identified. Therefore, I recommend that these shortcomings, as listed in the following, should be addressed before it can be considered for publication;

1. Abstract section, present in more detail and clarity

Thanks for the reviewer's kind suggestion. The abstract section was thoroughly rewritten in the revised manuscript. More details were added in the abstract.

"This paper develops a combined cooling and power system, which consists of a carbon dioxide Brayton cycle, a dual-pressure organic Rankine cycle and an ejector refrigeration cycle, to recover waste heat from exhaust gas and jacket water in internal combustion engines. Thermodynamic models of the system are performed and exergoeconomic methods are used to calculate the levelized exergy cost of the component products. Effects of seven parameters, including temperature and pressure at the Brayton cycle turbine inlet, temperature and pressure at the high-pressure and low-pressure side of the organic Rankine cycle turbine inlet and pressure at the ejector primary inlet, are evaluated. Single-objective optimization is carried out by means of genetic algorithm to obtain the minimum levelized exergy cost of system product. Results show that the increase of pressure at Brayton cycle turbine inlet and high-pressure and low-pressure side of the organic Rankine cycle turbine inlet contributes to the decrease of levelized exergy cost of the system product. Optimization results show that minimum levelized exergy cost for system product is 53.25 \$ $(MWh)^{-1}$. When levelized exergy cost is minimum, system net power output, cooling capacity and exergy efficiency are 374.37 kW, 188.63 kW and 37.31%, respectively."

2. Please, Give more numerical results about the study results in the abstract section.

Thank the reviewer for the suggestion. The abstract section was rewritten in the revised manuscript and more numerical results were put in the abstract section.

3. Analysis of the state of the art in the introduction is insufficient, which undermines novelty of this work. An updated and complete literature review should be conducted.

The introduction section was thoroughly rewritten in the revised manuscript. More recent references were discussed and some old references were removed. The novelty of this work was further clarified.

4. Literature section should be given current papers after 2017.

We thank the reviewer for the kind suggestion. References in 2017 and 2018 were put in the introduction sections and some old references were removed in the revised manuscript.

[5] Rijpkema J, Munch K, Andersson S. Thermodynamic potential of twelve working

fluids in Rankine and flash cycles for waste heat recovery in heavy duty diesel engines. Energy 2018; 160:996-1007.

[6] Su X, Shedd T A. Towards working fluid properties and selection of Rankine cycle based waste heat recovery (WHR) systems for internal combustion engines – A fundamental analysis. Appl Therm Eng 2018; 142:502-10.

[10] Wang X, Shu G, Tian H, Liu P, Jing D, Li X. Dynamic analysis of the dual-loop Organic Rankine Cycle for waste heat recovery of a natural gas engine. Energy Convers Manage 2017; 148:724-736.

[11] Wang E, Yu Z, Zhang H, Yang F. A regenerative supercritical dual-loop organic Rankine cycle system for energy recovery from the waste heat of internal combustion engines. Appl Energy 2017; 190:574-90.

[12] Huang H, Zhu J, Deng W, Ouyang T, Yan B, Yang X. Influence of exhaust heat distribution on the performance of dual-loop organic Rankine Cycle (DORC) for waste heat recovery. Energy 2018; 151:54-65.

[13] Rajabloo T, Bonalumi D, Lora P. Effect of a partial thermal decomposition of the working fluid on the performances of ORC power plants. Energy 2017; 133:1013-26.

[14] Shi L, Shu G, Tian H, Deng S. A review of modified Organic Rankine cycles (ORCs) for internal combustion engine waste heat recovery (ICE-WHR). Renew Sustain Energy Rev 2018; 92:95-110.

5. How were reference conditions (environmental pressure and temperature) considered?

In this paper, environment temperature is 20 ℃ and environment pressure is 101.3

kPa. They are based on the following reference:

Yang X, Zheng N, Zhao L, Deng S, Li H, Yu Z. Analysis of a novel combined power and ejector refrigeration cycle. Energy Convers Manage; 2016; 108:266-74.

6. The level of English throughout the manuscript does not meet the journal's desired standard. There are a number of grammatical errors.

Thank the reviewer for the kind suggestion. We have checked the grammatical errors and thoroughly rewrote the paper in the revised manuscript.

7. Introduction part needs to be extended by some of the recently published papers to show the importance of multigeneration systems in high-quality journals

We thank the reviewer for the kind suggestion. We have expressed the importance of the multigeneration systems with three recently published paper in the introduction section of the revised manuscript.

[27] Li Fan, Sun Bo, Zhang C, Zhang L. Operation optimization for combined cooling, heating, and power system with condensation heat recovery. Appl Energy 2018; 230:305-16.

[28] Yari Mortaza, Ariyanfar Leyli, Aghdam EA. Analysis and performance assessment of a novel ORC based multigeneration system for power, distilled water and heat. Renew Energy 2018; 119:262-81.

[29] Bai Z, Liu T, Liu Q, Lei J, Gong L, Jin H. Performance investigation of a new cooling, heating and power system with methanol decomposition based chemical recuperation process. Appl Energy 2018; 229: 1152-63.

8. Originality of the paper should be emphasized clearly. How this study differs from

related published papers?

The introduction section was rewritten in the revised manuscript. We analyzed the gaps existing in the published papers and provided our original solutions. The innovative features of the paper were summarized at the end of the introduction section.

There are three innovative features in this paper:

(1) We investigated a CO_2 Brayton cycle to prevent the risk of the decomposition of organic working fluid and provide power with high efficiency.

Organic Rankine cycles are used by many researchers to recover waste heat from internal combustion engines. Refrigerants are widely used as working in organic Rankine cycles but their decomposition temperatures are relatively low (200-300 ℃). When the high-temperature (above 450 ℃) engine exhaust gas transfers heat with these organic working fluids, there are risks of decomposition of the organic working fluids. Though organic working fluids with high decomposition temperature were investigated researchers, their flammability hindered their further applications. Some high-temperature loops for waste heat recovery were proposed by some researchers such as thermoelectric generator, steam Rankine cycle. But the thermal efficiency of the thermoelectric generator is low and the bulk of components in steam Rankine cycle is large, which might limit their application. Thus, we use a CO_2 Brayton cycle work as a high-temperature loop in the system to prevent the decomposition risks and provide power with high efficiency and compact structure.

(2) We developed a dual-pressure organic Rankine cycle to increase the utilization

efficiency of the jacket water energy.

The previous internal combustion engine waste heat recovery systems, energy in jacket water was not fully utilized. In some studies, energy in jacket water was not utilized as all. Jacket water was mainly used to preheat the organic working fluid in the organic Rankine cycle based internal combustion engine waste heat recovery system. But there is mismatch of the mass flow rate of the organic working fluid in the preheater and evaporator. Thus, only a small part of the energy in jacket water was harnessed. We developed a dual-pressure organic Rankine cycle as a bottom cycle after the CO_2 Brayton cycle. Dual-pressure organic Rankine cycle can provide a large amount of power output. Moreover, organic working fluid in both high-pressure and low-pressure are preheated by the jacket water, which increases the utilization rate of the jacket water.

(3) We developed an ejector refrigeration cycle to fully utilize the jacket water waste heat and provide refrigeration.

Combined cooling and power system driven by engine waste heat shows the advantages of high efficiency and multiple energy supply. Ammonia absorption refrigeration cycle are widely used for refrigeration in these systems. But the configuration of it is complex and it requires a high driven temperature. We coupled an ejector refrigeration cycle with the organic Rankine cycle system instead of ammonia absorption refrigeration cycle to provide refrigeration. The ejector refrigeration cycle has a simple structure and requires relatively low driven temperature. Thus, jacket water is used to drive the ejector refrigeration cycle to provide refrigeration and fully utilize the waste heat.

This paper differs from the previous paper mainly in the following four point:

(1) We used a CO_2 Brayton cycle to prevent the risk of decomposition of the organic working fluid and comprehensively analyzed its performance.

(2) We designed a dual-pressure organic Rankine cycle as a bottom cycle to increase the utilization efficiency of the jacket water.

(3) We used jacket water to drive the ejector refrigeration cycle to fully utilize the jacket water energy and provide refrigeration.

(4) We used exergoeconomic method to analyze the system performance.

9. Discuss and elaborate more on the exergy destruction rates of system and sub-systems. They were not written in the text.

Exergy destruction rates of the components in the system were calculated and presented in the revised manuscript from line 708 to 716 as following:

"Fig. 16 shows the exergy destruction of different components of the system under the optimization conditions. The largest exergy destruction takes place in the ORC turbine (41.26%), which is mainly caused by the mixing of the high-pressure working fluid and the low-pressure working fluid. Gas heater contributes 13.44% of the total exergy destruction. Three vapor generators take up 4.13%, 11.67% and 3.73% of the exergy destruction, respectively. The exergy destruction for the ejector is 5.61%, which is also caused by the working fluid mixing. For BC turbine, condenser 1, precooler and preheater, the exergy destruction are 3.31%, 4.64%, 3.69% and 3.65%, respectively. Other components contribute to the rest 4.87% of the exergy destruction."

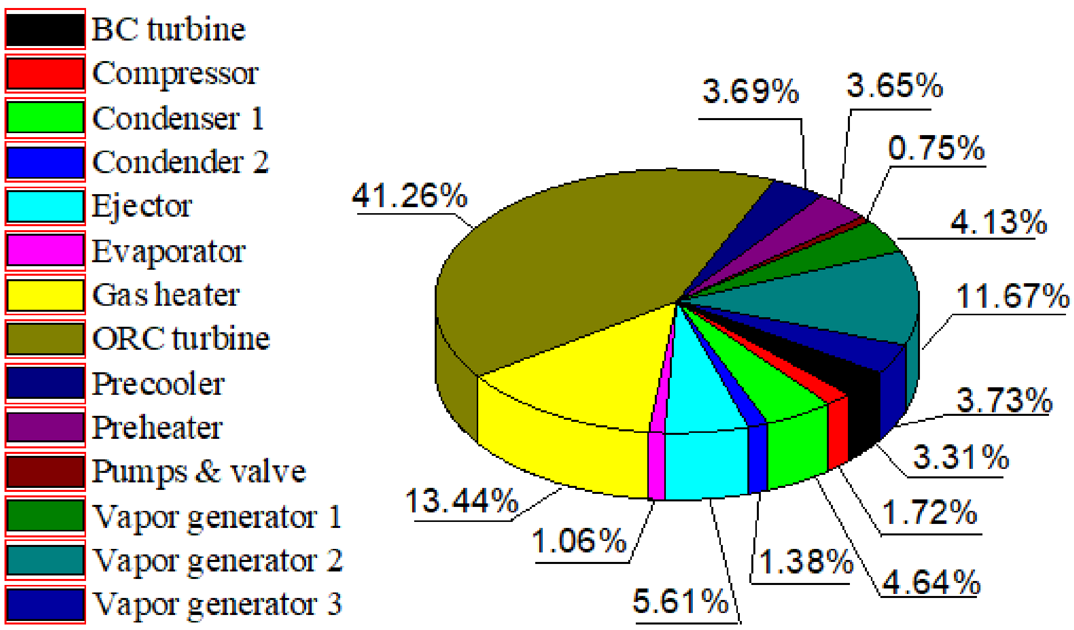

Fig. 16. Exergy destruction of different components

Performance analysis and optimization of a combined cooling and power system using low boiling point working fluid driven by engine waste heat

Wenge Huang, Jiangfeng Wang*, Jiaxi Xia, Pan Zhao, Yiping Dai

Institute of Turbomachinery, Shaanxi Engineering Laboratory of Turbomachinery and Power Equipment, State Key Laboratory of Multiphase Flow in Power Engineering, School of Energy and Power Engineering, Xi'an Jiaotong University, Xi'an 710049, China

Corresponding author: Jiangfeng Wang

Mailing address:

Institute of Turbomachinery, Shaanxi Engineering Laboratory of Turbomachinery and Power Equipment, State Key Laboratory of Multiphase Flow in Power Engineering, School of Energy and Power Engineering

Xi'an Jiaotong University, Xi'an 710049, China

E-mail address: jfwang@mail.xjtu.edu.cn (JF Wang).

Performance analysis and optimization of a combined cooling and power system using low boiling point working fluid driven by engine waste heat

Wenge Huang, Jiangfeng Wang*, Jiaxi Xia, Pan Zhao, Yiping Dai

Institute of Turbomachinery, Shaanxi Engineering Laboratory of Turbomachinery and Power Equipment, State Key Laboratory of Multiphase Flow in Power Engineering, School of Energy and Power Engineering, Xi'an Jiaotong University, Xi'an 710049, China

Abstract

This paper develops a combined cooling and power system, which consists of a carbon dioxide Brayton cycle, a dual-pressure organic Rankine cycle and an ejector refrigeration cycle, to recover waste heat from exhaust gas and jacket water in internal combustion engines. Thermodynamic models of the system are performed and exergoeconomic methods are used to calculate the levelized exergy cost of the component products. Effects of seven parameters, including Brayton cycle turbine inlet temperature and inlet pressure, organic Rankine cycle turbine high-pressure side and low-pressure side inlet temperature and ejector primary inlet pressure, are evaluated. Single-objective optimization is carried out by means of genetic algorithm to obtain the minimum levelized exergy cost of system product. Results show that the increase of pressure at Brayton cycle turbine inlet and high-pressure and low-pressure side of the organic Rankine cycle turbine inlet contributes to the decrease of levelized

exergy cost of the system product. Optimization results show that minimum levelized exergy cost for system product is 53.25 \$ (MWh)$^{-1}$. When system product levelized exergy cost is minimum, system net power output, cooling capacity and exergy efficiency are 374.37 kW, 188.63 kW and 37.31 %, respectively.

Nomenclature

Latin symbols		ρ	density, kg m^{-3}
A	area, m^2	μ	dynamic viscosity, m^2 s^{-1}
B_o	boiling number	η	efficiency, %
c	levelized average cost, \$(MWh)$^{-1}$	δ	thickness, m
c_p	specific heat, kJ kg^{-1} K^{-1}	*Subscribes*	
C	cost rate, \$ year^{-1}	1-31	state points
D	diameter, m	g1-g3	state points
e	exergy, kJ kg^{-1}	w1-w3	state points
E	exergy flow rate, kJ s^{-1}	Bt	Brayton cycle turbine
E_y	exergy flow rate per year, kJ year^{-1}	BM	bare module
F	multiplying factor	cond	condenser
f	friction factor	comp	compressor
G	mass flow rate, kg s^{-1}	D	destruction
h	enthalpy, kJ kg^{-1}	elec	electricity
H	depth, m	es	equivalent diameter
i_{eff}	interest rate	ev	evaporation/evaporator
l	length, m	ex	exergy

M	mass flow rate, kg s^{-1}	F	fuel
n	lifetime, year	g	exhaust gas
Nu	Nusselt number	gh	gas heater
P	pressure, MPa	he	heat exchanger
Pr	Prandtl number	L	loss
Pt	center distance between tubes, m	l	liquid
P_r	reduced pressure	M	material
Q	heat transfer rate, kW	Ot	ORC turbine
Q_{cool}	cooling capacity, kW	P	product
q_{m}	average imposed wall heat flux, W m^{-2}	p1	pump 1
r_{f}	enthalpy of vaporization, kJ kg^{-1}	p2	pump 2
T	temperature, K	p3	pump 3
U	overall heat transfer coefficient, W m^{-2} K^{-1}	p4	pump 4
W	power, kW	pf	primary flow
W_{y}	annually power, MWh $year^{-1}$	prec	precooler
x	vapor quality	preh	preheater
Z	annually levelized cost value, \$ $year^{-1}$	s	shell
z	capital cost, k\$	t	tube
Acronyms		th	thermal
BC	Brayton cycle	turb	turbine
CBC	CO_2 Brayton cycle	vg	vapor generator
CCP	combined cooling and power	w	tube wall

CRF	capital recovery factor
CEPCI	chemical engineering plant cost index
DORC	dual-pressure organic Rankine cycle
ERC	ejector refrigeration cycle
GA	genetic algorithm
TEG	thermoelectric generator
AARC	ammonia absorption refrigeration cycle
Greek symbols	
α	convection heat transfer coefficient, W m^{-2} K^{-1}
λ	heat conductivity, W m^{-1} K^{-1}

1. Introduction

Nowadays, internal combustion engine (ICE) is the major motive power source in energy field, which are widely used in transport, construction, agriculture, etc. Over 50 % of the total transportation fuel is consumed by ICEs [1]. However, only 30-45 % of the fuel energy is converted into effective power output, while the remaining energy is discharged to the environment via exhaust gas, jacket water and charge air, causing a large amount of waste fuel energy [2]. Thus, technology for waste heat recovery from ICEs has drawn much interest of researchers in the last decade. Much effort has been devoted to the study of organic Rankine cycle (ORC) based ICE waste heat recovery system for its advantages of high efficiency and simple structure [3].

There are two important pathways that will lead to the improvement of the ORC system for ICE waste heat recovery. One will be selecting organic working fluids which are suitable for the system under certain conditions. Another is to optimize the system configuration to make full use of the waste heat.

The work of selecting suitable organic working fluids for ORC was carried out by many researchers to improve the efficiency of the ICE waste heat recovery. Tian et al. [4] evaluated the performance of 20 different working fluids in an ORC system for ICE waste heat recovery. Rijpkema et al. [5] compared the performance of twelve working fluids in an ORC-based ICE waste heat recovery system to find the suitable candidate. Su et al. [6] developed a theoretical efficiency model about working fluids selecting for ORC-based ICE waste heat recovery system via strict mathematical derivation.

Configuration optimization in ORC-based ICE waste heat recovery system mainly focuses on reducing the system irreversible rate to fully utilize the engine waste heat. Vaja and Gambarotta [7] added a preheater and a recuperator separately to a simple ORC system to improve the performance for the ICE waste heat recovery. Kim et al. [8] proposed a novel single-loop ORC system to recovery engine waste heat. They employed two recuperators in series to heat the working fluid. Comparison showed that the net power output of the system was 35.6 % more than simple ORC system. Because that the maximum power output of single-loop ORC is lower than that of the dual-loop ORC system [9], more attention has been focused on dual-loop ORC based ICE waste heat recovery system in recent years. Wang et al. [10] modeled a dual-loop ORC system for engine waste heat recovery. The high-temperature loop absorbed heat from exhaust gas and its residual heat acted as heat source for the low-temperature loop. Wang et al. [11] investigated a dual-loop ORC system for ICE waste heat recovery. The high-temperature loop absorbed heat from exhaust gas for the first time. Then the low-temperature loop absorbed heat from the residual heat of the exhaust gas to realize the cascading utilization of the waste heat. Huang et al. [12] proposed a complex dual-loop ORC system for engine waste heat recovery. The high-temperature loop absorbed heat from the exhaust gas and residual heat from both the exhaust gas and the high-temperature loop provided heat for the low-temperature loop.

When referring to heat transfer in the high-temperature loop, thermal stability of organic working fluid is necessary to be considered. In previous studies, refrigerants were most selected as working fluids. The decomposition temperatures of refrigerants are relatively low (200-300 ℃) [13], while the temperature of exhaust gas is above 450 ℃ [14]. Direct heat transfer between high-temperature exhaust gas and refrigerant caused the risk of working fluid decomposition. Though high decomposition temperature working fluids such as siloxanes and alkanes were adopted by some researchers, their flammability hindered their further applications [15]. Though placing a heat transfer oil intermediate loop between the exhaust gas and the ORC system could address this issue [16], it would cause a large amount of the high-temperature waste heat unharnessed. Therefore, some other high-temperature loops for waste heat recovery were employed by researchers to couple with the ORC. Miller et al. [17] introduced thermoelectric generator (TEG) technology. High-temperature exhaust gas was first exploited by the TEG, then the cooled exhaust gas could drive the ORC safely. But the energy conversion capacity of TEG is low because of the material limitation. Steam Rankine for its high efficiency and stable operation attracted much attention of researchers. Shu et al. [18] placed a steam Rankine cycle between the ORC and the exhaust gas. Yu et al. [19] coupled a steam Rankine cycle with an ORC for the ICE waste heat recovery. However, the large bulk of the components in steam Rankine cycle limits further applications (such as application in vehicles) [20]. Considering the requirement of high thermal efficiency and compact configuration, Brayton cycle could be a compromise solution. Brayton cycle with CO_2 (carbon dioxide) as working fluid has the advantage of low environmental impact and good thermodynamic performance [21]. Few studies about ORC system coupled with CO_2 Brayton cycle (CBC) for ICE waste heat recovery have been published. Though Zhang et al. [20] carried out some relevant studies, their attention was focused on comparing the performance of CBC, TEG and steam Rankine cycle when coupled with the same bottom ORC. Detailed analysis of the CBC was not given and the energy in jacket water was not harnessed.

Jacket water, though containing large amounts of energy [22], obtained little attention in the previous studies. For its relatively low temperature, jacket water was mainly used to preheat the organic working fluid in the ORC system. In the ORC-based ICE waste heat recovery system designed by Zhang et al. [23] jacket water was used to preheat the organic working fluid. Then the organic working fluid was heat by the high-temperature exhaust gas to vapor state and expanded in the ORC turbine. In Yang's [24] ICE waste heat recovery system, jacket water and secondary exhaust gas were used to preheat the organic working fluids in ORC. In the dual-loop ORC based ICE waste heat recovery system investigated by Song et al. [25], jacket water was used to preheat the low-temperature-loop. Yu et al. [26] calculated the energy recovery efficiency from an ORC-based ICE waste heat recovery system. 75 % waste heat could be recovered from the exhaust gas, while only 9.5 % waste heat was recovery from jacket water. The relatively low utilization rate of jacket water energy in the ORC system is caused by the mismatch of working fluid mass flow rate in the preheater and the evaporator. Thus, the utilization of energy in jacket water could be further explored.

Multigeneration system driven by waste heat has drawn increasing interest of researchers in light of the trend towards reducing emissions, increasing the efficiency of energy use and providing variable energy. Li et al. [27] modeled a combined cooling, heating and power system to highly utilize the waste heat. Yari et al. [28] proposed a waste heat recovery system to provide power, distilled water and heat. Bai et al. [29] investigated a cooling, heating and power system driven by exhaust gas to recovery the waste heat. Combined cooling and power (CCP) systems driven by ICE waste heat were also investigated by some researchers. Chen et al. [30] designed an ammonia-water combined cooling and power system using the waste heat from the ICEs. Ammonia-water was heated by exhaust gas and jacket water. One part of the ammonia-water vapor flew into the turbine to provide power and the other part flew into the evaporator to provide refrigeration. Salek et al. [31] coupled an ammonia absorption refrigeration cycle and a bottoming Rankine cycle with internal combustion engine to produce power and cooling capacity.

Ammonia absorption refrigeration cycle (AARC) were widely used in the combined cooing and power system for its large refrigeration output. However, the complex cycle structure and high driven temperature requirement of AARC might sometimes limit its applications. On the contrary, ejector refrigeration cycle (ERC) exhibits the advantages of easy maintenance and high reliability [32] and it can be driven by low-temperature heat source such as the jacket water. Thus, ICE waste heat recovery system with ERC driven by jacket water not only simultaneously generate power and refrigeration but also fully utilized the jacket water waste heat.

In this study, a combined cooling and power system is developed, which comprises a CO_2 Brayton cycle, a dual-pressure organic Rankine (DORC) cycle and an ejector refrigeration cycle. The CO_2 Brayton cycle absorbs heat from the high-temperature exhaust gas directly to prevent the decomposition risk. The turbine exhaust in the CO_2 Brayton cycle and the engine exhaust gas after heat transfer are respectively regarded as the heat sources for the high-pressure side and low-pressure side of the dual-pressure ORC, realizing the cascading utilization of exhaust gas. Meanwhile, organic working fluids in high-pressure side and low-pressure side are both preheated by jacket water which increases the mass flow rate of the organic working fluid preheated by jacket water. What’s more, the ejector refrigeration cycle is adopted to produce refrigeration and fully utilize waste heat in jacket water. Thermodynamic and exergoeconomic analysis is carried out to examine the effects of key parameters on system performance. Then a system optimization is conducted to obtain the minimum levelized exergy cost for the system product by means of genetic algorithm (GA).

The innovative features of this paper are as follow:

- A CO_2 Brayton cycle is investigated to prevent the risk of decomposition of organic working fluid and provide power.
- A novel dual-pressure ORC system is developed to cascading utilize the waste heat in exhaust gas and jacket water and provide large amounts of power output.
- An ejector refrigeration cycle driven by jacket water is designed to provide refrigeration and fully utilize the jacket water waste heat.

2. System description

The combined cooling and power system is shown in Fig. 1. The system integrates a dual-pressure organic Rankine cycle with a CO_2 Brayton cycle and an ejector refrigeration, which can produce power and refrigeration simultaneously. High-temperature gas heat from the ICE enters the gas heater to provide heat for the CBC. In the CBC, compressor compresses the CO_2 to a supercritical state. The high-pressure CO_2 flows into the gas heater to absorb heat. Then CO_2 with high temperature and high pressure expands through the BC turbine to produce power.

After expanding in the BC turbine, the high-temperature exhaust CO_2 flows into vapor generator 2 to heat the organic working fluid. High-pressure side organic working fluid heated by the CO_2 then flows into the ORC turbine to produce power. Meanwhile low-pressure side organic working fluid absorbs heat from the secondary engine exhaust gas in vapor generator 1 and then enters ORC turbine to produce power.

Exhaust vapor from the ORC turbine is cooled by condenser 1 to liquid state and pressured by pump 1. Jacket water with large mass flow rate is used to preheat the organic working fluid in the preheater. The preheated organic working fluid then separates. One part of the fluid is pumped by pump 3 to the vapor generator 1 to cycle in the low-pressure side. The other part is pumped by pump 2 to the vapor generator 2 to cycle in the high-pressure side.

The jacket water then flows into vapor generator 3 to provide heat for the ejector refrigeration cycle. After the condensation process in condenser 2, liquid working fluid is divided into two separated parts. One part of the fluid is pumped to the vapor generator 3 to absorb heat from jacket water and then becomes superheated vapor. The other part of the working fluid flows through the throttle valve to become low-pressure vapor-liquid mixture. The low-pressure mixture enters the evaporator to produce cooling capacity when absorbing heat from the environment and become low-pressure vapor. After that, the superheated vapor mixes with the low-pressure vapor in the ejector. The mixed working fluid enters the condenser 2 to be condensed to liquid.

R245fa is selected as the working fluid for the organic Rankine cycle and the ejector refrigeration cycle because of the great thermodynamic performance [33] and the low environment effects [34].

3. System model

Several assumptions are made to simplify the simulation of the system, which are: (1) the system keeps a steady state; (2) the heat and frication in the system are not considered; (3) the pressure losses in the vapor generators, preheater, evaporator, condensers and pipes are neglected; (4) the gas temperature at the outlet of the vapor generator 1 is higher than 110 ℃ [35], considering the low gas dew point temperature; (5) the working fluids at the outlet of the condensers and the preheater are saturated liquids, and the evaporator outlet state is saturated vapor; (6) the process through the throttle valve is isenthalpic.

3.1.Energy model

The net power of the CO_2 Brayton cycle is expressed as:

$$W_{\mathrm{BC}} = W_{\mathrm{Bt}} - W_{\mathrm{comp}} \tag{1}$$

The net power of the DORC is given as:

$$W_{\mathrm{ORC}} = W_{\mathrm{Ot}} - W_{\mathrm{p1}} - W_{\mathrm{p2}} - W_{\mathrm{p3}} \tag{2}$$

The cooling capacity of the ERC is given as:

$$Q_{\mathrm{cool}} = M_{\mathrm{cool}} \cdot (h_{21} - h_{20}) \tag{3}$$

The net power output of the whole system is calculated as:

$$W_{\mathrm{net}} = W_{\mathrm{ORC}} + W_{\mathrm{BC}} - W_{\mathrm{p4}} \tag{4}$$

The thermal efficiency of the system is given as:

$$\eta_{\mathrm{th}} = \frac{W_{\mathrm{net}} + Q_{\mathrm{cool}}}{M_{\mathrm{g1}} \cdot (h_{\mathrm{g1}} - h_{\mathrm{g3}}) + M_{\mathrm{w1}} \cdot (h_{\mathrm{w1}} - h_{\mathrm{w3}})} \tag{5}$$

The detailed energy model equations of each component are list in Table 1. Note that there are two expanding processes in the ORC turbine. The high-pressure vapor expands in the turbine and then mixes with the vapor from vapor generator 1. After that, the mixed vapor expands in the turbine for the second time.

3.2.Exergy model

The energy model of the system is based on the first law of thermodynamics. From the viewpoint of the first law, it is equivalent for work and heat. Nevertheless, according to the second law of the thermodynamics, the irreversibility of work and heat is different. The exergy is used to quantifies the difference between them. The exergy model of the system is based on a dead state (the ambient condition in this study). Definition of exergy is given as:

$$e = (h - h_0) - T_0 \cdot (s - s_0) \quad (6)$$

where h_0, T_0 and s_0 are the parameters under the ambient conditions.

The exergy flow rate in this study is given by:

$$E = M \cdot e \quad (7)$$

In this study, all the components in the system are associated directly or indirectly with fuel of other heat sources, such as exhaust as and jacket water. The heat sources provide exergy for the components to operate. For each component, there is an exergy balance equation, being expressed as [36]:

$$E_F = E_P + E_D + E_L \quad (8)$$

where E_F, E_P, E_D, E_L donate the rate of exergy for the component fuel, the rate of exergy for component product, the rate of component exergy destruction and the rate of component exergy loss, respectively.

The details of the exergy balance equations for each component are listed in Table 1.

The exergy efficiency represents the degree of the utilization of the waste heat in the system, being expressed as:

$$\eta_{ex} = \frac{W_{net} + E_{cool}}{E_{g1} - E_{g3} + E_{w1} - E_{w3}} \tag{9}$$

where E_{cool} is the exergy rate of the cooling process, being expressed as:

$$E_{cool} = E_{25} - E_{24} \tag{10}$$

3.3.Capital cost calculation

A method of modeling the capital costs of main components is used in this study. According to Ref. [37], the bare module cost of the components is calculated as the basic cost. The basic cost of the components includes the direct project cost (such as component cost, material cost of the installation, etc.) and the indirect project cost (like the taxes, insurance engineering expenses, etc.). The bare module cost of the components is calculated under basic conditions. For deviations from the based conditions, multiplying factors (the specific component type, the specific system pressure and the specific material of construction) are added in the calculation to correct the results. In the following text, equations from Eq. (11) to Eq. (21) are proposed in Ref. [37].

Axial turbines (BC turbine and ORC turbine) are used in this study. The bare module cost equation of the turbine is:

$$\log_{10} C^0_{\text{turb}} = K_{1,\text{turb}} + K_{2,\text{turb}} \cdot \log_{10} W + K_{3,\text{turb}} \cdot (\log_{10} W)^2 \quad (11)$$

where $K_{\text{i, turb}}$ are constants corresponding to the turbine type; and W is the power output of the turbine.

Turbines used in this study are made of carbon steel (CS) and operate under high pressure. Thus, a multiplying factor is used to correct the result. The capital cost of the turbine is given as:

$$C_{\text{turb}} = F_{\text{BM,turb}} \cdot C^0_{\text{turb}} \quad (12)$$

where $F_{\text{BM,turb}}$ is the multiplying factor corresponding to the working conditions of the turbine.

Reciprocating pumps are used in this study. The bare module cost equation of the pumps is given as:

$$\log_{10} C^0_{\text{pump}} = K_{1,\text{pump}} + K_{2,\text{pump}} \cdot \log_{10} W + K_{3,\text{pump}} \cdot (\log_{10} W)^2 \quad (13)$$

where $K_{\text{i, pump}}$ are the constants corresponding to the pump type; and W is the power input of the pump.

Pumps used in this study are made of stainless steel (SS) and work under high pressure. Thus, multiplying factors are used to correct the bare module cost. The capital cost of the pump is given as:

$$C_{\text{pump}} = \left(B_{1,\text{pump}} + B_{2,\text{pump}} \cdot F_{\text{M,pump}} \cdot F_{\text{P,pump}} \right) \cdot C^0_{\text{pump}} \quad (14)$$

where $B_{\mathrm{i,\ pump}}$ are the constants corresponding to the type of the pump; $F_{\mathrm{M,pump}}$ is the material factor of the pump and $F_{\mathrm{P,pump}}$ is the pressure factor of the pump. The equation of the pressure factor is given as:

$$\log_{10} F_{\mathrm{P,pump}} = C_{1,\mathrm{pump}} + C_{2,\mathrm{pump}} \cdot \log_{10} P_{\mathrm{pump}} + C_{3,\mathrm{pump}} \cdot (\log_{10} P_{\mathrm{pump}})^2 \tag{15}$$

where $C_{\mathrm{i,\ pump}}$ are the constants corresponding to the type of the pump; and P_{pump} is the pressure of the pump under working conditions.

Axial compressor is used in this study. The bare module cost equation of the compressor is given as:

$$\log_{10} C^0_{\mathrm{comp}} = K_{1,\mathrm{comp}} + K_{2,\mathrm{comp}} \cdot \log_{10} W + K_{3,\mathrm{comp}} \cdot (\log_{10} W)^2 \tag{16}$$

where $K_{\mathrm{i,comp}}$ are the constants corresponding to the type of the compressor; W is the power input of the compressor.

The compressor is made of carbon steel (CS) and works under high pressure. Correction equation of the bare module cost is given as:

$$C_{\mathrm{comp}} = F_{\mathrm{BM,comp}} \cdot C^0_{\mathrm{comp}} \tag{17}$$

where $F_{\mathrm{BM,comp}}$ is the constant corresponding to the type of the compressor.

Shell-and-tube heat exchangers (gas heater, vapor generators, precooler, preheater, evaporator and condensers) are used in this study. The bare module cost equation of the heat exchanger is given as:

$$\log_{10} C^0_{\mathrm{he}} = K_{1,\mathrm{he}} + K_{2,\mathrm{he}} \cdot \log_{10} A + K_{3,\mathrm{he}} \cdot (\log_{10} A)^2 \tag{18}$$

where $K_{\mathrm{i,he}}$ are the constants corresponding to the type of the heat exchanger; A is the heat transfer area of the heat exchanger. The calculation of the heat exchanger areas is presented in Appendix A.

Heat exchangers used in this study are made of carbon steel (CS) and work under different pressure. Multiplying factors are needed to correct the results, the equation is given as:

$$C_{\mathrm{he}} = \left(B_{1,\mathrm{he}} + B_{2,\mathrm{he}} \cdot F_{\mathrm{M,he}} \cdot F_{\mathrm{P,he}}\right) \cdot C_{\mathrm{he}}^{0} \tag{19}$$

where $B_{\mathrm{i,he}}$ are the constants corresponding to the type of the heat exchanger. $F_{\mathrm{M,he}}$ and $F_{\mathrm{P,he}}$ are the material factor and pressure factor, respectively. The pressure factor is obtained from the following equation:

$$\log_{10} F_{\mathrm{P,he}} = C_{1,\mathrm{he}} + C_{2,\mathrm{he}} \cdot \log_{10} P_{\mathrm{he}} + C_{3,\mathrm{he}} \cdot (\log_{10} P_{\mathrm{he}})^2 \tag{20}$$

where $C_{\mathrm{i,he}}$ are the constants corresponding to the type of the heat exchanger; P_{he} is the designed working pressure for the heat exchanger.

The values of the constants mentioned above for the main components are listed in Appendix B.

The calculation of the bare module cost depends on past records or published correlations for price information. It is necessary to update the costs because of the inflation. This can be achieved by the following equation:

$$C_2 = C_1 \cdot \left(\frac{I_2}{I_1}\right) \tag{21}$$

where C is the purchased cost and I is the cost index. The subscript 1 refers to base time when cost is known and subscript 2 refers to time when cost is desired. The *CEPCI* (Chemical Engineering Plant Cost Index) is employed to calculate the inflation. The values of $CEPCI_{2016}$ and $CEPCI_{\mathrm{ref},2001}$ are 541.7 and 397, respectively [38].

3.4. Exergoeconomic model

Exergoeconomic is a branch of engineering which combines the thermodynamic analysis and economic principles. Thermodynamic performance and economic cost of the system are all taken into consideration.

To find the relationship between the present value of the expenditure and the equivalent annually levelized costs, the capital recovery factor (CRF) is employed, being expressed as [36]:

$$Z_{\mathrm{i}} = CRF \cdot C_{\mathrm{i}} \tag{22}$$

$$CRF = \frac{i_{\mathrm{eff}} \cdot (1+i_{\mathrm{eff}})^{n}}{(1+i_{\mathrm{eff}})^{n} - 1} \tag{23}$$

where i_{eff} is the effective discount rate with a value of 0.05 [39]; and n is the lifetime of the CCP system, being assumed as 30 years [40].

In order to calculate the equivalent annually levelized costs, the annual working time of the system is assumed as 8000 h [41]. Then the annual exergy rates and annual power output or consumption are obtained.

In a steady system, there are a number of entering and outing working fluid streams and heat and work interactions with the surroundings. In exergoeconomic analysis, each flowing stream is associated with a levelized exergy cost. The equations to calculate the cost of the stream product are given as:

$$C_{\mathrm{in}} = c_{\mathrm{in}} \cdot E_{\mathrm{y,in}} \tag{24}$$

$$C_{\mathrm{out}} = c_{\mathrm{out}} \cdot E_{\mathrm{y,out}} \tag{25}$$

$$C_{\mathrm{work}} = c_{\mathrm{work}} \cdot W_{\mathrm{y}} \tag{26}$$

$$C_{\text{heat}} = c_{\text{heat}} \cdot E_{\text{y,heat}} \tag{27}$$

where c denotes levelized exergy cost of the streams; $E_{\text{y,in}}$ and $E_{\text{y,out}}$ are the exergy transfer rate of the stream flowing in and out of a component; W_{y} and $E_{\text{y,heat}}$ are the power and the heat transfer rate of the components considering the annual working time.

The cost balance equation applied to the kth system component is given as:

$$\sum_{\text{out}} C_{\text{out,k}} + C_{\text{w,k}} = C_{\text{heat,k}} + \sum_{\text{in}} C_{\text{in,k}} + Z_{\text{k}} \tag{28}$$

Details of the cost balance equation are listed in Table 2.

The levelized exergy cost for system product is chosen to indicate the exergoeconomic performance, being expressed as [42,43]:

$$c_{\text{product}} = c_{\text{capital}} + c_{\text{fuel}} \tag{29}$$

where c_{capital} is the capital-cost-related part of the levelized exergy cost for the system product, being expressed as:

$$c_{\text{capital}} = \frac{Z_{\text{total}}}{W_{\text{net}} + E_{\text{cool}}} \tag{30}$$

where c_{fuel} is the fuel-cost-related part of the levelized exergy cost for the system product, being expressed as:

$$c_{\text{fuel}} = \frac{c_{\text{Bt}} \cdot W_{\text{y,comp}} + c_{\text{Ot}} \cdot W_{\text{y,pump1}} + c_{\text{Ot}} \cdot W_{\text{y,pump2}} + c_{\text{Ot}} \cdot W_{\text{y,pump3}} + c_{\text{Ot}} \cdot W_{\text{y,pump4}}}{W_{\text{net}} + E_{\text{cool}}} \tag{31}$$

where c_{Bt} and c_{Ot} are the levelized exergy cost for the BC turbine power output and the ORC turbine power output, which are calculated in Table 3. Likewise, they can be expressed as the capital-cost-related part and the fuel-cost-related part, given by Eq. (32) and Eq. (33).

$$c_{\mathrm{Bt}} = \frac{Z_{\mathrm{Bt}}}{W_{\mathrm{y,Bt}}} + \frac{c_3 \cdot \left(E_{\mathrm{y},3} - E_{\mathrm{y},4}\right)}{W_{\mathrm{y,Bt}}} \tag{32}$$

$$c_{\mathrm{Ot}} = \frac{Z_{\mathrm{Ot}}}{W_{\mathrm{y,Ot}}} + \frac{c_{10} \cdot \left(E_{\mathrm{y},10} + E_{\mathrm{y},11} - E_{\mathrm{y},12}\right)}{W_{\mathrm{y,Ot}}} \tag{33}$$

In addition, the levelized exergy cost for the condensers and the precooler is equal to zero, being given by:

$$c_{26}=c_{28}=c_{30}=0 \tag{34}$$

The levelized exergy cost for the exhaust gas as well as the jacket water is zero, being expressed as:

$$c_{g1}=c_{w1}=0 \tag{35}$$

3.5.Internal combustion engine

In this study, the engine selected [7] is a 12-cylinder 4-stroke supercharged engine. The main designed parameters of the engine are listed in Table 3. The composition of the engine exhaust gas is presented in Table 4. The thermal load of the engine exhaust gas is about 1700 kW and 1000 kW can be obtained from the engine jacket water.

3.6.Simulation conditions for the system

The thermodynamic parameters of the working fluid are calculated under the environment of MATLAB with the help of REFPROP 9.1 [44]. The basic conditions of simulation for the CCP system are listed in Table 5.

Seven key parameters : BC turbine inlet temperature ($T_{\mathrm{Bt,in}}$), BC turbine inlet pressure ($P_{\mathrm{Bt,\,in}}$), inlet temperature at the high-pressure side of ORC turbine ($T_{\mathrm{Ot,\,in,\,h}}$), inlet pressure at the high-pressure side of ORC turbine ($P_{\mathrm{Ot,\,in,\,h}}$), inlet temperature at the low-pressure side of ORC turbine ($T_{Ot, in, l}$), inlet pressure at the low-pressure side of ORC turbine ($P_{Ot, in, l}$) and the ejector primary inlet pressure ($P_{ej, in}$), are chosen to analyze the thermodynamic and exergoeconomic performance of the system. When one parameter is investigated to analyze the system performance, other parameters are maintained constants based on the conditions in Table 5.

In the thermodynamic aspect, the net power output of the CO_2 Brayton cycle (W_{BC}), net power output of the DORC (W_{ORC}), net power of the whole system (W_{net}), cooling capacity of the system (Q_{cool}) and the exergy efficiency of the system (η_{exergy}) are selected to reflect the system performance. Levelized exergy cost for the BC turbine power output (c_{Bt}), levelized exergy cost for the ORC turbine power output (c_{Ot}), levelized exergy cost the system product ($c_{product}$) and the system capital cost ($z_{capital}$) are chosen to represent the exergoeconomic performance.

4. Results and discussion

The influence of the BC turbine inlet temperature ($T_{Bt,in}$) on the output and the exergy efficiency of the system are shown in Fig. 2. The net power output of the CBC increases with the rise of $T_{Bt,in}$. That can be explained by the large decrease of the compressor power consumption. With the increase of the CO_2 temperature at the BC turbine inlet, the mass flow rate of CO_2 decreases, leading to the decrease of the compressor power consumption. Although the drop of CO_2 mass flow rate would cut down the BC turbine power output, the decrease quantity of compressor power consumption is larger than the decrease of the BC turbine power output. Thus, the large decrease of the compressor power consumption determines the increase trend of the CBC net power output.

It is presented that the net power output of the DORC increases with the rise of the BC turbine inlet temperature. Since the residual heat in exhaust CO_2 acts as the heat source for the high-pressure side of DORC, the temperature rise of the exhaust CO_2, caused by the rise of $T_{Bt,in}$, would offer more heat for the bottom cycle, which causes the increase of the mass flow rate of the organic working fluid in the high-pressure side of DORC . Hence, the power output of the ORC turbine increases, leading to the increase of the net power output of the DORC.

With the increase of $T_{Bt,in}$, the cooling capacity of the ERC decreases, as shown in Fig. 2. The increase of the organic working fluid mass flow rate in DORC would absorb more heat from jacket water, resulting in the decrease of energy available for the ERC. As a result, less secondary flow working fluid from the evaporator is entrained to the ejector, resulting the decrease of the cooling capacity of the CCP system.

The increase of the CBC net power output and the DORC net power output account for the increase of the net power output of the whole CCP system. Though the cooling capacity of the ERC is large, it produces only a small amount of exergy. The decrease of the exergy output caused by the cooling capacity drop can be made up by the increase of the power exergy output. Thus, the exergy efficiency of the system increases.

The influences of the BC turbine inlet temperature on the levelized exergy cost and the system capital cost of the system are shown in Fig. 3. The levelized exergy cost for the BC turbine power output (c_{Bt}) drops with the rise of the BC turbine inlet temperature ($T_{Bt,in}$). That can be explained by the decrease of the capital-cost-related part of c_{Bt}. The capital-cost-related part of c_{Bt} decreases with the decrease of cost of compressor, which is cut down by the drop of the compressor power consumption. The increase of the ORC turbine power output causes the decrease of both the capital-cost related part and the fuel-cost-related part of c_{Ot}, resulting in the decrease of c_{Ot}.

The system capital cost ($z_{capital}$) rises with the rise of $T_{Bt,in}$. The large increase of the ORC turbine power output increases the cost of the ORC turbine. Moreover, the increase of the mass flow rate of the organic working fluid in the DORC causes the increase of cost for the vapor generator 2 and the preheater. Though the cost of compressor decreases, it can’t change the ascending trend of the total system capital.

It can be obtained in Fig. 3 that the levelized exergy cost for the system product ($c_{product}$) decreases with the rise of $T_{Bt,in}$. The decline in levelized exergy cost for the BC turbine and ORC turbine power output, according to Eq. (31), would cause the decrease of the fuel-cost related part of $c_{product}$. Though the increase of $z_{capital}$ would cut down the capital-cost-related part of $c_{product}$, the impact of levelized exergy cost for the BC turbine and ORC turbine is greater, which leads to the descending trend of $c_{product}$.

The influence of the BC turbine inlet pressure ($P_{Bt, in}$) on the output and the exergy efficiency of the system are shown in Fig. 4. The net power output of the CBC increases with the increase of $P_{Bt, in}$, which can be explained by the rise of enthalpy drop of the CO_2 in the BC turbine. Though the rise of $P_{Bt, in}$ requires more compressor power consumption, the increase of the BC turbine power output is larger in quantity than the consumption, which leads to the increase of the CBC net power output.

The net power output of the DORC decreases with the rise of $P_{Bt, in}$. On the one hand, the temperature of the exhaust CO_2 at the BC turbine outlet decreases with the increase of $P_{Bt, in}$. Thus, less heat is offered to the high-pressure cycle of DORC, resulting in the decrease of the high-pressure cycle power output. On the other hand, the increase of $P_{Bt, in}$ causes the increase of the compressor power consumption, which results in the rise of the CO_2 temperature at the compressor outlet. Thus, less heat is released in the gas heater and more heat is provided to the low-pressure cycle of DORC, which leads to the increase of the low-pressure cycle power output. However, the increase of the power output in low-pressure side is smaller than the decrease of the power output in the high-pressure side. Thus, the net power of the DORC decreases slightly.

The cooling capacity of the system increases with the increase of $P_{Bt, in}$. Just like the variation of the power output, the decrease of the mass flow rate in the high-pressure side of DORC is larger than the increase of mass flow rate in the low-pressure side. Therefore, the total mass flow rate in the DORC decreases, resulting in the reduction of heat provided for the ejector refrigeration cycle. Thus, the cooling capacity of the ERC decreases.

The net power output of the whole system increases with the increase of the BC turbine inlet pressure. Though the net power output of the DORC decreases, the increase of CBC net power output is much larger. Thus, the net power output of the CCP system increases with the increase of $P_{Bt,\,in}$. The exergy efficiency of the system likewise has the same rising trend.

The influences of the BC turbine inlet pressure ($P_{Bt,\,in}$) on the levelized exergy cost and the system capital cost of the system are depicted in Fig. 5. The levelized exergy cost for the BC turbine output c_{Bt} increases with the rise of the $P_{Bt,\,in}$, which can be explained by the variations of the capital-cost-related part and the fuel-cost-related part. The increase of $P_{Bt,\,in}$ causes the increase of cost for both the BC turbine and the compressor, which lead to the rise of the two related parts.

The levelized exergy cost for the ORC turbine product (c_{Ot}) increases with the rise of $P_{Bt,in}$. The decrease of the mass flow rate in the DORC causes that less exergy is produced in vapor generator 2, causing the increase of the fuel-related part of c_{Ot}. Therefore, the levelized exergy cost for the ORC turbine (c_{Ot}) increases.

The system capital cost ($z_{capital}$) increases with the rise of ($P_{Bt,\,in}$). The increase of the mass flow rate in the ERC causes the rise of capital cost for the evaporator and vapor generator 3, which combined with the rise of the BC turbine cost and compressor cost accounts for the system capital cost rise.

The levelized exergy cost for the system product decreases with the rise of $P_{Bt,\,in}$ as presented in Fig. 5. According to Eq. (31), the rise of the c_{Ot}, c_{Bt} would cause the rise of the fuel-cost-related part of $c_{product}$. However, because of the large increase of the system net power output, the capital-cost-related part and the fuel-cost-related part decrease actually, which determines the decrease of $c_{product}$.

The influence of inlet temperature at the high-pressure side of ORC turbine ($T_{\mathrm{Ot,\,in,\,h}}$) on the output and the exergy efficiency of the system are shown in Fig. 6. The net power output of the CBC remains unchanged since thermal parameters in dual-pressure ORC are irrelevant to the thermodynamic performance of the CBC.

The net power output of the DORC decreases with the increase of $T_{\mathrm{Ot,\,in,\,h}}$. Though the increase of the vapor temperature could lead to the rise of the enthalpy drop in the ORC turbine, it would also cause the decrease of the mass flow rate in the high-pressure side, whose impact is greater than that of the enthalpy drop. Therefore, the power output of the DORC decreases.

The cooling capacity of the ejector refrigeration cycle increases with the rise of $T_{\mathrm{Ot,\,in,\,h}}$. More heat is provided for the ERC because of the decrease of the mass flow rate in the DORC, leading to the increase of the mass flow rate in vapor generator 3. Thus, more secondary flow from the evaporator is entrained into the ejector, resulting in the increase of the cooling capacity.

The net power output of the CCP system decreases with the rise of $T_{\mathrm{Ot,\,in,\,h}}$. The unchanged CBC power output and the drop of the DORC power output determine the decrease of the net power output of the CCP system. The exergy efficiency of the system as well drops with the increase of the increase of $T_{\mathrm{Ot,\,in,\,h}}$.

The influences of inlet temperature at the high-pressure side of ORC turbine on the levelized exergy cost and the system capital cost of the system are presented in Fig. 7. The levelized exergy cost for the ORC turbine output (c_{Ot}) increases with the increase of $T_{\mathrm{Ot,\,in,\,h}}$. The reason is that the two related parts of c_{Ot} increase with the drop of the

ORC turbine power output.

The levelized exergy cost for the BC turbine power output (c_{Bt}) increases with the rise the $T_{Ot, in, h}$. Since the decrease of the mass flow rate in the high-pressure side of DORC, the exergy generated in the vapor generator 2 decreases, causing the increase of the levelized exergy cost of the vapor. Thus, the increase levelized exergy cost of the vapor, which is heated by the BC turbine residual heat, causes the increase of the levelized exergy cost for the exhaust CO_2. According to Eq. (32), the fuel-cost-related part of c_{Bt} increases, leading to the increase of c_{Bt}.

The system capital cost ($z_{capital}$) decreases with the increase of $T_{Ot, in, h}$. The decrease of the DORC power output causes the drop of the ORC turbine cost, which leads to the descending trend of $z_{capital}$.

The levelized exergy cost for the system product ($c_{product}$) increases with the rise of $T_{Ot, in, h}$, as shown in Fig. 7. The increase of the levelized exergy cost for the BC turbine and ORC turbine power output cause the rise of fuel-cost-related part of $c_{product}$. Meanwhile, the large decrease of the net power of the CCP system causes the increase of the capital-cost-related part. The two increase parts determine the rise of $c_{product}$.

The influences of the inlet pressure at the high-pressure side of ORC turbine ($P_{Ot, in, h}$) on the output and exergy efficiency of the system are presented in Fig. 8. The net power of the CBC keeps unchanged because of the unchanged thermal parameters in the cycle.

The net power output of the DORC increase with the rise of $P_{Ot, in, h}$. The increase of the evaporation pressure cuts down the latent heat of the organic working fluid, which causes the increase of the mass flow rate in the high-pressure side of DORC. As a result, the net power output of the ORC turbine increases, leading to the increase of the net power output of the DORC.

Considering the increase of the DORC net power output and the unchanged CBC net power output, the net power output of the whole system increases. Also, the exergy efficiency of the system increases.

The increase of the mass flow rate in the DORC absorbs more heat from the jacket water in the preheater. Thus, less heat is released in the vapor generator 3, causing the decrease of the mass flow rate of the working fluid in the ERC. As a result, the cooling capacity of the system decreases.

The influence of the inlet pressure at the high-pressure side of the ORC turbine ($P_{Ot, in, h}$) on the levelized exergy cost and system capital cost of the system are presented in Fig. 9. The large increase of the ORC turbine power output accounts for the decrease of the levelized exergy cost for the ORC turbine power output (c_{Ot}). The increase of the mass flow rate in the high-pressure side of DORC means that more exergy in the vapor is generated by the vapor generator 2, which leads to the decrease of its levelized exergy cost. Thus, the levelized exergy cost for the BC turbine exhaust CO_2, which provides heat for the vapor, decreases with the vapor levelized exergy cost. Moreover, the drop of the CO_2 levelized exergy cost causes the decrease of the fuel-cost-related part of c_{Bt}, which further results in the decrease of c_{Bt}.

The increase of the ORC turbine power output and the increase of mass flow rate in the DORC cause the increase of cost for the turbine and the vapor generator 2, leading to the rise of the system capital cost.

The levelized exergy cost for the system product ($c_{product}$) decreases with the increase of $P_{Ot, in, h}$. The decrease of c_{Ot} and c_{Bt} account for the decrease of the fuel-cost-related part of the levelized exergy for the system product. The impact of c_{Ot} and c_{Bt} is greater than that of the system capital cost which would result in the increase of the capital-cost-related part of $c_{product}$. Thus, the levelized exergy cost of the system product ($c_{product}$) shows a descending trend.

The influences of the inlet temperature at the low-pressure side of ORC turbine ($T_{Ot, in, l}$) on the output and the exergy efficiency of the system are presented in Fig. 10. Parameters changes in the DORC are irrelevant to the thermodynamic performance of the CBC. Thus, the net power of the CBC remains unchanged.

The net power output of the DORC decreases with the increase of $T_{Ot, in, l}$. The increase of the inlet temperature causes the decrease of the mass flow rate in the low-pressure side of the DORC, leading to the decrease of the DORC net power output.

Considering the decrease of the DORC net power output and the unchanged CBC net power output, the net power output of the whole system deceases. Likewise, the exergy efficiency of the system decreases.

The cooling capacity of the ejector refrigeration cycle increases with the increase of $T_{Ot, in, l}$. The decrease of the mass flow rate in the low-pressure side means that more heat is offered to the ERC. Thus, the mass flow rate of the working fluid in the vapor generator 3 increases and more working fluid is entrained to the ejector from the evaporator, which leads to the increase of the refrigeration cycle.

The influence of inlet temperature at the low-pressure side of the ORC turbine ($T_{Ot, in, 1}$) on the levelized exergy cost and system capital cost of the system are presented in Fig. 11. The levelized cost for the BC turbine power output increase with the increase of $T_{Ot, in, 1}$. The decrease of the mass flow rate in the vapor generator 1 leads to the drop of the vapor exergy output, which results in the increase of the levelized exergy cost for the vapor. The levelized exergy cost for vapor in vapor generator 2, which is the equal to that of the vapor in vapor generator 1, increases as a result, causing the increase of the levelized exergy cost of the exhaust CO_2 after the BC turbine. Thus, the fuel-cost-related part of c_{Bt} increases, resulting in the rise of c_{Bt}.

The levelized exergy cost for the ORC turbine (c_{Ot}) increases with the increase of $T_{Ot, in, 1}$. That can be explained by the increase of the levelized exergy cost of the ORC low-pressure inlet vapor and the decrease of the power output of the ORC turbine power output. Both the fuel-cost-related part and the capital-cost-related part of c_{Ot} increases.

The decrease of the mass flow rate and the ORC turbine power output cause the decrease of the vapor generator 1 cost and the turbine cost. Thus, the capital cost of the system decreases.

The levelized exergy cost for the system product increases with the increase of $T_{Ot, in, 1}$. The increase of c_{Bt} and c_{Ot} cause the increase of the fuel-cost-related part of the levelized exergy cost for the system product. Though of, the decease of the system capital cost causes the decrease of the capital-cost-related part, its effect is less important. Thus, the increase of the fuel-cost-related part determines the increase of the levelized exergy cost for the system product.

The influences of the inlet temperature of the low-pressure side of the ORC turbine ($P_{Ot,\ in,\ l}$) on the output of the exergy efficiency of the system are shown in Fig. 12. The net power of the CBC keeps unchanged with the increase of the increase of the low evaporation pressure. The reason is that the thermodynamic of the CBC is irrelevant to the thermal parameters in DORC.

The net power output of the DORC increases with the rise of $P_{Ot,\ in,\ l}$. The increase of enthalpy drop of the organic working fluid in the low-pressure side, which is caused by the rise of $P_{Ot,\ in,\ l}$, results in the increase of the power output of the low-pressure side. Though mass flow rate in the low-pressure side would decrease, its impact is less important than that of the enthalpy drop. Thus, the net power output of DORC increases.

The unchanged CBC power output and the increase of the DORC power accounts for the increase of the system net power output and exergy efficiency of the system.

The cooling capacity increases slightly with the increase of $P_{Ot,\ in,\ l}$. Because of the decrease of the mass flow rate in DORC, less heat is released in the preheater and more heat is provided in vapor generator 3. Thus, the mass flow rate of the working fluid in the ERC increases, resulting in the slight increase of the cooling capacity.

The influences of inlet pressure at the low-pressure side of the ORC turbine ($P_{Ot,\ in,\ l}$) on the levelized exergy cost and system capital cost of the system are shown in Fig. 13. The levelized exergy cost for the ORC turbine power output decreases with the increase of $P_{Ot, in, 1}$. That can be explained by the decrease of the vapor generator 1 cost, caused by the decrease of the mass flow rate in DORC, and the increase of the DORC power output. Both the capital-cost-related part and the fuel-cost-related part of c_{Ot} decrease.

The levelized exergy cost for the BC turbine power output decreases with of $P_{Ot, in, 1}$. The decrease of the c_{Ot} causes the drop of levelized exergy cost for the vapor in vapor generator 2, which is heated by the residual heat in the BC turbine exhaust CO_2. Thus, the levelized exergy cost of the exhaust CO_2 decreases, which further leads to the drop of the fuel-cost-related part of c_{Bt}. Therefore, the levelized exergy cost for the BC turbine power output (c_{Bt}) decreases, as shown in Fig. 13.

The increase of the ORC turbine power output causes the increase of the ORC turbine cost. Meanwhile, the increase of the cooling capacity causes the increase of the heat transfer area in the evaporator which requires the rise of the evaporator cost. Thus, the capacity cost of the system increases.

The levelized exergy cost for the system product decreases with the increase of $P_{Ot, in, 1}$. The decrease of the levelized exergy cost for the BC turbine power output and ORC turbine power cause the decrease of the fuel-cost-related part of the system levelized exergy cost, which determined the decrease of the levelized exergy cost for the system product.

The influence of ejector primary inlet pressure ($P_{ej, in}$) on the output and the exergy efficiency of the system are shown in Fig. 14. Thermal parameter changes in the ERC can't affect the thermodynamic performance of the CBC and DORC. Thus, the net power output of the two cycles remain unchanged. With the increase of the ejector primary inlet pressure, the power consumption of pump 4 increases, leading to the slight decrease of the power output of the whole system.

The increase of the ejector primary inlet pressure causes the increase of the entrainment ratio of the ejector. Thus, more secondary flow is entrained to the ejector from the evaporation, leading to the increase of the cooling capacity.

With the increase of the ejector primary inlet pressure, the power consumption of pump 4 increases gradually. At first, the exergy loss in pump 4 is smaller than the exergy produced by the cooling capacity. Then, with the increase of the pump power consumption, the exergy loss in pump 4 becomes larger than the cooling exergy increase. Thus, the exergy efficiency for the system increases at first and then decreases with the increase of the ejector primary inlet pressure.

The influence of the ejector primary inlet pressure on the levelized exergy cost and the system capital cost of the system are presented in Fig. 15. The increase of the ejector primary inlet pressure can’t affect the power output of the BC turbine and the ORC turbine. Thus, the levelized exergy cost for the BC turbine and the ORC power output remain unchanged.

The increase of the pump power consumption results in the increase of the pump 4 cost. The increase of the mass flow rate in the evaporator causes the increase of the evaporator cost. Thus, the system capital cost increases, which leads to the increase of the capital-cost-related part of c_{product}. As a result, the levelized exergy cost for the system increases.

The parametric analysis reveals the potential of optimization for the CCP system. With the increase of the BC turbine inlet temperature, the net power output of the system increases while the cooling capacity decreases. With the increase of the inlet temperature at the high-pressure side of ORC turbine, the net power output of the system decreases while the cooling capacity increases. In this study, seven key parameters (BC turbine inlet temperature, BC turbine inlet pressure, inlet temperature at the high-pressure side of ORC turbine, inlet pressure at the high-pressure side of ORC turbine, inlet temperature at the low-pressure side of ORC turbine, inlet pressure at the low-pressure side of ORC turbine and the ejector primary inlet pressure) are chosen as the variables to optimize the system. The ranges of these parameters are listed in Table 6.

Considering that the levelized exergy cost reflects the thermodynamic and the exergoeconomic aspect of the system, the levelized exergy cost for the system product is selected as the objective function and genetic algorithm is selected to conduct the single-objective optimization.

Genetic algorithm (GA) is an optimization method based on the natural biological evaluation. [45] It simulates the natural genetic rules and searches the optimization result in all the generation. The control parameters of the GA are listed in Table 7.

The optimization results of GA are listed in Table 8. It can be obtained that the minimum levelized exergy cost for the system product $c_{product}$ is 53.25 \$(MWh)$^{-1}$. The net power output, exergy efficiency of the CCP system are 374.37 kW, 37.31 % respectively. The inlet pressure at the high-pressure side of ORC turbine is 1.85 MPa.

Meanwhile, it can be evidenced from Fig. 8 and 9 that the highest output power (about 374.37 kW), exergy efficiency (about 37.31 %) and the lowest levelized exergy cost (about 53.25 $\$(MWh)^{-1}$) at the highest inlet pressure at the high-pressure side ORC turbine (about 1.85 MPa). The results shown in Fig. 8 and 9 are close to the optimization results. The inlet pressure at the high-pressure side ORC turbine is varied while other six parameters are kept as constants in Fig. 8 and 9. Thus, inlet pressure at the high-pressure side ORC turbine plays a more important role than other six parameters when determining the performance of the system. When the inlet pressure at the high-pressure side ORC turbine is close to the highest permitted pressure, the system performance is close to the optimization performance.

Fig. 16 shows the exergy destruction of different components of the system under the optimization conditions. The largest exergy destruction takes place in the ORC turbine (41.26 %), which is mainly caused by the mixing of the high-pressure vapor and the low-pressure vapor. Gas heater contributes 13.44 % of the total exergy destruction. Three vapor generators take up 4.13 %, 11.67 % and 3.73 % of the exergy destruction, respectively. The exergy destruction for the ejector is 5.61 %, which is also caused by the working fluid mixing. For BC turbine, condenser 1, precooler and preheater, the exergy destruction are 3.31 %, 4.64 %, 3.69 % and 3.65 %, respectively. Other components contribute to the rest 4.87 % of the exergy destruction.

5. Conclusion

In this paper, a combined cooling and power system is developed. Seven parameters are selected to analyze the thermodynamic and exergoeconomic performance of the system. Single-objective optimization is carried out with the help of GA. The conclusions of the study are presented as follows:

(1) In the CBC, the increase of $T_{\mathrm{Bt,in}}$ and $P_{\mathrm{Bt,\,in}}$ contribute to the increase of the system exergy efficiency and the decrease of the levelized exergy cost for the system product.

(2) In the DORC, the increase of $T_{\mathrm{Ot,\,in}}$ and $T_{\mathrm{Ot,\,in,\,l}}$ would cause the decrease of the system exergy efficiency and the increase of the levelized exergy cost for the system product. Meanwhile, the increase of $P_{\mathrm{Ot,\,in,\,h}}$ and $P_{\mathrm{Ot,\,in,\,l}}$ would result in the increase of the exergy efficiency and the decrease of the levelized exergy cost.

(3) In the ERC, the increase of $P_{\mathrm{ej,\,in}}$ would cause the increase of the refrigeration capacity and the decrease of the system net power output.

(4) Single -objective optimization results show that the minimum levelized exergy cost for the system product is obtain as 53.25 \$(MWh)$^{-1}$ with net power output of 374.37 kW, cooling capacity of 188.63 kW and system exergy efficiency of 37.31 %.

Acknowledgement

The authors gratefully acknowledge the financial support by the National Natural Science Foundation of China (Grant No. 51476121)

Appendix A

This section shows the calculation of the heat transfer area in the heat exchangers used in this study.

All the heat exchangers used in this study are shell-and-tube heat exchanger. The thermodynamic properties of the working fluid vary with the heat transfer process. Thus, to calculate the heat transfer area actually, the heat transfer processes are discretized into a lot of small sections. In each section, the heat transfer area is small and the thermodynamic properties are assumed to be constant.

For each section the heat transfer area is calculated as:

$$A_{\mathrm{i}} = Q_{\mathrm{i}} \big/ \left(\Delta T_{\mathrm{i}} \cdot U_{\mathrm{i}}\right) \tag{B1}$$

where ΔT_{i} is the log-mean temperature difference (LMTD) and U_{i} is the overall heat transfer coefficient.

$$\frac{1}{U_{\mathrm{i}}} = \frac{1}{\alpha_{\mathrm{t,i}}} + \frac{\delta}{\lambda} + \frac{1}{\alpha_{\mathrm{s,i}}} \tag{B2}$$

In Eq. (B2) δ and λ represent the thickness of the tube and the thermal conductivity of the tube wall, respectively. $\alpha_{\mathrm{t,i}}$ is the convection heat transfer coefficient in the tube side and $\alpha_{\mathrm{s,i}}$ is the convection heat transfer coefficient in the shell side.

For different heat transfer process, the convection heat transfer coefficient has different format. We classify the heat transfer processes into single-phase heat transfer process and two-phase heat transfer process. In gas heater, precooler and the preheater, single-phase heat transfer process happens. In evaporator, two-phase heat transfer process occurs. In vapor generators and the condensers, both the single-phase and the two-phase heat transfer process happen.

In the single-phase heat transfer process, the convection heat transfer coefficient in the tube side and the shell side are expressed as [46]:

$$\alpha_{\mathrm{t,i}} = \frac{\lambda \cdot Nu}{D_{\mathrm{i}}} \tag{B3}$$

$$\alpha_{\mathrm{s,i}} = 0.36\left(\frac{\lambda}{D_{\mathrm{es}}}\right)\cdot\left(\frac{D_{\mathrm{es}}\cdot G_{\mathrm{s}}}{\mu}\right)^{0.55}\cdot \mathrm{Pr}^{\frac{1}{3}}\cdot\left(\frac{\mu}{\mu_{\mathrm{w}}}\right)^{0.14} \tag{B4}$$

In Eq. (B3), the Nusselt number is calculated as [47,48]:

$$Nu = \left[\frac{(f/8)\cdot \mathrm{Re}\cdot \mathrm{Pr}}{12.7(f/8)^{0.5}\cdot\left(\mathrm{Pr}^{2/3}-1\right)+1.07}\right],\quad for\ \mathrm{Re}<10^4 \tag{B5}$$

$$Nu = \left[\frac{(f/8)\cdot(\mathrm{Re}-1000)\cdot \mathrm{Pr}}{12.7(f/8)^{0.5}\cdot\left(\mathrm{Pr}^{2/3}-1\right)+1.07}\right],\ for\ 10^4<\mathrm{Re}<5\times10^6 \tag{B6}$$

where f is the Darcy friction factor, Re is the Reynolds and Pr is the Prandtl number.

In Eq. (B4), D_{es} is the equivalent diameter of the shell, being expressed as:

$$D_{\mathrm{es}} = \frac{1.10\mathrm{Pt}^2}{D_{\mathrm{out,i}}} - D_{\mathrm{out,i}} \tag{B7}$$

where Pt is the center distance between the tubes.

Evaporation and condensation are two different two-phase heat transfer processes. In this study, the cold organic working fluid flows in the tubes of the heat exchangers. The convection heat transfer coefficient of evaporation and condensation are expressed as [49,50]:

$$\alpha_{\mathrm{ev,i}} = 0.023\left[\frac{G(1-x)}{\mu_{\mathrm{l}}}\right]^{0.8}\cdot \mathrm{Pr}_{\mathrm{l}}^{0.4}\cdot\frac{\lambda_{\mathrm{l}}}{d}\cdot\left[1+3000Bo^{0.86}+1.12\left(\frac{x}{1-x}\right)^{0.75}\cdot\left(\frac{\rho_{\mathrm{l}}}{\rho_{\mathrm{v}}}\right)^{0.41}\right] \tag{B8}$$

$$\alpha_{\mathrm{cond,i}} = 0.023\left[\frac{G(1-x)}{\mu_{\mathrm{l}}}\right]^{0.8}\cdot \mathrm{Pr}_{\mathrm{l}}^{0.4}\cdot\frac{\lambda_{\mathrm{l}}}{d}\cdot\left[(1-x)^{0.8}+\frac{3.8x^{0.76}(1-x)0.04}{P_r^{0.38}}\right] \tag{B9}$$

In Eq. (B9), P_r is the reduced pressure. In Eq. (B8) Bo is the boiling number, being expressed as:

$$Bo = \frac{q_{\mathrm{m}}}{G \cdot r_{\mathrm{f}}} \tag{B10}$$

Appendix B

The constants for component capital cost calculation are list in Table B1.

Reference

[1] Abdul-Wahhab H, Al-Kayiem H, Aziz A, Nasif M. Survey of invest fuel magnetization in developing internal combustion engine characteristics. Renew Sustain Energy Rev 2017; 79:1392-99.

[2] Heywood J. B. Internal combustion engine fundamentals. New York: McGraw-Hill; 1988.

[3] Chao H, Chao L, Hong G, Hui X, You L, Shuang W. The optimal evaporation temperature and working fluids for subcritical Organic Rankine Cycle. Energy 2012; 38: 136-143.

[4] Tian H, Shu G, Wei H, Liang X, Liu L. Fluids and parameters optimization for the organic Rankine cycles (ORCs) used in exhaust heat recovery of Internal Combustion Engine (ICE). Energy 2012; 47: 125-136.

[5] Rijpkema J, Munch K, Andersson S. Thermodynamic potential of twelve working fluids in Rankine and flash cycles for waste heat recovery in heavy duty diesel engines. Energy 2018; 160:996-1007.

[6] Su X, Shedd T A. Towards working fluid properties and selection of Rankine cycle based waste heat recovery (WHR) systems for internal combustion engines – A

fundamental analysis. Appl Therm Eng 2018; 142:502-10.

[7] Vaja I, Gambarotta A. Internal Combustion Engine (ICE) bottoming with Organic Rankine Cycles (ORCs). Energy 2010; 35(2):1084-93.

[8] Kim M, Shin G, Kim G, Cho B. Single-loop organic Rankine cycle for engine waste heat recovery using both low-and high-temperature heat sources. Energy 2016; 96:482-94.

[9] Ringer J, Seifert M, Guyotot V, Hübner W. Rankine cycle for waste heat recovery of IC engines. SAE. 2009. 2009-01-0174.

[10] Wang X, Shu G, Tian H, Liu P, Jing D, Li X. Dynamic analysis of the dual-loop Organic Rankine Cycle for waste heat recovery of a natural gas engine. Energy Convers Manage 2017; 148:724-736.

[11] Wang E, Yu Z, Zhang H, Yang F. A regenerative supercritical dual-loop organic Rankine cycle system for energy recovery from the waste heat of internal combustion engines. Appl Energy 2017; 190:574-90.

[12] Huang H, Zhu J, Deng W, Ouyang T, Yan B, Yang X. Influence of exhaust heat distribution on the performance of dual-loop organic Rankine Cycle (DORC) for waste heat recovery. Energy 2018; 151:54-65.

[13] Rajabloo T, Bonalumi D, Lora P. Effect of a partial thermal decomposition of the working fluid on the performances of ORC power plants. Energy 2017; 133:1013-26.

[14] Shi L, Shu G, Tian H, Deng S. A review of modified Organic Rankine cycles (ORCs) for internal combustion engine waste heat recovery (ICE-WHR). Renew Sustain Energy Rev 2018; 92:95-110.

[15] El-Harbawi M, Shaaran S, Ahmad F, Wahi M, Abdul A, Larid D, Yin C. Estimating the flammability of vapours above refinery wasterwater laden with hydrocarbon mixtures. Fire Safety J 2012; 51:61-67.

[16] Wang X, Tian H, Shu G. Part-load performance prediction and operation strategy design of organic Rankine cycles with a medium cycle used for recovering waste heat from gaseous fuel engines. Energies 2016; 9: 527.

[17] Miller E, Hendricks T, Wang H, Peterson R. Integrated dual-cycle energy recovery using thermoelectric conversion and an organic Rankine bottoming cycle. Proceedings of the Institution of Mechanical Engineers, Part A: J Power Energy 2011; 225:33-43.

[18] Shu G, Wang X, Tian H. Theoretical analysis and comparison of Rankine cycle and different organic Rankine cycles as waste heat recovery system for a large gaseous fuel internal combustion engine. Appl Therm Eng 2016; 108:525-37.

[19] Yu G, Shu G, Tian H, Huo Y, Zhu W. Experimental investigations on a cascaded steam-/organic-Rankine-cycle (RC/ORC) system for waste heat recovery (WHR) from diesel engine. Energy Convers Manage 2016; 129:43-51.

[20] Zhang C, Shu G, Tian H, Wei H, Liang X. Comparative study of alternative ORC-based combined power systems to exploit high temperature waste heat. Energy Convers Manage 2015; 89:541-54.

[21] Galindo J, Guardiola C, Dolz V, Kleut P. Further analysis of a compression-expansion machine for a Brayton Waste Heat Recovery cycle on an IC engine. Applied Thermal Engineering 2018; 128: 345-356.

[22] Ma J, Liu L, Zhu T, Zhang T. Cascade utilization of exhaust gas and jacket water waste heat from an Internal Combustion Engine by a single loop Organic Rankine Cycle system. Appl Therm Eng 2016; 107:218-26.

[23] Zhang H G, Wang E H, Fan B Y. A performance analysis of a novel system of a dual loop bottoming organic Rankine cycle (ORC) with a light-duty diesel engine. Applied Energy 2013;102: 1504-1513.

[24] Yang F, Cho H, Zhang H, Zhang J. Thermoeconomic multi-objective optimization of a dual loop organic Rankine cycle (ORC) for CNG engine waste heat recovery. Applied Energy 2017; 205: 1100-1118.

[25] Song J, Gu C. Parametric analysis of a dual loop Organic Rankine cycle (ORC) system for engine waste heat recovery. 2015; 105:995-1005.

[26] Yu G, Shu G, Tian H, Wei H, Liu L. Simulation and thermodynamic analysis of a bottoming Organic Rankine Cycle (ORC) of diesel engine (DE). Energy 2013; 51:281-90.

[27] Li Fan, Sun Bo, Zhang C, Zhang L. Operation optimization for combined cooling, heating, and power system with condensation heat recovery. Appl Energy 2018; 230:305-16.

[28] Yari Mortaza, Ariyanfar Leyli, Aghdam EA. Analysis and performance assessment of a novel ORC based multigeneration system for power, distilled water and heat. Renew Energy 2018; 119:262-81.

[29] Bai Z, Liu T, Liu Q, Lei J, Gong L, Jin H. Performance investigation of a new cooling, heating and power system with methanol decomposition based chemical

recuperation process. Appl Energy 2018; 229: 1152-63.

[30] Chen Y, Han W, Jin H. Investigation of an ammonia-water combined power and cooling system driven by the jacket water and exhaust gas heat of an internal combustion engine. International Journal of Refrigeration 2017; 82: 174-188.

[31] Salek F, Moghaddam A, Naserian M. Thermodynamic analysis of diesel engine coupled with ORC and absorption refrigeration cycle. Energy Conversion and Management 2017; 140: 240-246.

[32] Wang J, Dai Y, Sun Z. A theoretical study on a novel combined power and ejector refrigeration cycle. Int J Refrig 2009; 32(6):1186-94.

[33] Dai Y, Wang J, Gao L. Parametric optimization and comparative study of organic Rankine cycle (ORC) for low grade waste heat recovery. Energy Convers Manage 2009; 50:576-82.

[34] Shu G, Zhao M, Tian H, Huo Y, Zhu W. Experimental comparison of R123 and R245fa as working fluids for waste heat recovery from heavy-duty diesel engine. Energy 2016; 115:756-69.

[35] Zhang J, Zhang H, Yang K, Yang F, Wang Z, Zhao G, Liu H, Wang E, Yao B. Performance analysis of regenerative organic Rankine cycle (RORC) using the pure working fluid and the zeotropic mixture over the whole operating range of a diesel engine. Energy Convers Manage 2014; 84:282-94.

[36] Bejan A, Tsatsaronis G, Moran M. Thermal design and optimization. New York: John Wiley & Sons; 1996.

[37] Turton R, Bailie RC, Whiting WB, Shaeiwitz JA. Analysis, synthesis, and design

of chemical processes. 3rd ed. Upper Saddle River, N.J: Prentice Hall; 2009.

[38] Li J, Ge Z, Liu Q, Duan Y, Yang Z. Thermo-economic performance analyses and comparison of two turbine layouts for organic Rankine cycles with dual-pressure evaporation. Energy Conversion and Management, 2018; 164: 603-614.

[39] Sheng Z, Huai W, Tao G. Performance comparison and parametric optimization of subcritical organic Rankine cycle (ORC) and transcritical power cycle system for low-temperature geothermal power generation. Appl Energy 2011;88(8):2740-54.

[40] Tempesti D, Fiaschi D. Thermo-economic assessment of a micro CHP system fueled by geothermal and solar energy. Energy 2013; 58: 45-51.

[41] Velez F, Segovia JJ, Martin MC, Antonlin G, Chejne F, Quijano A. A technical, economical and market review of organic Rankine cycles for the conversion of low-grade heat for power generation. Renew Sustain Energy Rev 2012; 16:4175-89.

[42] Akbari D, Mahmoudi M. Thermoeconomic analysis & optimization of the combined supercritical CO2 (carbon dioxide) recompression Brayton/ organic Rankine cycle. Energy 2014; 78:501-12.

[43] Zare V, Mahmoudi M, Yari M. An exergoeconomic investigation of waste heat recovery from the Gas Turbine-Modular Helium Reactor (GT-MHR) employing an ammonia–water power/cooling cycle. Energy 2013;61. 397-409.

[44] Lemmon EW, Huber ML, McLinden MO. NIST standard reference database 23, reference fluid thermodynamic and transport properties (REFPROP). Version 9.1. National Institute of Standards and Technology; 2010

[45] Wang J, Dai Y, Gao L. Parametric analysis and optimization for a combined

power and refrigeration cycle. Appl Energy 2008;85(11):1071-85.

[46] Kern DQ. Process heat transfer. New York: McGraw-Hill; 1950

[47] Kandylas IP, Stamatelos AM. Engine exhaust system design based on heat transfer computation. Energy Convers Manage 1999; 40:1057-72.

[48] Incropera FP, DeWitt DP. Fundamentals of heat and mass transfer. New York: Wiley; 2002

[49] Gungor KE, Winterton RHS. Simplified general correlation for saturated flow boiling and comparisons of correlations with data. Chem Eng Res and Des, 1987; 65:148-56.

[50] Shah MM. A general correlation for heat transfer during film condensation inside pipes. Int J Heat Mass Transf 1979; 22:547-56.

Figure captions

Fig. 1. Schematic diagram of the CCP system

Fig. 2. Influences of BC turbine inlet temperature on the output and the exergy efficiency of the system.

Fig. 3. Influences of BC turbine inlet temperature on the levelized exergy cost and the system capital cost of the system.

Fig. 4. Influences of BC turbine inlet pressure on the output and the exergy efficiency of the system.

Fig. 5. Influences of BC turbine inlet pressure on the levelized exergy cost and the system capital cost of the system.

Fig. 6. Influences of inlet temperature at the high-pressure side of ORC turbine on the output and the exergy efficiency of the system.

Fig. 7. Influences of inlet temperature at the high-pressure side of ORC turbine on the levelized exergy cost and the system capital cost of the system.

Fig. 8. Influences of inlet pressure at the high-pressure side of ORC turbine on the output and the exergy efficiency of the system.

Fig. 9. Influences of inlet pressure at the high-pressure side of ORC turbine on the levelized exergy cost and the system capital cost of the system.

Fig. 10. Influences of inlet temperature at the low-pressure side of ORC turbine on the output and the exergy efficiency of the system.

Fig. 11. Influences of inlet temperature at the low-pressure side of ORC turbine on the levelized exergy cost and system capital cost of the system.

Fig. 12. Influences of inlet pressure at the low-pressure side of ORC turbine on the output and the exergy efficiency of the system.

Fig. 13. Influences of inlet pressure at the low-pressure side of ORC turbine on the levelized exergy cost and system capital cost of the system.

Fig. 14. Influences of ejector primary inlet pressure on the output and the exergy efficiency of the system.

Fig. 15. Influences of ejector primary inlet pressure on the levelized exergy cost and the system capital cost of the system.

Fig. 16. Exergy destruction of different components

Table 1 Energy and exergy models for each component in CCP system

Component	Energy equation	E_F	E_P	E_D	E_L
Gas heater	$M_{g1}\cdot(h_{g1}-h_{g2})=M_2\cdot(h_3-h_2)$	$E_{g1}-E_{g2}$	E_3-E_2	$E_{g1}+E_2-E_3-E_{g2}$	/
BC turbine	$W_{Bt}=M_3\cdot(h_3-h_4)=M_3\cdot(h_3-h_{4s})\cdot\eta_{Bt}$	E_3-E_4	W_{Bt}	$E_3-E_4-W_{Bt}$	/
Vapor generator 2	$M_4\cdot(h_4-h_5)=M_9\cdot(h_{10}-h_9)$	E_4-E_5	$E_{10}-E_9$	$E_4+E_9-E_5-E_{10}$	/
Precooler	$M_1\cdot(h_5-h_1)=M_{26}\cdot(h_{27}-h_{26})$	/	/	$E_5+E_{26}-E_1-E_{27}$	$E_{27}-E_{26}$
Compressor	$W_{comp}=M_1\cdot(h_2-h_1)=M_1\cdot(h_{2s}-h_1)/\eta_{comp}$	W_{comp}	E_2-E_1	$E_1-E_2+W_{comp}$	/
Vapor generator 1	$M_{g2}\cdot(h_{g2}-h_{g3})=M_8\cdot(h_{11}-h_8)$	$E_{g2}-E_{g1}$	$E_{11}-E_8$	$E_{g2}+E_8-E_{11}-E_{g3}$	/
ORC turbine	$W_{Ot}=M_{10}\cdot(h_{10}-h_{12})+M_{11}\cdot(h_{11}-h_{12})$	$E_{10}+E_{11}-E_{12}$	W_{Ot}	$E_{10}+E_{11}-E_{12}-W_{Ot}$	/
Condenser 1	$M_{12}\cdot(h_{12}-h_{13})=M_{28}\cdot(h_{29}-h_{28})$	/	/	$E_{12}+E_{28}-E_{13}-E_{29}$	$E_{29}-E_{28}$
Pump 1	$W_{p1}=M_{13}\cdot(h_{14}-h_{13})=M_{13}\cdot(h_{14s}-h_{13})/\eta_{p1}$	W_{p1}	$E_{14}-E_{13}$	$E_{13}-E_{14}+W_{p1}$	/
Preheater	$M_{15}\cdot(h_{15}-h_{14})=M_{w1}\cdot(h_{w1}-h_{w2})$	$E_{w1}-E_{w2}$	$E_{15}-E_{14}$	$E_{w1}+E_{14}-E_{15}-E_{w2}$	/
Pump 2	$W_{p2}=M_7\cdot(h_9-h_7)=M_7\cdot(h_{9s}-h_7)/\eta_{p2}$	W_{p2}	E_9-E_7	$E_7-E_9+W_{p2}$	/
Pump 3	$W_{p3}=M_6\cdot(h_8-h_6)=M_6\cdot(h_{8s}-h_6)/\eta_{p3}$	W_{p3}	E_8-E_6	$E_6-E_8+W_{p3}$	/
Vapor generator 3	$M_{23}\cdot(h_{23}-h_{22})=M_{w2}\cdot(h_{w2}-h_{w3})$	$E_{w2}-E_{w3}$	$E_{23}-E_{22}$	$E_{w2}+E_{22}-E_{23}-E_{w3}$	/
Condenser 2	$M_{16}\cdot(h_{16}-h_{17})=M_{30}\cdot(h_{31}-h_{30})$	/	/	$E_{16}+E_{30}-E_{17}-E_{31}$	$E_{31}-E_{30}$
Valve	$h_{19}=h_{20}$	/	/	$E_{19}-E_{20}$	/
Pump 4	$W_{p4}=M_{22}\cdot(h_{22}-h_{18})=M_{22}\cdot(h_{22s}-h_{18})/\eta_{p4}$	W_{p4}	$E_{22}-E_{18}$	$E_{18}-E_{22}+W_{p4}$	/
Ejector	$M_{16}\cdot h_{16}=M_{23}\cdot h_{23}+M_{21}\cdot h_{21}$	$E_{23}+E_{21}$	E_{16}	$E_{23}+E_{21}-E_{16}$	/
Evaporator	$M_{20}\cdot(h_{21}-h_{20})=M_{24}\cdot(h_{24}-h_{25})$	$E_{20}-E_{21}$	$E_{25}-E_{24}$	$E_{20}+E_{24}-E_{21}-E_{25}$	/

Table 2 Cost balance and auxiliary relation [30] for each component of CCP system

Component	Cost balance	Auxiliary relation

Gas heater	$c_{g2} \cdot E_{y,g2} + c_3 \cdot E_{y,3} = c_{g1} \cdot E_{y,g1} + c_2 \cdot E_{y,2} + Z_{gh}$	$c_{g1}=c_{g2}=0$
Vapor generator 2	$c_5 \cdot E_{y,5} + c_{10} \cdot E_{y,10} = c_4 \cdot E_{y,4} + c_9 \cdot E_{y,9} + Z_{vg,2}$	$c_4=c_5$
BC turbine	$c_4 \cdot E_{y,4} + c_{Bt} \cdot W_{y,Bt} = c_3 \cdot E_{y,3} + Z_{Bt}$	$c_4=c_3$
Precooler	$c_1 \cdot E_{y,1} + c_{26} \cdot E_{y,26} = c_5 \cdot E_{y,5} + c_{27} \cdot E_{y,27} + Z_{prec}$	$c_1=c_5$
Compressor	$c_2 \cdot E_{y,2} = c_1 \cdot E_{y,1} + c_{elec,1} \cdot W_{y,comp} + Z_{comp}$	$c_{elec,1}=c_{Bt}$
Vapor generator 1	$c_{g3} \cdot E_{y,g3} + c_{11} \cdot E_{y,11} = c_{g2} \cdot E_{y,g2} + c_8 \cdot E_{y,8} + Z_{vg,1}$	$c_{g2}=c_{g3}$
ORC turbine	$c_{12} \cdot E_{y,12} + c_{Ot} \cdot W_{y,Ot} = c_{11} \cdot E_{y,11} + c_{10} \cdot E_{y,10} + Z_{Ot}$	$c_{10}=c_{11}=c_{12}$
Pump 1	$c_{14} \cdot E_{y,14} = c_{13} \cdot E_{y,13} + c_{elec,3} \cdot W_{y,pump1} + Z_{pump1}$	$c_{elec,3}=c_{Ot}$
Condenser 1	$c_{13} \cdot E_{y,13} + c_{29} \cdot E_{y,29} = c_{28} \cdot E_{y,28} + c_{12} \cdot E_{y,12} + Z_{cond1}$	$c_{13}=c_{12}$
Preheater	$c_{w2} \cdot E_{y,w2} + c_{15} \cdot E_{y,15} = c_{w1} \cdot E_{y,w1} + c_{14} \cdot E_{y,14} + Z_{preh}$	$c_{w1}=c_{w2}=0$
Pump 2	$c_9 \cdot E_{y,9} = c_7 \cdot E_{y,7} + c_{elec,2} \cdot W_{y,pump2} + Z_{pump2}$	$c_{elec,2}=c_{Ot}$
Pump 3	$c_8 \cdot E_{y,8} = c_6 \cdot E_{y,6} + c_{elec,3} \cdot W_{y,pump3} + Z_{pump3}$	$c_{elec,3}=c_{Ot}$
Vapor generator 3	$c_{w3} \cdot E_{y,w3} + c_{23} \cdot E_{y,23} = c_{w2} \cdot E_{y,w2} + c_{22} \cdot E_{y,22} + Z_{vg,3}$	$c_{w3}=c_{w2}$
Valve	/	$c_{19}=c_{20}$
Pump 4	$c_{22} \cdot E_{y,22} = c_{18} \cdot E_{y,18} + c_{elec,3} \cdot W_{y,pump4} + Z_{pump4}$	$c_{elec,4}=c_{Ot}$
Condenser 2	$c_{17} \cdot E_{y,17} + c_{31} \cdot E_{y,31} = c_{30} \cdot E_{y,30} + c_{16} \cdot E_{y,16} + Z_{cond2}$	$c_{16}=c_{17}$
Ejector	$c_{16} \cdot E_{y,16} = c_{23} \cdot E_{y,23} + c_{21} \cdot E_{y,21}$	/
Evaporator	$c_{21} \cdot E_{y,21} + c_{25} \cdot E_{y,25} = c_{20} \cdot E_{y,20} + c_{24} \cdot E_{y,24} + Z_{ev}$	$c_{20}=c_{21}$

Table 3 Main parameters of the engine [7]

Parameters	Value
Power output (kW)	2928
Rotation (r(min)$^{-1}$)	1000

Exhaust gas temperature (℃)	470
Exhaust gas mass flow rate (kg s^{-1})	4.35
Temperature of jacket water (℃)	90/79
Mass flow rate of jacket water (kg s^{-1})	25

Table 4 Composition of the exhaust gas [7]

Composition	Molecular $(g(mol)^{-1})$	Fraction (%)
O_2	32.00	9.3
CO_2	44.00	9.1
H_2O	18.01	7.4
N_2	28.01	74.2

Table 5 Condition of simulation for the CCP system

Parameter	Value
Ambient temperature (℃)	20
Ambient pressure (MPa)	0.101
Compressor inlet temperature (℃)	35
BC turbine inlet temperature (℃)	400
BC turbine inlet pressure (MPa)	18
BC turbine outlet pressure (MPa)	8
Inlet temperature at the high-pressure side of ORC turbine (℃)	150
Inlet pressure at the high-pressure side of ORC turbine (MPa)	1.6
Inlet temperature at the low-pressure side of ORC turbine (℃)	100
Inlet pressure at the low-pressure side of ORC turbine (MPa)	1.0

Outlet pressure of pump 1 (MPa)	0.9
Ejector primary inlet pressure (MPa)	0.4
Terminal temperature difference at gas heater outlet (℃)	100
Pinch point temperature difference in vapor generator 1 (℃)	30
Pinch point temperature difference in vapor generator 2 (℃)	30
Pinch point temperature difference in vapor generator 3 (℃)	25
Condensation temperature of condenser 1 (℃)	30
Condensation temperature of condenser 2 (℃)	30
Evaporation temperature of evaporator (℃)	5
Isentropic efficiency of BC turbine (%)	80
Isentropic efficiency of ORC turbine (%)	80
Isentropic efficiency of compressor (%)	80
Isentropic efficiency of pump 1 (%)	75
Isentropic efficiency of pump 2 (%)	75
Isentropic efficiency of pump 3 (%)	75
Inlet temperature of cooling water (℃)	20

Table 6 Parameters for GA

Parameter	Operation range
BC turbine inlet temperature (℃)	330-440
BC turbine inlet pressure (MPa)	15-20
Inlet temperature at the high-pressure side of ORC turbine (℃)	130-180
Inlet pressure at the high-pressure side of ORC turbine (MPa)	1.4-2

Inlet temperature at the low-pressure side of ORC turbine (℃)	90-150
Inlet pressure at the low-pressure side of ORC turbine (MPa)	0.9-1.3
Ejector primary inlet pressure (MPa)	0.3-1

959 **Table 7** Control parameters of GA

Tuning parameters	Value
Population size	20
Mutation probability	0.01
Crossover probability	0.8
Stop generation	200

960 **Table 8** Single-objective optimization results

Parameter	Value
BC turbine inlet temperature (℃)	425.46
BC turbine inlet pressure (MPa)	20.00
Inlet temperature at the high-pressure side of ORC turbine (℃)	144.32
Inlet pressure at the high-pressure side of ORC turbine (MPa)	1.85
Inlet temperature at the low-pressure side of ORC turbine (℃)	100.03
Inlet pressure at the low-pressure side of ORC turbine (MPa)	1.26
Ejector primary inlet pressure (MPa)	0.54
Net power output (kW)	374.37
Cooling capacity (kW)	188.63
Exergy efficiency (%)	37.31
Levelized exergy cost ($ (MWh)$^{-1}$)	53.25

Table B1 Constants for component costs [37]

Constant	Value	Constant	Value	Constant	Value
$B_{1,\mathrm{he}}$	1.63	$K_{3,\mathrm{pump}}$	0.1538	$C_{3,\mathrm{he}}$	0.08183
$B_{2,\mathrm{he}}$	1.66	$K_{1,\mathrm{turb}}$	2.7051	$C_{1,\mathrm{pump}}$	-0.3635
$B_{1,\mathrm{pump}}$	1.89	$K_{2,\mathrm{turb}}$	1.4398	$C_{2,\mathrm{pump}}$	0.3957
$B_{2,\mathrm{pump}}$	1.35	$K_{3,\mathrm{turb}}$	-0.1776	$C_{3,\mathrm{pump}}$	-0.0026
$K_{1,\mathrm{he}}$	4.3247	$K_{1,\mathrm{comp}}$	2.2897	$F_{\mathrm{M,he}}$	1.0
$K_{2,\mathrm{he}}$	-0.3030	$K_{2,\mathrm{comp}}$	1.3604	$F_{\mathrm{BM,turb}}$	3.5
$K_{3,\mathrm{he}}$	0.1634	$K_{3,\mathrm{comp}}$	-0.1027	$F_{\mathrm{BM,comp}}$	2.7
$K_{1,\mathrm{pump}}$	3.3892	$C_{1,\mathrm{he}}$	0.03881	$F_{\mathrm{M,pump}}$	2.2
$K_{2,\mathrm{pump}}$	0.0536	$C_{2,\mathrm{he}}$	-0.11272		

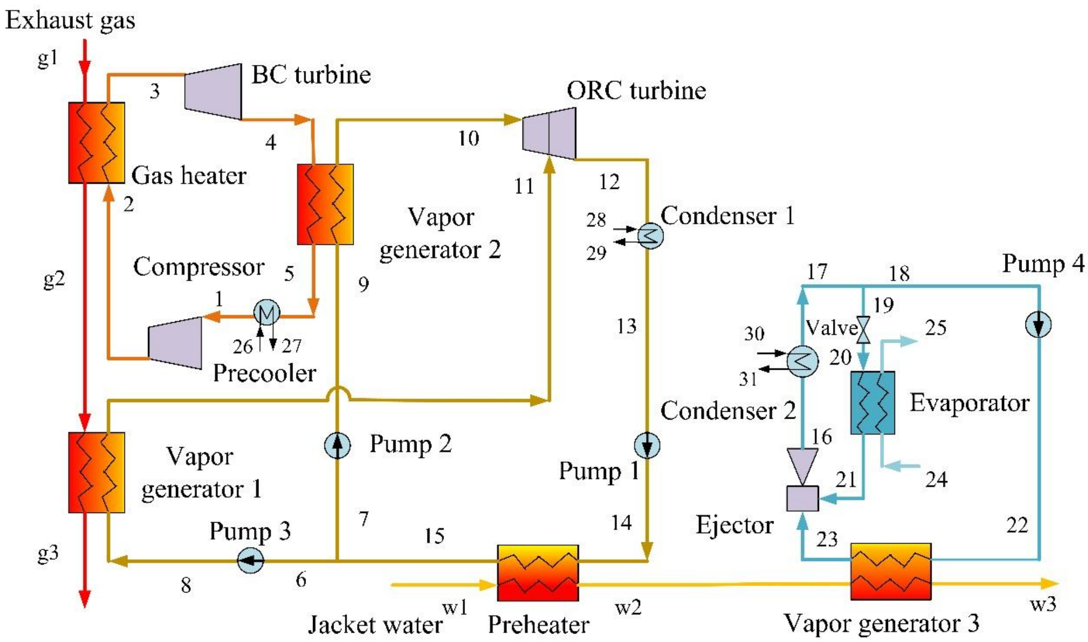

Fig. 1. Schematic diagram of the CCP system

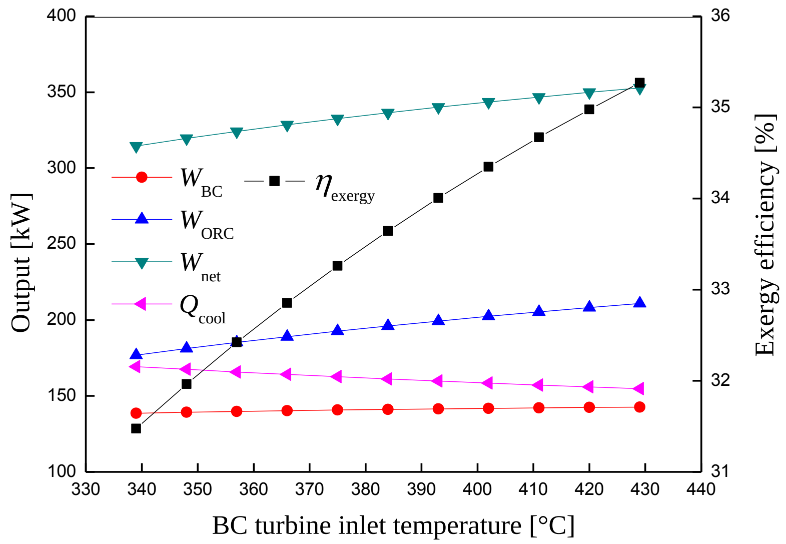

Fig. 2. Influences of BC turbine inlet temperature on the output and the exergy efficiency of the system.

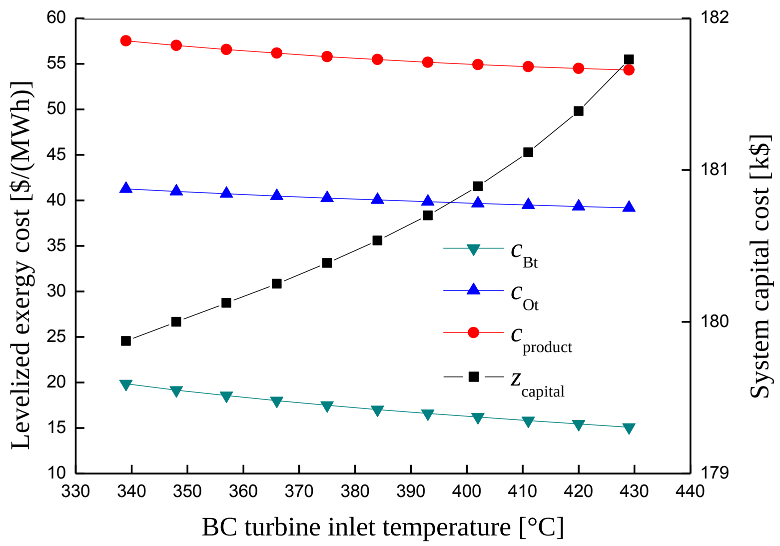

Fig. 3. Influences of BC turbine inlet temperature on the levelized exergy cost and the system capital cost of the system.

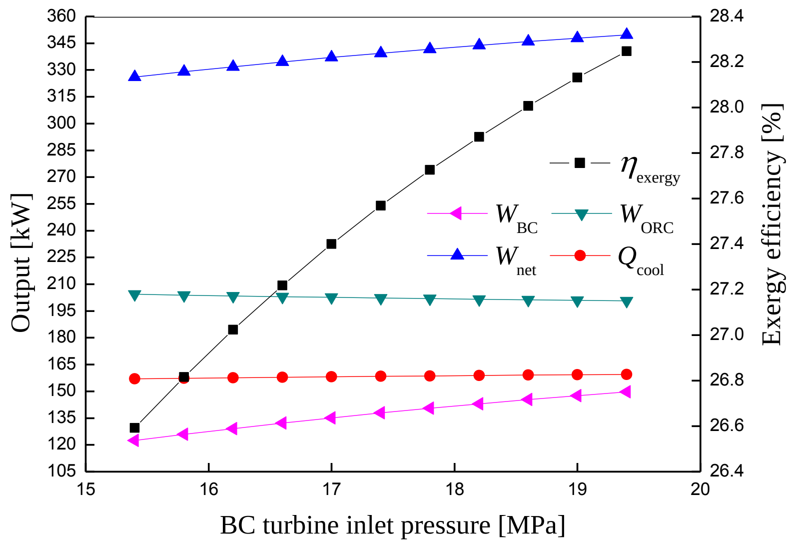

Fig. 4. Influences of BC turbine inlet pressure on the output and the exergy efficiency of the system.

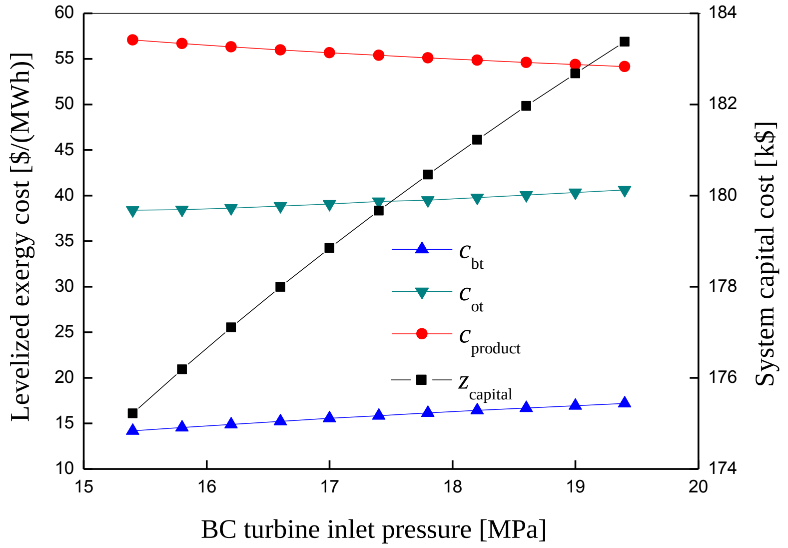

Fig. 5. Influences of BC turbine inlet pressure on the levelized exergy cost and the system capital cost of the system.

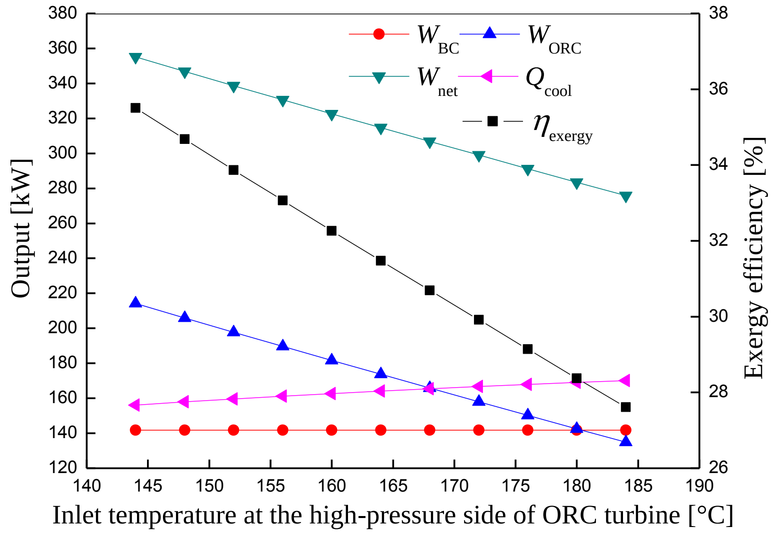

Fig. 6. Influences of inlet temperature at the high-pressure side of ORC turbine on the output and the exergy efficiency of the system.

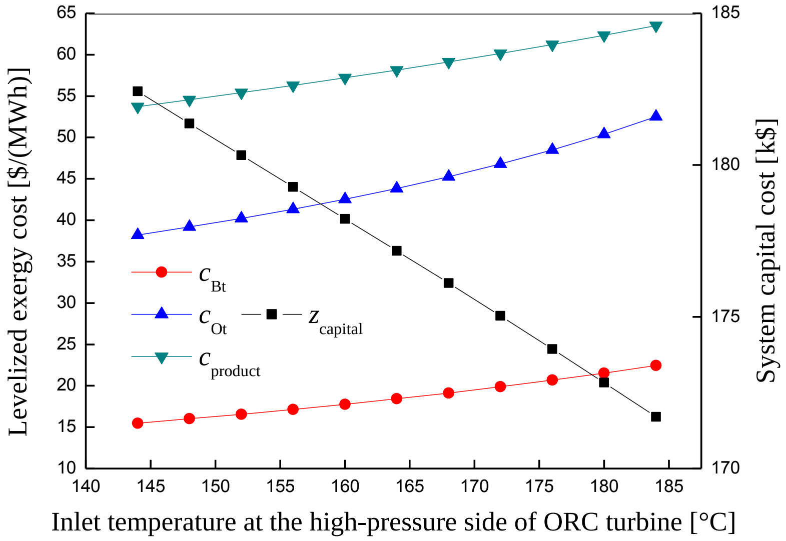

Fig. 7. Influences of inlet temperature at the high-pressure side of ORC turbine on the levelized exergy cost and the system capital cost of the system.

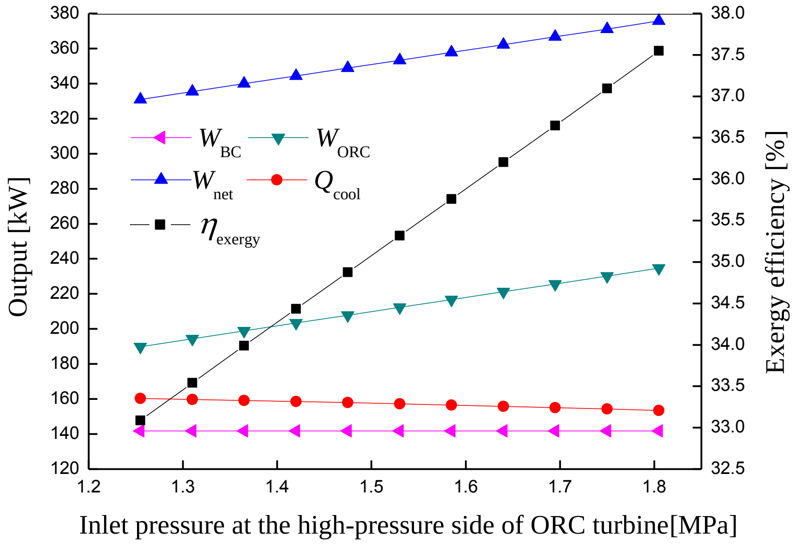

Fig. 8. Influences of inlet pressure at the high-pressure side of ORC turbine on the output and the exergy efficiency of the system.

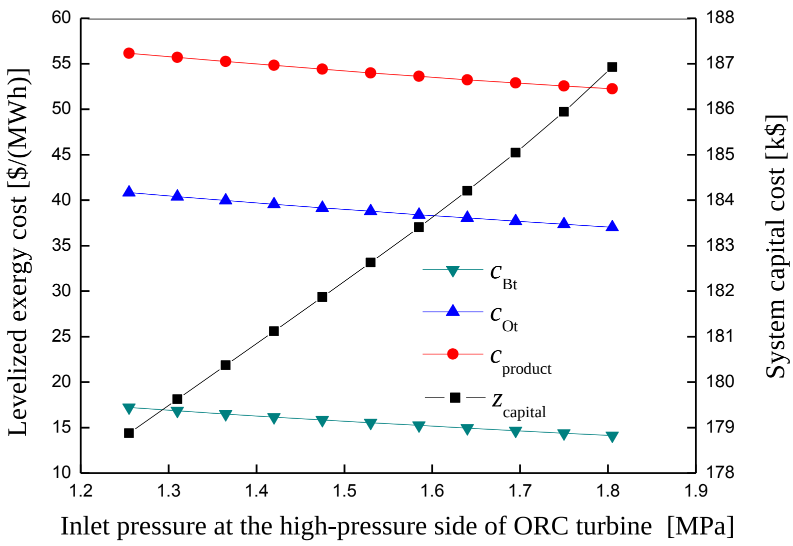

Fig. 9. Influences of inlet pressure at the high-pressure side of ORC turbine on the levelized exergy cost and the system capital cost of the system.

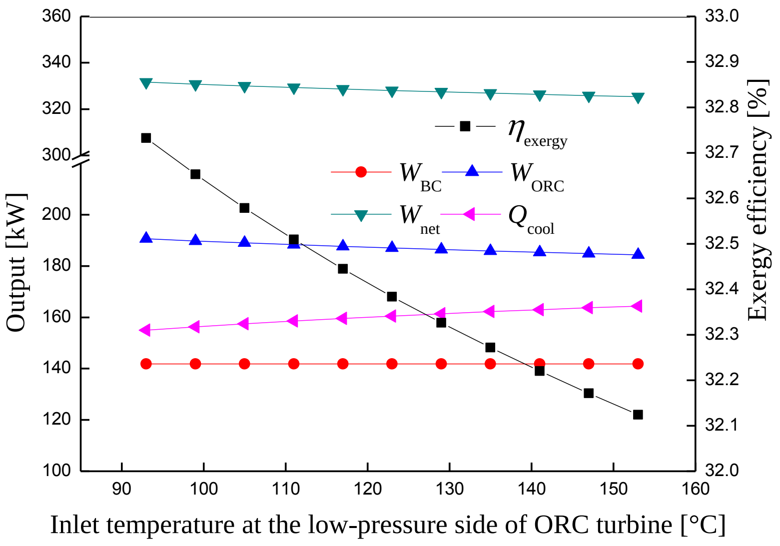

Fig. 10. Influences of inlet temperature at the low-pressure side of ORC turbine on the output and the exergy efficiency of the system.

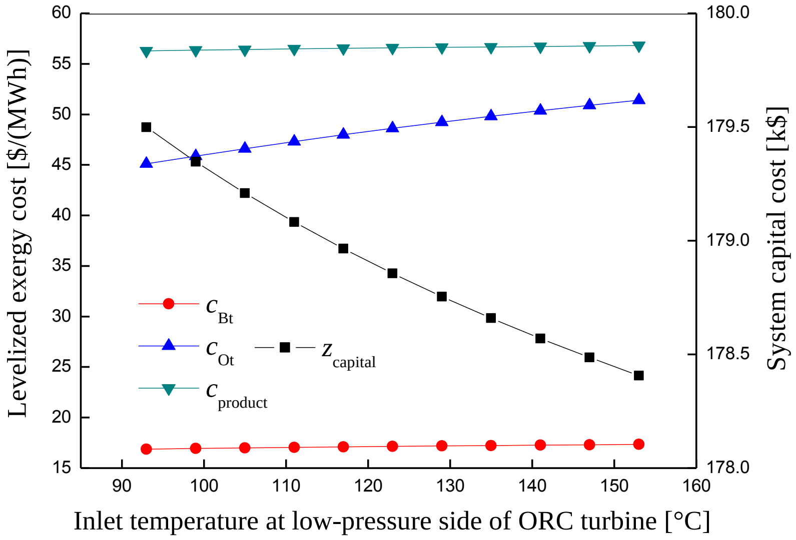

Fig. 11. Influences of inlet temperature at the low-pressure side of ORC turbine on the levelized exergy cost and system capital cost of the system.

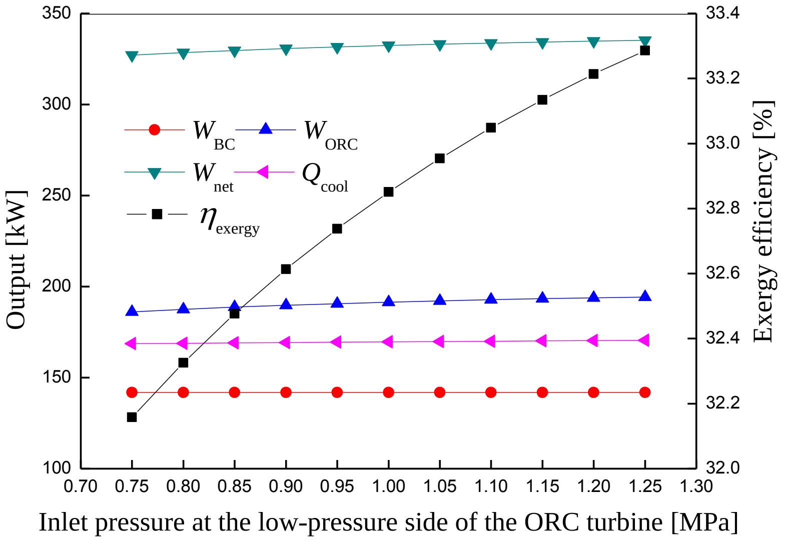

Fig. 12. Influences of inlet pressure at the low-pressure side of ORC turbine on the output and the exergy efficiency of the system.

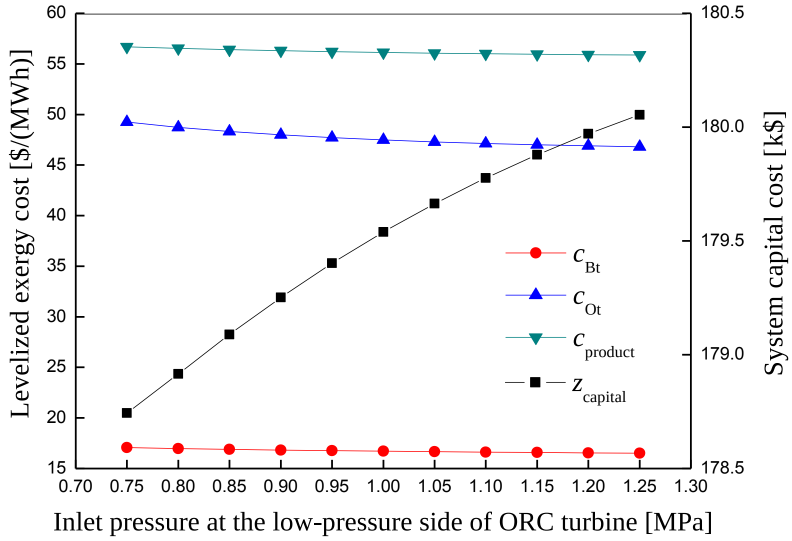

Fig. 13. Influences of the inlet pressure at the low-pressure side of ORC turbine on the levelized exergy cost and system capital cost of the system.

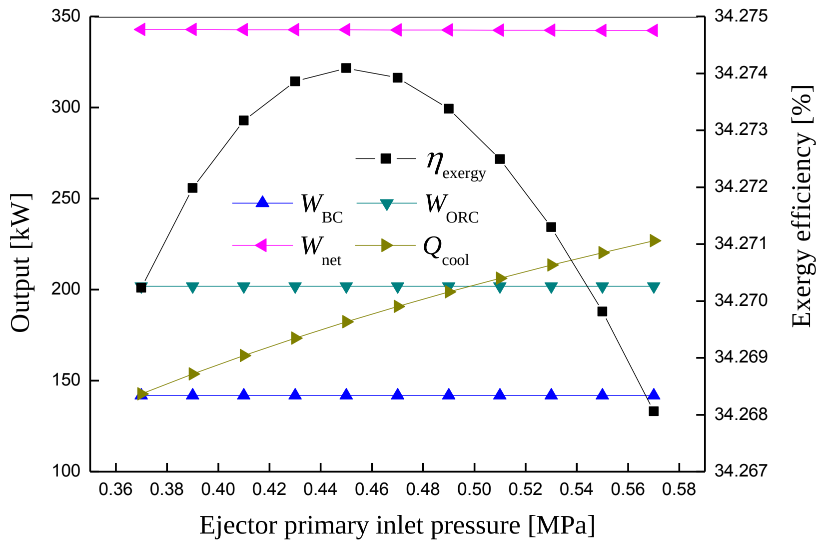

Fig. 14. Influences of ejector primary inlet pressure on the output and the exergy efficiency of the system.

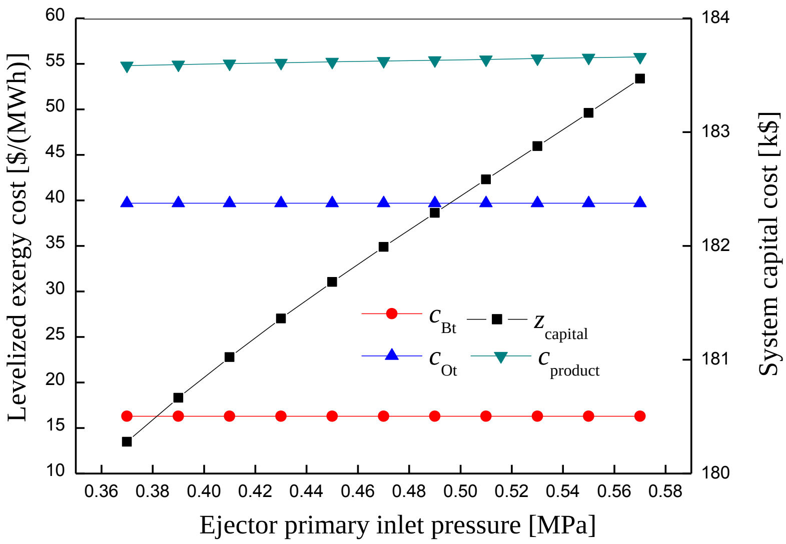

Fig. 15. Influences of ejector primary inlet pressure on the levelized exergy cost and the system capital cost of the system.

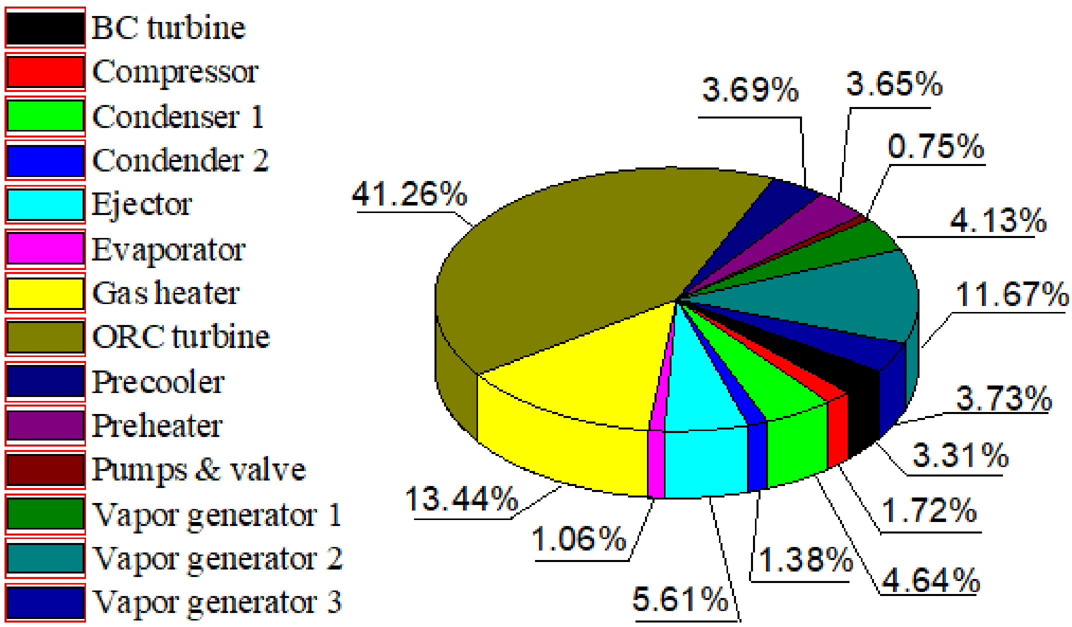

Fig. 16. Exergy destruction of different components